4.1.1.6 Flexural Cracking/Toe Crushing

Reference: Abrams & Shah (1992)
Specimen: W2
Material: Brick
Loading: Reversed quasistatic cyclic
Provided Information:
Prism f'_m= 911 psi, brick f'_m=3480 psi
L/h_{eff}= 9ft /6ft = 1.5
Nominal f_a= 50 psi
Cantilever conditions
Assumed Values:
v_{me1}=(0.75/1.5)*(0.75*100+f_a) psi
v_{me2}=(0.75/1.5)*(f_a) psi
Calculated Values (kips):
V_r=28 V_{tc}=29
V_{bjs1}=53 V_{bjs2}=21
V_{dt1}= 155 V_{dt2}= 175
FEMA 273 Predicted Behavior: Rocking at 28 kips with drift "d"=0.3%
ATC-43 Predicted Behavior: Flexural cracking/toe crushing at 29 kips
Actual Behavior: Flexural cracking/toe crushing, with a maximum capacity of 43-45 kips.

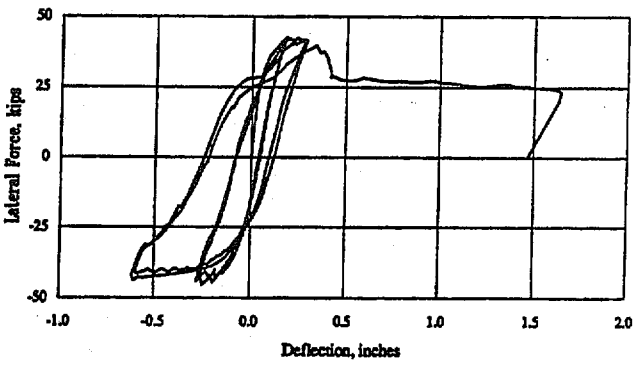

Test Wall W2

Reference: Epperson and Abrams (1989)
Specimen: E1
Material: Brick
Loading: Monotonic
Provided Information:
Prism f'_m= 1740 psi, brick f'_m=8280 psi
L/h_{eff}= 7.83ft /6ft = 1.31
Nominal f_a= 126 psi
Cantilever conditions
Assumed Values:
v_{me1}=(0.75/1.5)*(0.75*186+f_a) psi
v_{me2}=(0.75/1.5)*(f_a) psi
Calculated Values (kips):
V_r=118 V_{tc}=118
V_{bjs1}=250 V_{bjs2}=101
V_{dt1}= 336 V_{dt2}= 533
FEMA 273 Predicted Behavior: Rocking or toe crushing
ATC-43 Predicted Behavior: Flexural cracking/toe crushing at 118 kips
Actual Behavior: Flexural cracking/toe crushing, with a maximum capacity of 120 kips and final drift of 0.3%

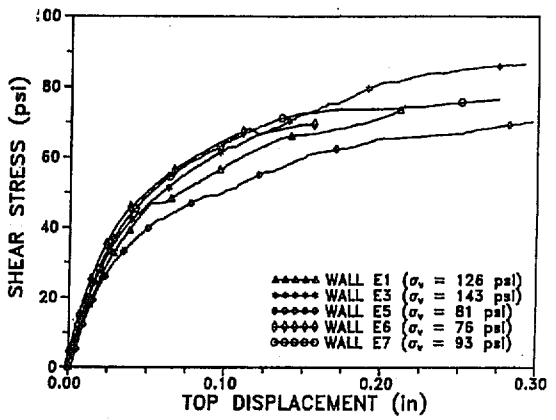

Summary of measured top level displacement of the Test Walls vs shear stress

Reference: Epperson and Abrams (1989)
Specimen: E3
Material: Brick
Loading: Monotonic
Provided Information:
Prism f'_m= 1740 psi, brick f'_m=8280 psi
L/h_{eff}= 9.5ft /6ft = 1.58
Nominal f_a= 141 psi
Cantilever conditions
Assumed Values:
v_{me1}=(0.75/1.5)*(0.75*186+f_a) psi
v_{me2}=(0.75/1.5)*(f_a) psi
Calculated Values (kips):
V_r=190 V_{tc}=186
V_{bjs1}=307 V_{bjs2}=133
V_{dt1}= 420 V_{dt2}= 635
FEMA 273 Predicted Behavior: Toe crushing at 186 kips
ATC-43 Predicted Behavior: Flexural cracking/toe crushing at 186 kips
Actual Behavior: Flexural cracking/toe crushing, with a maximum capacity of 164 kips and final drift of 0.4%

Reference: Epperson and Abrams (1989)
Specimen: E5
Material: Brick
Loading: Monotonic
Provided Information:
Prism f'_m= 1740 psi, brick f'_m=8280 psi
L/h_{eff}= 11.42ft /6ft = 1.90
Nominal f_a= 81 psi
Cantilever conditions
Assumed Values:
v_{me1}=(0.75/1.5)*(0.75*186+f_a) psi
v_{me2}=(0.75/1.5)*(f_a) psi
Calculated Values (kips):
V_r=150 V_{tc}=156
V_{bjs1}=289 V_{bjs2}=88
V_{dt1}= 367 V_{dt2}= 680
FEMA 273 Predicted Behavior: Rocking at 150 kips with "d" drift of 0.2%
ATC-43 Predicted Behavior: Flexural cracking/toe crushing at 156 kips
Actual Behavior: Flexural cracking/toe crushing, with a maximum capacity of 154 kips and final drift of 0.4%

Reference: Epperson and Abrams (1989)
Specimen: E6
Material: Brick
Loading: Monotonic
Provided Information:
Prism f'_m= 1740 psi, brick f'_m=8280 psi
L/h_{eff}= 11.42ft /6ft = 1.90
Nominal f_a= 76 psi
Cantilever conditions
Assumed Values:
v_{me1}=(0.75/1.5)*(0.75*186+f_a) psi
v_{me2}=(0.75/1.5)*(f_a) psi
Calculated Values (kips):
V_r=141 V_{tc}=147
V_{bjs1}=284 V_{bjs2}=82
V_{dt1}= 357 V_{dt2}= 675
FEMA 273 Predicted Behavior: Rocking at 141 kips with "d" drift of 0.2%
ATC-43 Predicted Behavior: Flexural cracking/toe crushing at 147 kips
Actual Behavior: Flexural cracking/toe crushing, with a maximum capacity of 150 kips and final drift of 0.2%

Reference: Epperson and Abrams (1989)
Specimen: E7
Material: Brick
Loading: Monotonic
Provided Information:
Prism f'_m= 1740 psi, brick f'_m=8280 psi
L/h_{eff}= 11.42ft /6ft = 1.90
Nominal f_a= 93 psi
Cantilever conditions
Assumed Values:
v_{me1}=(0.75/1.5)*(0.75*186+f_a) psi
v_{me2}=(0.75/1.5)*(f_a) psi
Calculated Values (kips):
V_r=173 V_{tc}=177
V_{bjs1}=302 V_{bjs2}=101
V_{dt1}= 390 V_{dt2}= 692
FEMA 273 Predicted Behavior: Rocking at 173 kips with "d" drift of 0.2%
ATC-43 Predicted Behavior: Flexural cracking/toe crushing at 177 kips
Actual Behavior: Flexural cracking/toe crushing, with a maximum capacity of 157 kips and final drift of 0.4%

4.1.2 Comments on FEMA 273 Component Force/Displacement Relationships

4.1.2.1 Conclusions from Review of the Research and Their Impact on the Evaluation Methodology

As the previous sections indicate, the FEMA 273 methodology leads to successful predictions in certain cases. In other cases, the predictions did not match the observed behavior. To help address this issue, some modifications were made in the Section 7.3 methodology in FEMA 306. Some of these issues and their resolution include:

- Rocking and toe crushing equations often yield very similar values; when they do differ, the lower value does not necessarily predict the governing mode. Section 7.3 in FEMA 306 thus identifies which mode will occur on the basis of aspect ratio, unless the axial stress is very high, since there have been no reported instances of rocking in stocky piers. The $L/h_{eff} > 1.25$ is a somewhat arbitrary threshold based simply on a review of test results.

- Stable rocking generally exceeds the proposed "d" drift value of $0.4h_{eff}/L$. Thus, this value is conservative (see Costley and Abrams, 1996 and Anthoine et al., 1995).

- Rocking does not appear to exhibit the FEMA 273 drop to the "c" capacity value in the above two tests nor, apparently, in the Magenes and Calvi (1995) tests. The only exception is Specimen W3 of Abrams and Shah (1992), which, after rocking for ten cycles at drifts of up to 0.5% ($0.5h_{eff}/L$), was then pushed to 0.8% drift ($0.8h_{eff}/L$) where it experienced toe crushing. The test was stopped at that point. Given the limited number of specimens, it is difficult to determine if this represents the drop from initial load to the "c" level, or a special, sequential mode. For simplicity, this case was combined with the rocking cases, and the "d" drift level was set to account for this level of toe crushing. In most cases, though, rocking capacities will not drop off significantly. The "d" drift value of $0.4h_{eff}/L$ was set based on Costley and Abrams (1996), with some conservatism (Abrams, 1997) to account for Specimen W3. The "c" drift value was conservatively set at 0.6, because of the limited test data (Abrams, 1997), but aside from Specimen W3, higher "c" values are probably likely.

- There are few pure bed-joint sliding tests. Specimen W1 of Abrams and Shah (1992) is one example, and Specimens MI2 and MI4 of Magenes and Calvi (1992) appear to be examples as well. The drop in lateral strength appears to occur at about 0.3-0.4% drift in W1 and MI4, so the proposed "d" value of 0.4 seems reasonable. The "c" of 0.6 also seems reasonable. The capacity for bed-joint sliding is based on the bond-plus-friction strength. After cracking, the bond capacity will be eroded, and the strength is likely to be based simply on the friction portion of the equation. Cyclic in-place push tests show this behavior; so does Specimen W1 of Abrams and Shah (1992). One could argue that the second cycle backbone curve of FEMA 273 (which, by definition, goes into the nonlinear, post-cracking range) should be limited only to the frictional capacity. But in many cases, other modes will be reached before the full bed-joint sliding capacity is reached. In some of these cases, interestingly, bed-joint sliding occurs after another mode has occurred. Manzouri et al. (1995), for example, show sequences such as initial toe crushing that progresses to bed-joint sliding at higher drift values. One explanation is that toe crushing degenerated into bed-joint sliding because the toe crushing and initial bed-joint sliding values were quite close. See Section 4.1.2.2 for further explanation.

- Mixed modes or, more accurately, sequences of different behavior modes are common in the experiments.

4.1.2.2 The Bed-Joint Sliding and Flexural Cracking/Toe Crushing/Bed-Joint Sliding Modes

The model of bed-joint sliding used in this document is shown in Figure 4-1. For estimating the strength and deformation capacity of the undamaged bed-joint sliding mode, FEMA 273 was used. The idealized relationship has a plateau at the bed-joint capacity V_{bjs1}, which includes the bond and friction components. After bond is lost, the residual strength is limited to 60% of V_{bjs1}. The actual backbone curve is likely to be smoother than the idealized model, since the loss of bond does not occur all at once in the entire masonry section. Instead, more heavily stressed portions crack, and shear demand is redistributed to the remaining

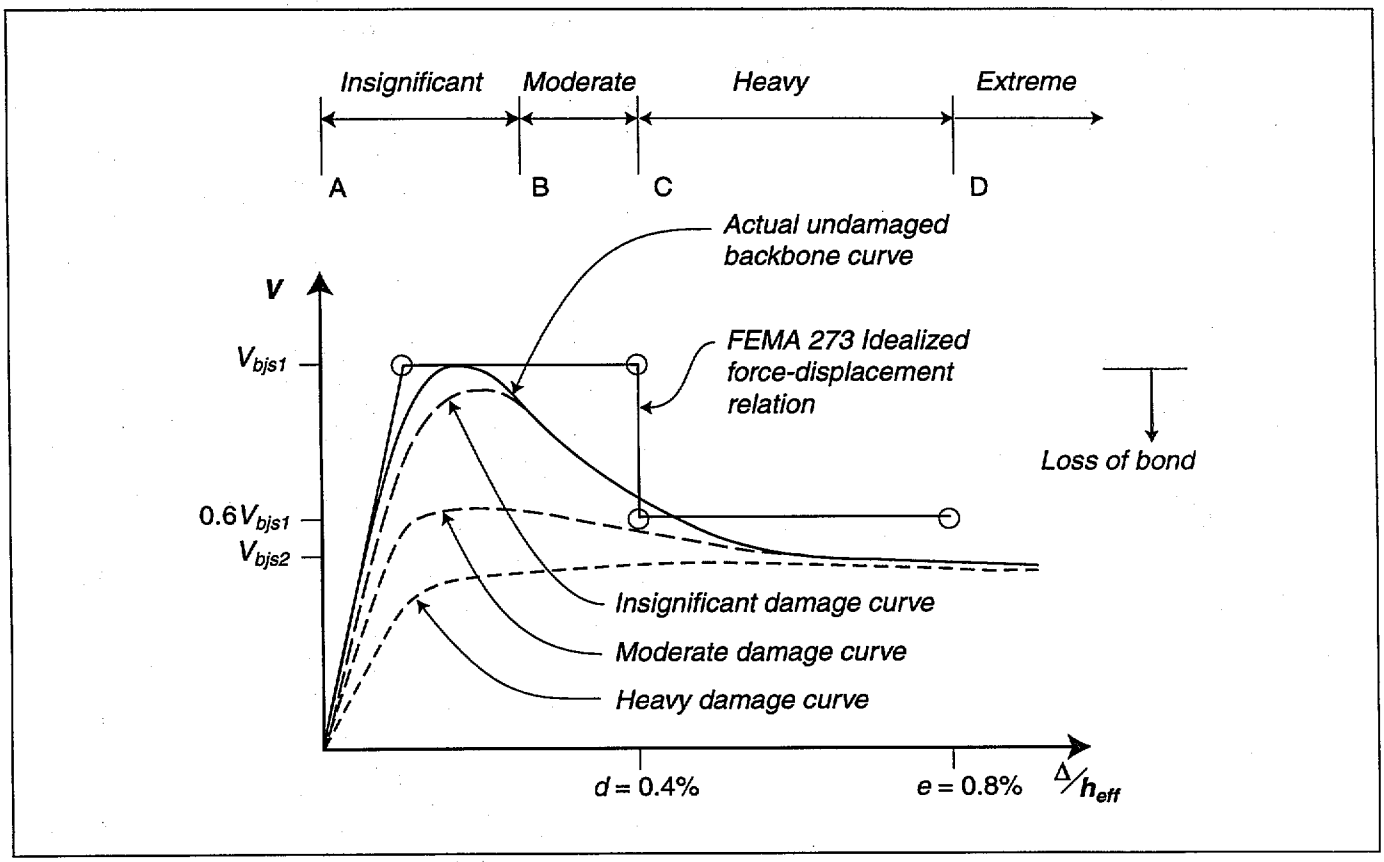

Figure 4-1 ***Bed-joint sliding force/displacement relationship***

sections. The actual residual strength could be higher or lower than $0.6V_{bjs1}$. One measure of the residual capacity is V_{bjs2}.

Figure 4-1 also shows the assumed changes to the force/displacement relationship following the damaging event. *Insignificant* damage is characterized by displacement during the damaging event that is between points A and B. Loss of bond is limited. Following the damaging event, the dashed "Insignificant Damage Curve" represents the force/displacement relationship. For damaging events that reach levels of initial displacement beyond point B, greater loss of bond occurs, and the subsequent damage curve achieves a lower strength. Eventually, with initial displacements beyond point C, the entire bond is lost and only friction remains. Thus, future cycles will no longer be able to achieve the original V_{bjs1} level, reaching only the V_{bjs2} level. With significant cyclic displacements, some erosion of the crack plane and deterioration of the wall is likely to lead to a small reduction in capacity below the V_{bjs2} level.

The varying level of bed-joint sliding strength is assumed in this document to be a possible explanation for some of the observed testing results in stocky walls, in particular results such as (1) Specimen W1 of Abrams and Shah (1992), in which bed-joint sliding was the only mode observed; (2) Manzouri et al. (1995), in which toe crushing behavior was followed by bed-joint sliding; and (3) Epperson and Abrams (1989), in which toe crushing was not followed by sliding. Figure 4-2 helps to explain the hypothesis.

In the top set of curves, toe-crushing strength substantially exceeds the V_{bjs1} level. As displacement occurs, the bed-joint sliding capacity is reached first, and it becomes the limit state. If displacement is such that *heavy* damage occurs, then in subsequent cycles, the strength will be limited to the V_{bjs2} level.

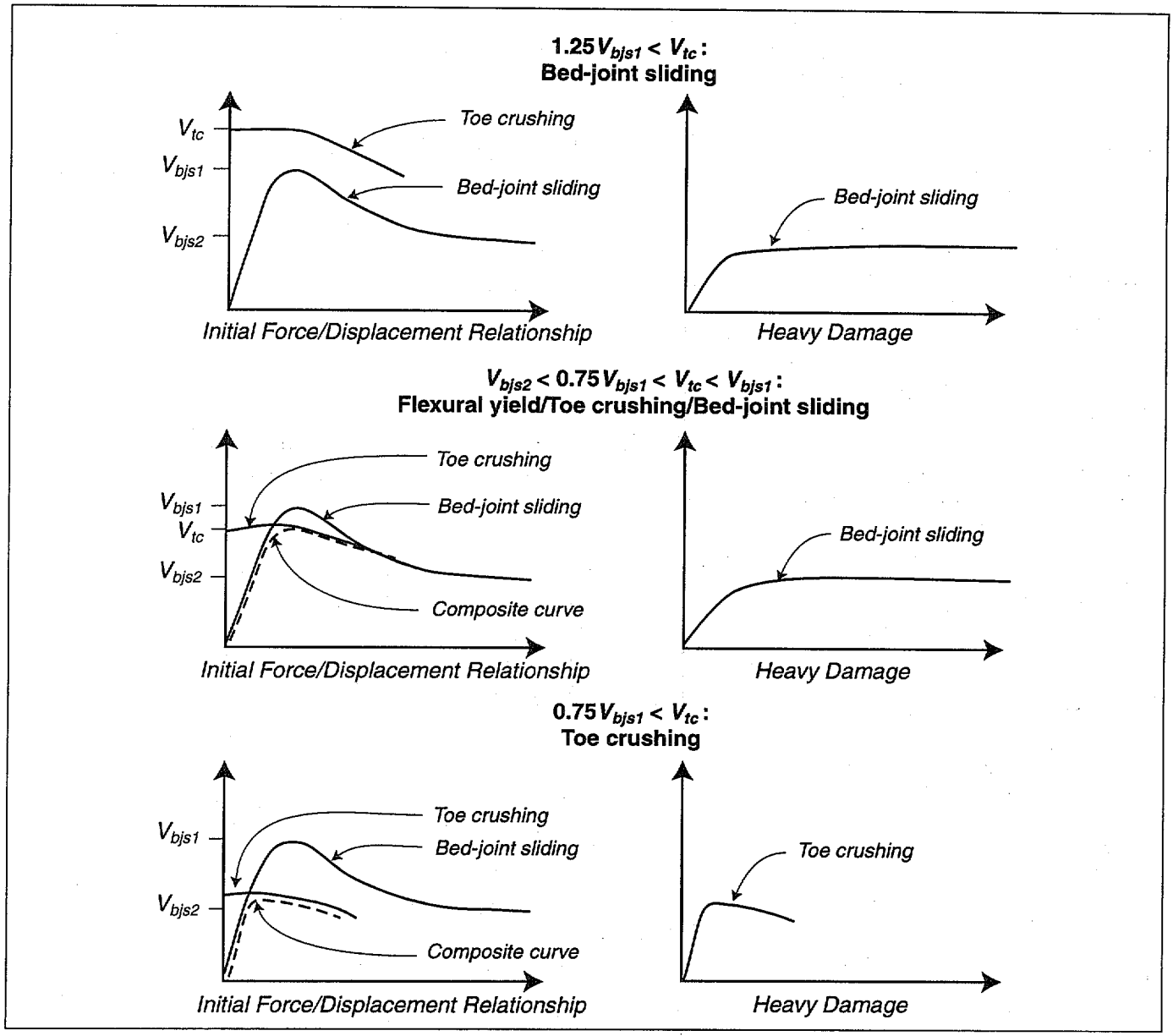

Figure 4-2 ***Relationship Between Toe Crushing and Bed-Joint Sliding***

In the second set of curves, toe-crushing and initial bed-joint sliding strengths are similar. As displacement occurs, the toe-crushing strength is reached first, cracking and movement occur within the wall, some of the bond is lost, and the wall begins to slide. The initial force/displacement curve is thus similar to that for bed-joint sliding, except that the peak is limited by the toe-crushing strength. If displacement is such that *Heavy* damage occurs, then in subsequent cycles, the strength will be limited to the V_{bjs2} level. This is one possible explanation for the Manzouri et al. (1995) tests.

In the third set of curves, toe-crushing strength is substantially lower than initial bed-joint sliding strength and the ductile mechanism of sliding is not achieved. This is one possible explanation for the Epperson and Abrams (1989) results, in which mortar shear strength was much higher and ductility was lower.

Section 7.3.2 in FEMA 306 makes use of the above hypotheses; cutoff values for the middle set of curves were based in part on review of the results shown in Section 4.1.1. Results are promising, but additional testing and verification of other tests should be done.

4.1.2.3 Out-of-Plane Flexural Response

The most comprehensive set of testing done to date on the out-of-plane response of URM walls was part of the ABK program in the 1980s, and it is documented in ABK (1981c). Input motions used in the ABK (1981c) were based on the following earthquake records: Taft 1954 N21E, Castaic 1971 N69E, Olympia 1949 S04E, and El Centro 1940 S00E. They were scaled in amplitude and were processed to represent the changes caused by diaphragms of varying stiffness to produce the final series of 22 input motion sets. Each set has a motion for the top of the wall and the bottom of the wall. Peak velocities range up to 39.8 in/sec; accelerations, up to 1.42g; and displacements, up to 9.72 inches. In ABK (1984), the mean ground input velocity for UBC Seismic Zone 4 was assumed to be 12 in/sec. For buildings with crosswalls, diaphragm amplification would increase this about 1.75-fold, to 21 in/sec. For buildings without crosswalls, wood roofs were assumed to have a velocity of about 24 in/sec and floors about 27 in/sec.

Since 1981, a significant number of ground motion records have been obtained, including a number of near-field records. In several instances, recent recordings substantially exceed the 12 in/sec value and even exceed the maximum values used by ABK (1981c). Of particular concern are near-field pulse effects and whether they were adequately captured by the original testing. When site-specific spectra and time histories that incorporate these effects are available, it may be possible to address this issue using the original research.

4.1.3 Development of *λ-factors*

One of the central goals of this document is to develop a method for quantitatively characterizing the effect of damage on the force/displacement relationship of wall components. Ideally, the most accurate approach would be to have two sets of cyclic tests for a component. One test would be of an initially undamaged wall displaced to failure. The second set would include walls initially displaced to various levels of damage (to represent the "damaging event") and then retested to failure. This would allow for direct determination of the λ-factors contained in the Component Guides in FEMA 306. Unfortunately, as noted in Section 4.1.1 there have been almost no experimental tests done on damaged URM walls; typically, tests were done on undamaged walls and either stopped or continued only after the damaged wall was repaired.

In the absence of test results on damaged walls, hysteresis curves of initially undamaged walls were reviewed. In reviewing these tests, the goal was to characterize how force/displacement relationships changed from cycle to cycle as displacement was increased. Early cycles were considered to represent "damaging" events, and subsequent cycles represented the behavior of an initially-damaged component. Particular attention was given to tests in which multiple runs on a specimen were performed. In these cases, initial runs (representing not just a damaging cycle, but a damaging earthquake record) were compared with subsequent runs to determine the extent of strength and stiffness deterioration.

Using these tests, the following general approaches were used to estimate λ-factors for this project. The reloading stiffnesses (i.e., the stiffness observed moving from the fourth quadrant to the first) at different cycles or different runs were compared to the intial stiffness to determine λ_K. This variable is estimated to be the ratio of stiffness at higher cycles to the initial stiffness. The assumption made is that if testing had been stopped and the displacement reset to zero and then restarted, the stiffness of the damaged component would have been similar to the reloading stiffness. See Figure 4-3 for an example.

For determining λ_Q, the approach shown in Figure 4-1 and discussed in the previous section is applied where appropriate to determine λ_Q, the ratio of strength at higher cycles to initial strength. The loss of strength is roughly equal to the capacity at high drift levels divided by the peak capacity. FEMA 273 describes both deformation-controlled and force-controlled modes. In a purely force-controlled mode, there is, by definition, little or no ductility. Deformation progresses until a brittle failure results. Thus, there are few, if any, damage states between *Insignificant* and *Extreme*, and there would be little, if any, post-cracking strength. Further, until a brittle mode occurs, the component would be expected to be minimally affected by previous displacement. Review of available hysteresis curves shows, though, that even modes defined as force-

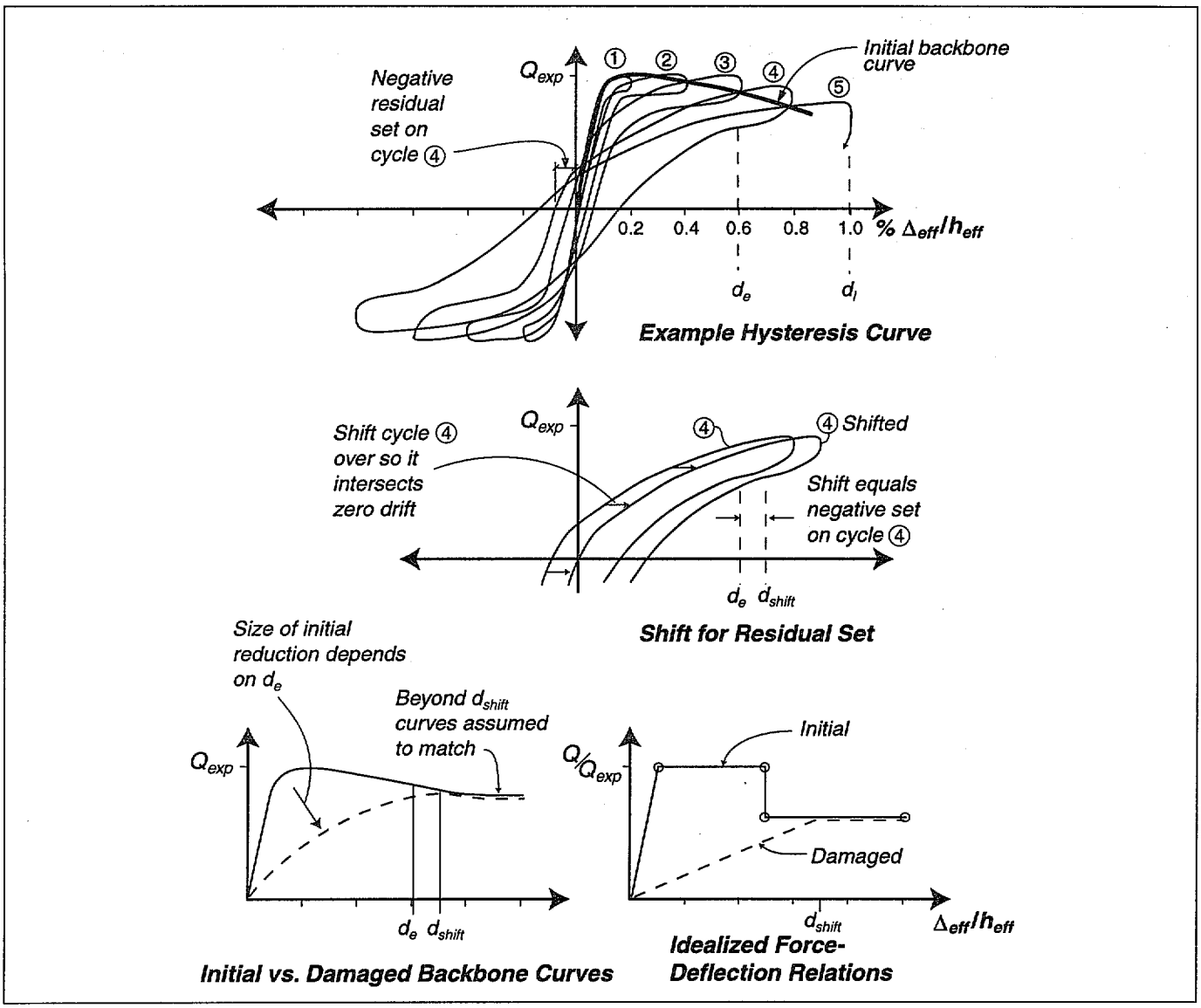

Figure 4-3 ***Developing the initial portion of the damaged force/displacement relationship***

controlled by FEMA 273 (such as diagonal tension) do have some residual strength.

There is little available information for determining λ_Δ, because retesting of damaged components to failure has not been done. Values were estimated using engineering judgment. In most cases, less-ductile modes are assumed to have higher λ_Δ values, even at higher damage levels. The basis of this assumption is the idea that in more-ductile modes, λ_Δ is assumed to be somewhat more dependent on cumulative inelastic deformation. In more-ductile modes, the available hysteretic energy has been dissipated in part by the damaging earthquake, and there is less available in the subsequent event. The result is the final displacement that can be achieved is reduced.

Values for λ_K^*, λ_Q^*, and λ_Δ^* are based, where possible, on tests of repaired walls. The values in URM1F, for example, are set at 1.0 because the hysteresis curves of repaired walls were equal to or better than those of the original walls. In most other cases, repairs typically involve injection of cracks, but since microcracking can never be fully injected, it may not be possible to restore

complete initial stiffness. In the bed-joint sliding modes without tests, it was assumed that the strength could not be fully restored by injection, because the horizontal crack planes are closed and bond cannot be restored in these locations. It is important to recognize that injection of walls with many cracks or unfilled collar joints and cavities, may enhance strength, but it may also lead to less ductile behavior, because other modes may then occur prior to bed-joint sliding.

Values for $\lambda_{h/t}$ are based on a review of the ABK (1981c) document, the model proposed in Priestley (1985), and engineering judgment. At low levels of damage, the portions of wall between the crack planes are essentially undamaged, and the effective thickness, t, remains unchanged. At higher levels of damage, deterioration, crushing, and spalling of the corners of the masonry at crack locations reduces the effective thickness and the ability of the wall to resist movements imparted by the diaphragm.

4.2 Tabular Bibliography for Unreinforced Masonry

Table 4-1 contains a brief description of the key technical reports that address specific reinforced masonry component behavior. The component types and their behavior modes are indicated. The full references can be found in Section 4.4.

Table 4-1 Summary of Significant Experimental Research or Research Summaries

Reference	Specimen/Loading	Aspect Ratio (L/h_{eff})	Axial Stress (f_a in psi)	Predictive Equations	Repair	Component-Type	Behavior Modes Addressed[1]												
							a	b	c	d	e	f	g	h	i	j	k	l	m	n
Abrams (1992)	Based on Abrams and Shah (1992) and Epperson and Abrams (1989)			Strength	None	URM1								•						
Abrams and Shah (1992)	3 cantilever brick piers with reversed static-cyclic loading	2 1.5 1	75 50 50	Strength	None	URM1		•			•			•						
ABK (1981c)	22 specimens with dynamic out-of-plane loading, including brick, grouted and ungrouted clay and concrete block	*h/t* from 14.0-25.2	2-23	None	Ferrocement surface coating on 2 specimens	URM1													•	
Anthoine et al. (1995)	3 brick piers in double curvature with reversed static cyclic loading	0.5 0.5 0.74	87 87 116	None	None	URM2	• •	•					•							
Costley and Abrams (1996b)	2 3/8th-scale brick buildings on shake table, each with two punctured walls lines in the in-plane direction	0.54-0.84 0.53-0.74 0.30-0.40 0.96-1.50	33-36 40-48 40-48 33-36	Strength	None	URM2	• • •	•												
Epperson and Abrams (1989)	5 cantilever brick piers with monotonic loading	1.31 1.58 1.90 1.90 1.90	126 143 81 76 93	Strength	None	URM1								• • • • •						
Kingsley et al. (1996)	1 2-story, full-scale brick building with reversed static-cyclic loading	na	na	None	None	URM2														•
Magenes and Calvi (1992)	4 brick piers in double curvature with reversed static cyclic loading	0.75 0.75 0.5 0.5	163 97 181 100	Strength	None	URM2		• •					• •							

Table 4-1 Summary of Significant Experimental Research or Research Summaries (continued)

Reference	Specimen/Loading	Aspect Ratio (L/h_{eff})	Axial Stress (f_a in psi)	Predictive Equations	Repair	Component-Type	Behavior Modes Addressed[1] a	b	c	d	e	f	g	h	i	j	k	l	m	n
Magenes and Calvi (1995)	8 brick piers in double curvature tested on a shake table, some run multiple times with varying axial load	0.74	59		None	URM2	•	•												
		0.74	68				•	•												
		0.74	152				•						•							
		0.5	62				•													
		0.5	91				•													
		0.5	149				•													
		0.5	160				•													
		0.74	91					•												
		0.74	161										•							
		0.5	91				•													
		0.5	173																	
		0.5	161										•				•		✓	
Manzourzi et. al. (1995)	4 virgin brick piers with reversed static-cyclic loading, 3 cantileved and 1 pair of piers with spandrels	1.7	150	Sophisticated finite-element modelling	Repair techniques include grout injection, pinning, and addition of rebar-filled chases	URM1						•								
		1.7	55			URM1						•								
		1.7	85			URM1						•								
		1.27	70			URM2														•
Rutherford & Chekene (1997)	Contains extensive set of research summaries of URM enhancement	na	na	Uses FEMA 273 and provides equations for enhanced walls	Grout and epoxy injection, surface coatings, adhered fabrics, shotcrete, reinforced and post-tensioned cores, infilled openings, enlarged openings, and steel bracing															
Tomasevic and Weiss (1996)	4 1/4-scale brick buildings on shake table	na	na	None	Compares effectiveness of various wall-diaphragm ties															•

[1] Behavior Mode:

a Wall-pier rocking
b Bed-joint sliding
c Bed-joint sliding at wall base
d Spandrel joint sliding
e Rocking/toe crushing
f Flexural cracking/toe crushing/bed-joint sliding
g Flexural cracking/diagonal tension
h Flexural cracking/toe crushing
i Spandrel unit cracking
j Corner damage
k Preemptive diagonal tension
l Preemptive toe crushing
m Out-of-plane flexural response
n Other: Includes complex modes and those reported as having "diagonal cracking"

4.3 Symbols for Unreinforced Masonry

Symbols used in the unreinforced masonry sections of FEMA 306 and 307 are the same as those given in Section 7.9 of FEMA 273 except for the following additions and modifications.

C Resultant compressive force in a spandrel, lb

L_{sp} Length of spandrel, in.

M_{spcr} Expected moment capacity of a cracked spandrel, lb-in.

M_{spun} Expected moment capacity of an uncracked spandrel, lb-in.

V_{spcr} Expected diagonal tension capacity of a cracked spandrel, lb

V_{spun} Expected diagonal tension capacity of an uncracked spandrel, lb

NB Number of brick wythes in a spandrel

NR Number of rows of bed joints in a spandrel

T Resultant tensile force in a spandrel, lb

V_{bjs1} Expected shear strength of wall or pier based on bed joint shear stress, including both the bond and friction components, lb

V_{bjs2} Expected shear strength of wall or pier based on bed joint shear stress, including only the friction component, lb

V_{sp} Shear imparted on the spandrel by the pier, lb

V_{dt} Expected shear strength of wall or pier based on diagonal tension using v_{me} for f'_{dt}, lb

V_{tc} Expected shear strength of wall or pier based on toe crushing using v_{me} for f'_{dt}, lb

W_w Expected weight of a wall, lb

b_{effcr} Effective length of interface for a cracked spandrel, in.

b_{effun} Effective length of interface for an uncracked spandrel, in.

b_h Height of masonry unit plus bed joint thickness, in.

b_l Length of masonry unit, in.

b_w Width of brick unit, in.

d_{sp} Depth of spandrel, in.

d_{effcr} Distance between resultant tensile and compressive forces in a cracked spandrel, in.

d_{effun} Distance between resultant tensile and compressive forces in an uncracked spandrel, in.

f'_{dt} Masonry diagonal tension strength, psi

v_{bjcr} Cracked bed joint shear stress, psi

v_{bjun} Uncracked bed joint shear stress in a spandrel, psi

v_{ccr} Cracked collar joint shear stress in a spandrel, psi

v_{cun} Uncracked collar joint shear stress in a spandrel, psi

β $=0.67$ when $L/h_{eff}<0.67$, $=L/h_{eff}$ when $0.67 \le L/h_{eff} \le 1.0$, and $= 1.0$ when $L/h_{eff}>1$

Δ_s Average slip at cracked spandrel (can be estimated as average opening width of open head joint), in.

ε Factor for estimating the bond strength of the mortar in spandrels

γ Factor for coefficient of friction in bed joint sliding equation for spandrels

η Factor to estimate average stress in uncracked spandrel. Equal to NR/2 or, for more sophistication, use $\Sigma_{i=1,NR}\,[(d_{sp}/2 - b_h(i))/(d_{sp}/2 - b_h)]$

$\lambda_{h/t}$ Factor used to estimate the loss of out-of-plane wall capacity to damaged URM walls

μ_Δ Displacement ductility demand for a component, used in FEMA 306, Section 5.3.4, and discussed in Section 6.4.2.4 of FEMA 273. Equal to the component deformation corresponding to the global target displacement, divided by the effective yield displacement of the component (which is defined in Section 6.4.1.2B of FEMA 273).

4.4 References for Unreinforced Masonry

ABK, 1981a, *Methodology for Mitigation of Seismic Hazards in Existing Unreinforced Masonry Buildings: Categorization of Buildings,* A Joint Venture of Agbabian Associates, S.B. Barnes and Associates, and Kariotis and Associates (ABK), Topical Report 01, c/o Agbabian Associates, El Segundo, California.

ABK, 1981b, *Methodology for Mitigation of Seismic Hazards in Existing Unreinforced Masonry Buildings: Diaphragm Testing*, A Joint Venture of Agbabian Associates, S.B. Barnes and Associates, and Kariotis and Associates (ABK), Topical Report 03, c/o Agbabian Associates, El Segundo, California.

ABK, 1981c, *Methodology for Mitigation of Seismic Hazards in Existing Unreinforced Masonry Buildings: Wall Testing, Out-of-Plane*, A Joint Venture of Agbabian Associates, S.B. Barnes and Associates, and Kariotis and Associates (ABK), Topical Report 04, c/o Agbabian Associates, El Segundo, California

ABK, 1984, *Methodology for Mitigation of Seismic Hazards in Existing Unreinforced Masonry Buildings: The Methodology*, A Joint Venture of Agbabian Associates, S.B. Barnes and Associates, and Kariotis and Associates (ABK), Topical Report 08, c/o Agbabian Associates, El Segundo, California.

Abrams, D.P., 1992, "Strength and Behavior of Unreinforced Masonry Elements," *Proceedings of Tenth World Conference on Earthquake Engineering*, Balkema Publishers, Rotterdam, The Netherlands, pp. 3475-3480.

Abrams, D.P., 1997, personal communication, May.

Abrams, D.P., and Epperson, G.S, 1989, "Evaluation of Shear Strength of Unreinforced Brick Walls Based on Nondestructive Measurements," *5th Canadian Masonry Symposium*, Department of Civil Engineering, University of British Columbia, Vancouver, British Columbia., Volume 2.

Abrams, D.P., and Epperson, G.S, 1989, "Testing of Brick Masonry Piers at Seventy Years", *The Life of Structures: Physical Testing*, Butterworths, London.

Abrams, D.P., and Shah, N., 1992, *Cyclic Load Testing of Unreinforced Masonry Walls,* College of Engineering, University of Illinois at Urbana, Advanced Construction Technology Center Report #92-26-10.

Adham, S.A., 1985, "Static and Dynamic Out-of-Plane Response of Brick Masonry Walls," *Proceedings of the 7th International Brick Masonry Conference*, Melbourne, Australia.

Anthoine, A., Magonette, G., and Magenes, G., 1995, "Shear-Compression Testing and Analysis of Brick Masonry Walls," *Proceedings of the 10th European Conference on Earthquake Engineering*, Duma, editor, Balkema: Rotterdam, The Netherlands.

ATC, 1997a, *NEHRP Guidelines for the Seismic Rehabilitation of Buildings*, prepared by the Applied Technology Council (ATC-33 project) for the Building Seismic Safety Council, published by the Federal Emergency Management Agency, Report No. FEMA 273, Washington, D.C.

ATC, 1997b, NEHRP *Commentary on the Guidelines for the Seismic Rehabilitation of Buildings*, prepared by the Applied Technology Council (ATC-33 project) for the Building Seismic Safety Council, published by the Federal Emergency Management Agency, Report No. FEMA 274, Washington, D.C.

BSSC, 1992, *NEHRP Handbook for the Seismic Evaluation of Existing Buildings* , prepared by the Building Seismic Safety Council for the Federal Emergency Management Agency, Report No. FEMA-178, Washington, D.C.

Calvi, G.M., Kingsley, G.R., and Magenes, G., 1996, "Testing of Masonry Structures for Seismic Assessment," *Earthquake Spectra*, Earthquake Engineering Research Institute, Oakland, California, Vol. 12, No. 1, pp. 145-162.

Calvi, G.M, and Magenes, G., 1994, "Experimental Results on Unreinforced Masonry Shear Walls Damaged and Repaired," *Proceedings of the 10th International Brick Masonry Conference*, Vol. 2, pp. 509-518.

Calvi, G.M., Magenes, G., Pavese, A., and Abrams, D.P., 1994, "Large Scale Seismic Testing of an Unreinforced Brick Masonry Building," *Proceedings of Fifth U.S. National Conference on Earthquake Engineering*, Chicago, Illinois, July 1994, pp.127-136.

City of Los Angeles, 1985, "Division 88: Earthquake Hazard Reduction in Unreinforced Masonry Buildings," *City of Los Angeles Building Code*, Los Angeles, California.

City of Los Angeles, 1991, *Seismic Reinforcement Seminar Notes*, City of Los Angeles Department of Building and Safety.

Costley, A.C., Abrams, D.P., and Calvi, G.M., 1994, "Shaking Table Testing of an Unreinforced Brick Masonry Building," *Proceedings of Fifth U.S. National Conference on Earthquake Engineering*, Chicago, Illinois, July 1994, pp.127-136.

Costley, A.C., and Abrams, D.P, 1996a, "Response of Building Systems with Rocking Piers and Flexible Diaphragms," *Worldwide Advances in Structural Concrete and Masonry, Proceedings of the Committee on Concrete and Masonry Symposium*, ASCE Structures Congress XIV, Chicago, Illinois.

Costley, A.C., and Abrams, D.P., 1996b, *Dynamic Response of Unreinforced Masonry Buildings with Flexible Diaphragms*, National Center for Earthquake Engineering Research, Technical Report NCEER-96-0001, Buffalo, New York.

Epperson, G.S., and Abrams, D.P., 1989, *Nondestructive Evaluation of Masonry Buildings,* College of Engineering, University of Illinois at Urbana, Advanced Construction Technology Center Report No. 89-26-03, Illinois.

Epperson, G.S., and Abrams, D.P., 1992, "Evaluating Lateral Strength of Existing Unreinforced Brick Masonry Piers in the Laboratory," *Journal of The Masonry Society*, Boulder, Colorado, Vol. 10, No. 2, pp. 86-93.

Feng, Jianguo, 1986, "The Seismic Shear Strength of Masonry Wall," *Proceedings of the US-PRC Joint Workshop on Seismic Resistance of Masonry Structures*, State Seismological Bureau, PRC and National Science Foundation, USA, Harbin, China.

Gambarotta, L. and Lagomarsino, S., 1996, "A Finite Element Model for the Evaluation and Rehabilitation of Brick Masonry Shear Walls," *Worldwide Advances in Structural Concrete and Masonry, Proceedings of the Committee on Concrete and Masonry Symposium*, ASCE Structures Congress XIV, Chicago, Illinois.

ICBO, 1994, *Uniform Code for Building Conservation*, International Conference of Building Officials, Whittier, California.

Kariotis, J.C., 1986, "Rule of General Application - Basic Theory," *Earthquake Hazard Mitigation of Unreinforced Pre-1933 Masonry Buildings*, Structural Engineers Association of Southern California, Los Angeles, California.

Kariotis, J.C., Ewing, R.D., and Johnson, A.W., 1985a, "Predictions of Stability for Unreinforced Brick Masonry Walls Shaken by Earthquakes," *Proceedings of the 7th International Brick Masonry Conference*, Melbourne, Australia.

Kariotis, J.C., Ewing, R.D., and Johnson, A.W., 1985b, "Strength Determination and Shear Failure Modes of Unreinforced Brick Masonry with Low Strength Mortar," *Proceedings of the 7th International Brick Masonry Conference*, Melbourne, Australia.

Kariotis, J.C., Ewing, R.D., and Johnson, A.W., 1985c, "Methodology for Mitigation of Earthquake Hazards in Unreinforced Brick Masonry Buildings," *Proceedings of the 7th International Brick Masonry Conference*, Melbourne, Australia.

Kingsley, G.R., 1995, "Evaluation and Retrofit of Unreinforced Masonry Buildings," *Proceedings of the Third National Concrete and Masonry Engineering Conference*, San Francisco, California, pp. 709-728.

Kingsley, G.R., Magenes, G., and Calvi, G.M., 1996, "Measured Seismic Behavior of a Two-Story Masonry Building," *Worldwide Advances in Structural Concrete and Masonry, Proceedings of the Committee on Concrete and Masonry Symposium*, ASCE Structures Congress XIV, Chicago, Illinois.

Magenes, G., 1997, personal communication, May.

Magenes, G., and Calvi, G.M., 1992, "Cyclic Behavior of Brick Masonry Walls," *Proceedings of the Tenth World Conference*, Balkema: Rotterdam, The Netherlands.

Magenes, G. and Calvi, G.M., 1995, "Shaking Table Tests on Brick Masonry Walls," *10th European Conference on Earthquake Engineering*, Duma, editor, Balkema: Rotterdam, The Netherlands.

Manzouri, T., Shing, P.B., Amadei, B., Schuller, M., and Atkinson, R., 1995, *Repair and Retrofit of Unreinforced Masonry Walls: Experimental Evaluation and Finite Element Analysis*, Department of Civil, Environmental and Architectural Engineering, University of Colorado: Boulder, Colorado, Report CU/SR-95/2.

Manzouri, T., Shing, P.B., Amadei, B., 1996, "Analysis of Masonry Structures with Elastic/Viscoplastic Models, 1996," *Worldwide Advances in Structural Concrete and Masonry, Proceedings of the Committee on Concrete and Masonry Symposium*, ASCE Structures Congress XIV, Chicago, Illinois.

Priestley, M.J.N, 1985, "Seismic Behavior of Unreinforced Masonry Walls," *Bulletin of the New*

Zealand National Society for Earthquake Engineering, Vol. 18, No. 2.

Proposal for Change G7-7, 1997, proposal to change the in-plane URM wall provisions of FEMA 273 (1996).

Rutherford & Chekene, 1990, *Seismic Retrofitting Alternatives for San Francisco's Unreinforced Masonry Buildings: Estimates of Construction Cost and Seismic Damage for the San Francisco Department of City Planning*, Rutherford and Chekene Consulting Engineers: San Francisco, California.

Rutherford & Chekene, 1997, *Development of Procedures to Enhance the Performance of Rehabilitated Buildings*, prepared by Rutherford & Chekene Consulting Engineers, published by the National Institute of Standards and Technology as Reports NIST GCR 97-724-1 and 97-724-2.

SEAOC/CALBO, 1990, "Commentary on the SEAOC-CALBO Unreinforced Masonry Building Seismic Strengthening Provisions," *Evaluation and Strengthening of Unreinforced Masonry Buildings*, 1990 Fall Seminar, Structural Engineers Association of Northern California, San Francisco, California.

SEAOSC, 1986, "RGA (Rule of General Application) Unreinforced Masonry Bearing Wall Buildings (Alternate Design to Division 88)," *Earthquake Hazard Mitigation of Unreinforced Pre-1933 Masonry Buildings*, Structural Engineers Association of Southern California: Los Angeles, California.

Sheppard, P.F. and Tercelj, S., 1985, "Determination of the Seismic Resistance of an Historical Brick Masonry Building by Laboratory Tests of Cut-Out Wall Elements," *Proceedings of the 7th International Brick Masonry Conference*, Melbourne, Australia.

Tena-Colunga, A., and Abrams, D.P., 1992, *Response of an Unreinforced Masonry Building During the Loma Prieta Earthquake*, Department of Civil Engineering, University of Illinois at Urbana-Champaign, Structural Research Series No. 576.

Tomazevic, M., and Anicic, 1989, "Research, Technology and Practice in Evaluating, Strengthening, and Retrofitting Masonry Buildings: Some Yugoslavian Experiences," *Proceedings of the International Seminar on Evaluating, Strengthening and Retrofitting Masonry Buildings*, The Masonry Society: Boulder, Colorado.

Tomazevic, M., Lutman, M., and Weiss, P., 1996, "Seismic Upgrading of Old Brick-Masonry Urban Houses: Tying of Walls with Steel Ties," *Earthquake Spectra,* EERI: Oakland, California, Volume 12, No. 3.

Tomazevic, M., and Weiss, P., 1990, "A Rational, Experimentally Based Method for the Verification of Earthquake Resistance of Masonry Buildings," *Proceedings of the Fourth U.S. National Conference on Earthquake Engineering*, EERI: Oakland, California.

Turnsek, V., and Sheppard, P., 1980, "The Shear and Flexural Resistance of Masonry Walls," *Proceedings of the International Research Conference on Earthquake Engineering*, Skopje, Yugoslavia.

Willsea, F.J., 1990, "SEAOC/CALBO Recommended Provisions", *Evaluation and Strengthening of Unreinforced Masonry Buildings*, 1990 Fall Seminar, Structural Engineers Association of Northern California, San Francisco, California.

Xu, W., and Abrams, D.P., 1992, *Evaluation of Lateral Strength and Deflection for Cracked Unreinforced Masonry Walls*, U.S. Army Research Office, Report ADA 264-160, Triangle Park, North Carolina.

Zsutty, T.C., 1990, "Applying Special Procedures", *Evaluation and Strengthening of Unreinforced Masonry Buildings*, 1990 Fall Seminar, Structural Engineers Association of Northern California, San Francisco, California.

5. Infilled Frames

5.1 Commentary And Discussion

There is a wealth of experimental data reported in the literature on infilled frames. Unfortunately, only a limited amount of the research has been performed under *cyclic* loading and conducted on specimens that reflect U.S. construction practice. For these test results, it is evident that infilled frames can possess stable hysteresis loops and continue to carry substantial lateral loads at significant interstory drifts. This is true in spite of the highly damaged appearance and even complete loss of some of the masonry units within an infill panel.

Most experimental results on infilled-frame systems show a mixture of behavior modes that take place at various stages of loading. At low interstory drift levels (0.2% - 0.4%), corner crushing and some diagonal cracking in the panel tend to occur first. This is followed by frame yielding (0.5% - 1.0% interstory drift) and possible bed-joint sliding. As the drift amplitude increases beyond about 1%, cracking in the infill panel becomes more extensive, along with further frame damage. The frame damage takes the form of cracking, crushing, and spalling of concrete in the case of reinforced concrete frames or prying damage to bolted semi-rigid connections in steel frames. The coexistence of several behavior modes makes it difficult to determine what λ-factors should be used for quantitative strength and deformation analysis. Therefore, it is necessary to resort to individual component tests to assess λ-values. The results of experiments conducted by Aycardi et al. (1994) are illustrative of the performance of nonductile reinforced concrete frames. These tests give results for each of the failure modes (except column shear).

In the experimental studies on infilled frames by Mander et al. (1993a,b), steel frames were used and were instrumented with numerous strain gauges so the behavior of the frame could be uncoupled from the behavior of the infill panel. It was, therefore, possible to plot the net lateral load-drift capacity of the brick masonry infill panel. These results were helpful in identifying the λ-factors for corner crushing, diagonal cracking and general shear-failure behavior modes for masonry. The bed-joint sliding behavior mode tends to occur mostly in steel frames with ungrouted/ unreinforced masonry infill with low panel height-to-length aspect ratios. The experimental results of Gergely et al. (1994) were useful for identifying λ-factors for this behavior mode.

When investigating the out-of-plane behavior of infilled frame panels, it is difficult to enforce a complete failure, as evidenced by recent tests by Angel and Abrams (1994). It should be noted that these investigators first loaded their specimens in-plane before conducting their out-of-plane tests. Results of this study indicate that lateral strength capacity is generally well in excess of 200 psf. Thus, it is unlikely that out-of-plane failure should occur for normal infill height-to-thickness aspect ratios. These results suggest that if an out-of-plane failure is observed in the field, then some other (in-plane) behavior mode has contributed to the failure of the infill.

Dealing with infill panels with openings is difficult due to the many potential types of openings that may occur in practice. Evidently, when openings are present, the strength capacity is bounded by that of bare frame (lower bound) and that of a system with solid infill panels (upper bound). Although these results are derived from monotonic tests, they suggest that the deformation capacity is not impaired if openings exist.

5.1.1 Development of λ-Factors for Component Guides

The Component Damage Classification Guides and component modification factors (λ-factors) for infilled frames were based on an extensive review of research in the area of both nonductile reinforced concrete frames, as well as masonry structures. The principal references used in this work are listed in the tabular bibliography presented in Section 5.2. For each component behavior mode, three types of λ-factors are used: stiffness reduction factors (λ_K), strength reduction factor (λ_Q) and a displacement reduction factor (λ_D). Description of how each of these λ-factors were derived from experimental evidence and theoretical considerations is presented in what follows.

5.1.2 Development of Stiffness Deterioration—λ_K

As the displacement ductility of a member progressively increases, the member also softens. Even though the strength may be largely maintained at a nominal yield level, softening is manifest in the form of stiffness reduction. The degree of softening is generally related to the maximum displacement ductility the member has previously achieved.

There are several analytical models that can be used to give guidance on how one can assess the degree of softening in an element. For example, Chang and Mander (1994) describe several computational hysteretic models calibrated for reinforced concrete components. Utilizing their information obtained from a calibrated modified Takeda model, the λ_K-factor for stiffness reduction can be related by the following relationship:

$$\lambda_K = \left(\frac{\Delta_{max}}{\Delta_y}\right)^{-\alpha} = (\mu_\Delta)^{-\alpha} \qquad (5\text{-}1)$$

where Δ_{max} = maximum displacement in the displacement history, Δ_y = yield displacement, μ_Δ = displacement ductility factor, and α = an experimentally calibrated factor that is material- or specimen-dependent.

Strictly, α should be established on a component-by-component basis. However, for reinforced concrete components there is a range of values from $\alpha = 0.25$ to $\alpha = 1$ that may be applicable, $\alpha = 0.5$ being typical for most specimens. Well detailed members tend to have low α values, whereas higher α values are common for poorly detailed members. Although specific research on infill panels is not developed to the same extent, it seems reasonable that similar trends would be found for these components.

5.1.3 The Determination of λ_Q for Strength Deterioration

In structural elements not specifically designed for seismic resistance, there is generally a lack of adequate transverse reinforcement necessary to provide adequate confinement and shear resistance. As a result, under reversed cyclic loading the strength of such elements deteriorates progressively. Furthermore, if the non-seismically designed frame elements have inadequate anchorage for the reinforcing steel, there can be a gradual loss in strength and then a sudden drop in strength when the anchorage zone or lap splice zone fails. An energy approach can be used to assess the loss of strength in a reinforced concrete column or beam element where inadequate transverse reinforcement is found. The energy-based approach advanced by Mander and Dutta (1997) has been used in developing this process. A summary of the underlying theoretical concepts is given below.

Assuming the moment capacity contributed by the concrete is gradually consumed by the propagating level of damage, then at the end of the i-th cycle it can be shown that the reduced strength $F_i = \lambda_Q F_n$ can be evaluated through

$$\lambda_Q = \frac{F_i}{F_n} = 1 - \frac{M_c}{M_n}\Sigma D_{ci} = 1 - \frac{M_c}{M_n}\frac{\Sigma\theta_{pi}}{\Sigma\theta_{PC}} \qquad (5\text{-}2)$$

in which ΣD_{ci} = accumulated damage, $\Sigma\theta_{ci}$ = cumulative plastic drift, M_n = nominal moment capacity, M_c = the moment generated by the eccentric concrete stress block and $\Sigma\theta_{PC}$ = cumulative plastic rotation capacity considering concrete fatigue alone. Using energy concepts where it is assumed that the finite energy reserve of an unconfined concrete section is gradually consumed to resist the concrete compression force, a work expression can be formulated as

$$EWD = IWD \qquad (5\text{-}3)$$

where EWD = external work done on the section by the concrete compression force defined by the left hand side of the equation below, and IWD = internal work or energy absorption capacity of the section defined by the right hand side of the following equation

$$C_c \times \left(\phi_p \frac{c}{2}\right) \times 2N_c = A_g \int_0^{\varepsilon_{cu}} f_c \, d\varepsilon \qquad (5\text{-}4)$$

in which C_c = concrete compression force, ϕ_p = plastic curvature, c = neutral axis depth, $2N_c$ = total number of reversals and A_g = gross area of the concrete section. The integral in the above expression actually denotes the finite energy capacity of an unconfined concrete section which in lieu of a more precise analysis, can be approximated as $0.008\, f_c'$. Note also that the term in brackets in the above equation denotes the plastic strain at the location of the concrete compression force.

Assuming that in a cantilever column the plastic rotation is entirely confined to the plastic hinge zone (of length L_p), using the moment-area theorem and rearranging terms in the above equation, it is possible to solve for the cumulative plastic drift capacity as

$$\Sigma\theta_{PC} = \frac{0.016\left(\frac{L_p}{D}\right)}{\left(\frac{C_c}{f_c' A_g}\right)\left(\frac{c}{D}\right)} \qquad (5\text{-}5)$$

where $\Sigma\theta_P = 2N_c\theta_p$ is the *cumulative plastic drift* defined as the sum of all positive and negative drift amplitudes up to a given stage of loading; and D = overall depth/diameter of the column.

The concrete damage model described so far is generally applicable to beam and/or column elements with adequate bonding between the longitudinal reinforcement and the surrounding concrete. Thus following Equation 5-2, the concrete strength continues to decay until the moment capacity of the eccentric concrete block is fully exhausted. At this point the residual moment capacity entirely consists of the steel contribution. This is schematically portrayed in Figure 5-1a. However, more often than not, older buildings possess lap splice zones at their column bases. Such splices are not always equipped with adequate lap length to ensure proper development of bond strength. The lap splice thus becomes the weak point in the column which shows a drastic reduction in the strength almost immediately following the lap splice failure. This is depicted in Figure 5-1b where the bond failure in the lap splice is assumed to occur over one complete cycle. The residual strength immediately after F_i is determined by the extent of confinement around the lap splice, if any. Subsequently the lateral strength is entirely dependent on the performance of pure concrete which continues to decay following the same Equation 5-2 until the residual rocking strength F_r is obtained.

This theory has been validated with experimental results as shown in Figures 5-1c and 5-1d. In Figure 5-1c, the lateral strength envelope is compared with test results with instances of unconfined concrete failure only. In Figure 5-1d, the strength envelope is plotted for column specimen with a clear indication of lap splice failure. Satisfactory agreement between theory and experiment is observed.

Therefore, with the mechanism of failure and the progression of strength deterioration clearly identified and quantified, it is possible to assess, analytically, λ_Q factors for reinforced concrete elements with specific detailing. The research has not been developed to the same extent for infill panels, although an examination of test results indicates that similar trends are present.

5.1.4 Development of λ_D—Reduction in Displacement Capability

The reduction in displacement capability is more difficult to ascertain from traditional, quasi-static, reversed-cyclic-loading, laboratory tests on members. Generally such tests are conducted using two cycles at each ductility factor (or drift angle percentages) of ±1, ±2, ±6... until failure occurs. The reduction in displacement capacity depends on the severity of the previous loading history—that is, the amount of energy absorbed with respect to the total energy absorption capacity. Strictly this cannot be ascertained without resorting to fatigue type of testing.

Mander et al. (1994, 1995) and Mander and Dutta (1997) have shown that the displacement capability of structural concrete and steel elements follows a well-known Manson-Coffin fatigue relationship that can be written in displacement ductility terms as follows:

$$\mu_\Delta = \mu_m N_f^c \tag{5-6}$$

where N_f = number of equi-amplitude cycles required to produce failure at ductility amplitude μ_Δ; μ_m = monotonic ductility capacity; and c = fatigue exponent. Typical values of the latter are c = -1/3 for steel failure and c = -1/2 for nonductile reinforced concrete.

The above equation can be written in terms of a "damage fraction" ($D = n_d / N_f$) that can be sustained for n_d cycles of loading in the damaging earthquake:

$$D = \frac{n_d}{N_f} = n_d \left(\frac{\mu_\Delta^d}{\mu_m} \right)^{-\frac{1}{c}} \tag{5-7}$$

The remaining fatigue life then is (1 - D). The displacement-based λ_D-factor can thus be defined as

$$\lambda_D = \frac{\mu_\Delta^r}{\mu_m} = (1-D)^{-c} = \left[\frac{1}{n_d} - \left(\frac{\mu_\Delta^d}{\mu_m} \right)^{-\frac{1}{c}} \right]^{-c} \tag{5-8}$$

In the above two equations superscripts d and r refer to the damaging earthquake and remaining life, respectively.

Thus for nonductile reinforced concrete failure taking c = -1/2 gives

$$\lambda_D = \sqrt{\frac{1}{n_d} - \left(\frac{\mu_\Delta}{\mu_m} \right)^2} \tag{5-9}$$

For frictional or sliding behavior modes such as lap-splice failure of masonry infill panels, there is no limit to the displacement capability. Therefore, for these two behavior modes, $\lambda_D = 1$ at all times.

Although specific research on infill components is less developed, it is reasonable to assume that similar trends would be observed.

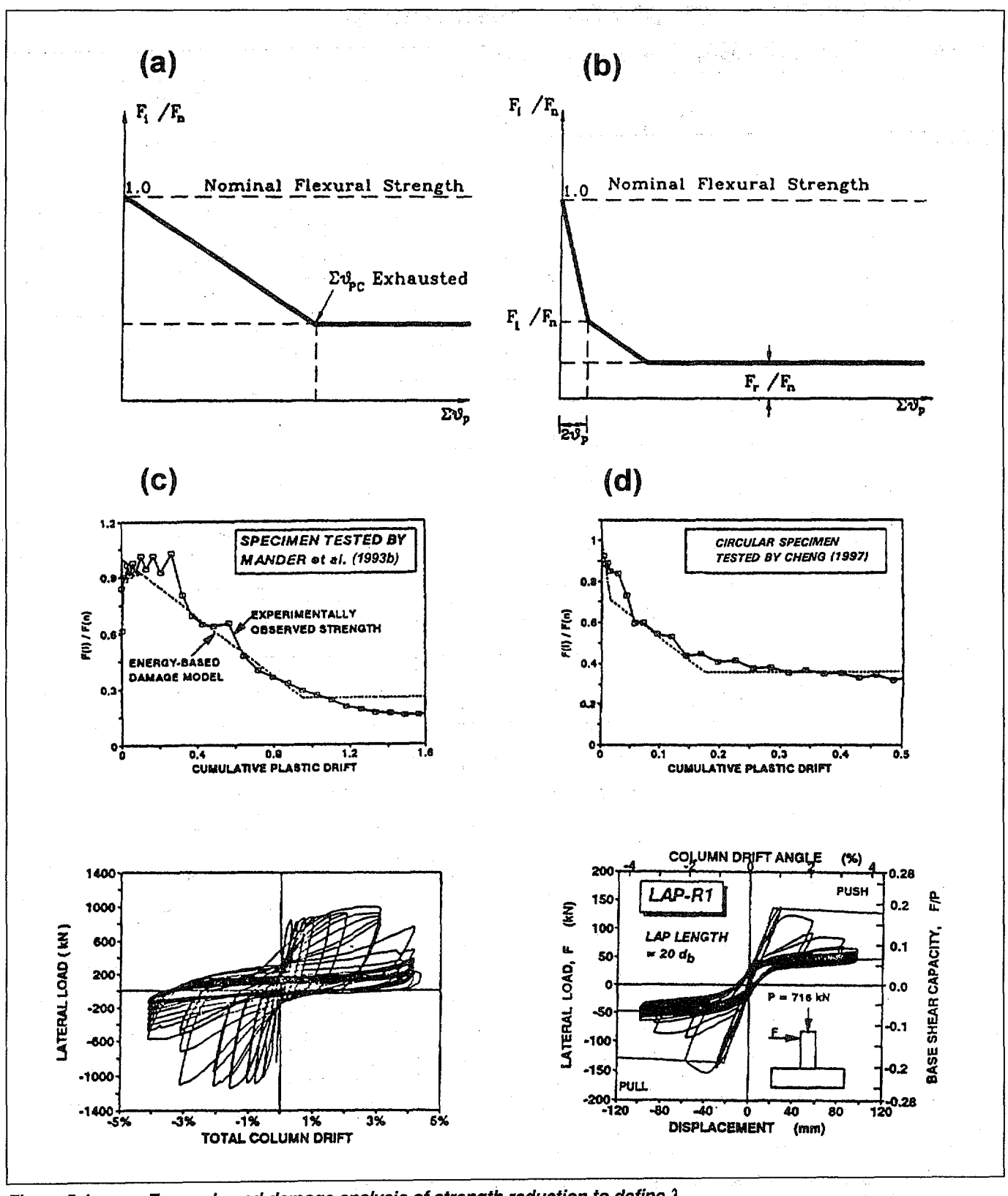

Figure 5-1 *Energy-based damage analysis of strength reduction to define λ_Q*

5.2 Tabular Bibliography for Infilled Frames

Table 5-1 Tabular Bibliography for Infilled Frames

References	Categories*									Remarks
	A	B	C	D	E	F	G	H	I	
Abrams, 1994								✓		
Al-Chaar et al., 1994								✓		
Aycardi et al., 1992									✓	Nonductile concrete frame performance
Aycardi et al., 1994									✓	Nonductile concrete frame performance
Axely and Bertero, 1979	✓							✓		Experiments on multistory frames
Benjamin and Williams, 1958		✓				✓		✓		Classic brick infilled steel frame experiments
Bertero and Brokken, 1983		✓	✓					✓		
Bracci et al., 1995									✓	Emphasis on nonductile frame performance
Brokken and Bertero, 1981								✓		
Coul, 1966						✓				
Crisafully et al., 1995		✓								
Dawe and McBride, 1985		✓				✓		✓		Steel frame with pierced brick infills
Dhanasekar et al., 1985		✓								
Flanagan and Bennett, 1994								✓		Steel frame-clay tile infill
Focardi and Manzini, 1984		✓								
Gergely et al., 1993				✓						Steel frame-clay tile infill
Hamburger and Chakradeo, 1993		✓								
Hill, 1994		✓								
Holmes, 1961						✓				
Kadir, 1974	✓	✓	✓					✓		
Kahn and Hanson, 1977				✓						
Klingner and Bertero, 1976								✓		Multistory infilled frame performance
Klingner and Bertero, 1978								✓		Multistory infilled frame performance
Kodur et al., 1995		✓								
Liauw and Lee, 1977	✓	✓				✓				
Liauw, 1979	✓							✓		Multistory steel frames-concrete infills
Liauw and Kwan, 1983a	✓							✓		Steel frame-concrete infill plastic failure modes
Liauw and Kwan, 1983b	✓	✓								Plastic-strength theory
Maghaddam and Dowling, 1987	✓	✓	✓	✓	✓	✓	✓	✓		General treatise on infilled-frame behavior
Mainstone and Weeks, 1970			✓					✓		

*A = Modes of Failure, B = Strength, C = Stiffness, D = Ductility, E = Hysteretic Performance, F = Openings, G = Repairs, H = Experimental Performance of Infilled Frames, I = Steel and Concrete Frame Behavior

Table 5-1 Tabular Bibliography for Infilled Frames (continued)

References	Categories*									Remarks
	A	B	C	D	E	F	G	H	I	
Mainstone, 1971		✓	✓	✓				✓		Classical work on strut methods of analysis
Mallick and Garg, 1971						✓				
Mander and Nair, 1993a	✓				✓			✓		Steel frames-brick infills under cyclic loading
Mander et al., 1993b	✓				✓		✓	✓		Effect of ferrocement repairs
Mander et al., 1994									✓	Low-cycle fatigue of steel frame connections
Mander et al., 1995									✓	
Mehrabi et al., 1996								✓		Concrete frame-block infill experiments
Mosalam et al., 1994				✓						Steel frame brick infills finite-element analysis
Parducci and Mezzi, 1980		✓			✓					
Paulay and Priestley, 1992	✓	✓	✓						✓	Classical text on design
Polyakov, 1956	✓	✓	✓					✓		Earliest work on infills translated from Russian
Prawel and Lee, 1994							✓			Ferrocement repairs for masonry
Priestley, 1996									✓	Most recent work on RC in shear
Priestley et al., 1996									✓	Most recent work on RC in shear
Reinhorn et al., 1995					✓					Advanced analysis methods for infills
Riddington and Stafford-Smith, 1977	✓	✓	✓							Early work on strut methods of analysis
Riddington, 1984		✓						✓		Emphasis on gap effects
Sachanski, 1960								✓		
Saneinejad and Hobbs, 1995	✓	✓	✓							Most up-to-date reference on analysis methods
Shapiro et al., 1994								✓		
Shen and Zhu, 1994								✓		Pseudo-dynamic tests
Shing et al., 1994								✓		
Stafford-Smith, 1966		✓	✓					✓		Early experimental work
Stafford-Smith and Carter, 1969			✓							Pioneering work on analysis using strut methods
Thomas, 1953								✓		Emphasis on brick work
Wood, 1978	✓	✓								Early work on plastic methods of analysis
Yoshimura and Kikuchi, 1995								✓		
Zarnic and Tomazevic, 1984				✓	✓			✓		
Zarnic and Tomazevic, 1985a				✓	✓			✓		
Zarnic and Tomazevic, 1985b		✓		✓	✓			✓		

*A = Modes of Failure, B = Strength, C = Stiffness, D = Ductility, E = Hysteretic Performance, F = Openings, G = Repairs, H = Experimental Performance of Infilled Frames, I = Steel and Concrete Frame Behavior

5.3 References for Infilled Frames

This list contains references from the infilled frames chapters of both FEMA 306 and 307.

Abrams, D.P. (Ed.), 1994, *Proceedings of the NCEER Workshop on Seismic Response of Masonry Infills*, National Center for Earthquake Engineering Research, Technical Report NCEER-94-0004.

Al-Chaar, G., Angel, R. and Abrams, D., 1994, "Dynamic testing of unreinforced brick masonry infills," *Proc. of the Structures Congress '94*, Atlanta, Georgia., ASCE, 1: 791-796.

Angel R., and Abrams, D.P., 1994, "Out-Of-Plane Strength evaluation of URM infill Panels," *Proceedings of the NCEER Workshop on Seismic Response of Masonry Infills,* D.P. Abrams editor, NCEER Technical Report NCEER-94-0004.

Aycardi, L.E., Mander, J.B., and Reinhorn, A.M., 1992, *Seismic Resistance of RC Frame Structures Designed only for Gravity Loads, Part II: Experimental Performance of Subassemblages*, National Center for Earthquake Engineering Research, Technical Report NCEER-92-0028.

Aycardi, L.E., Mander, J.B., and Reinhorn, A.M., 1994, "Seismic resistance of reinforced concrete frame structures designed only for gravity loads: Experimental performance of subassemblages", *ACI Structural Journal,* (91)5: 552-563.

Axely, J.W. and Bertero, V.V., 1979, "Infill panels: their influence on seismic response of buildings," Earthquake Eng. Research Center, University of California at Berkeley, Report No. EERC 79-28.

Benjamin, J.R., and Williams, H.A., 1958, "The behavior of one-story shear walls," *Proc. ASCE,* ST. 4, Paper 1723: 30.

Bertero, V.V. and Brokken, S.T., 1983, "Infills in seismic resistant building," *Proc. ASCE,* 109(6).

Bracci, J.M., Reinhorn, A.M., and Mander, J.B., 1995, "Seismic resistance of reinforced concrete frame structures designed for gravity loads: Performance of structural system", *ACI Structural Journal,* (92)5: 597-609.

Brokken, S.T., and Bertero, V.V., 1981, *Studies on effects of infills in seismic resistance R/C construction*, Earthquake Engineering Research Centre, University of California at Berkeley, Report No. EERC 81-12.

Chang, G. A., and Mander, J.B.,1994, *Seismic Energy Based Fatigue Damage Analysis of Bridge Columns: Part I - Evaluation of Seismic Capacity,* Technical Report NCEER-94-0006, and *Part II - Evaluation of Seismic Demand,* Technical Report NCEER-94-0013, National Center for Earthquake Engineering Research, State University of New York at Buffalo.

Cheng, C.T., 1997, *New Paradigms for the Seismic Design and Retrofit of Bridge Piers*, Ph.D. Dissertation, Science and Engineering Library, State University of New York at Buffalo, Buffalo, New York.

Chrysostomou, C.Z., Gergely, P, and Abel, J.F., 1988, *Preliminary Studies of the Effect of Degrading Infill Walls on the Nonlinear Seismic Response of Steel Frames*, National Center for Earthquake Engineering Research, Technical Report NCEER-88-0046.

Coul, A., 1966, "The influence of concrete infilling on the strength and stiffness of steel frames," *Indian Concrete Journal.*

Crisafulli, F.J., Carr, A.J., and Park, R., 1995, "Shear Strength of Unreinforced Masonry Panels," *Proceedings of the Pacific Conference on Earthquake Engineering*; Melbourne, Australia, Parkville, Victoria, 3: 77-86.

Dawe, J.L. and McBride, R.T., 1985, "Experimental investigation of the shear resistance of masonry panels in steel frames," *Proceedings of the 7th Brick Masonry Conf.*, Melbourne, Australia.

Dawe, J.L. and Young, T.C., 1985, "An investigation of factors influencing the behavior of masonry infill in steel frames subjected to in-plane shear," *Proceedings of the 7th International. Brick Masonry Conference*, Melbourne, Australia.

Dhanasekar, K., Page, A.W., and Kleeman, P.W., 1985, "The behavior of brick masonry under biaxial stress with particular reference to infilled frames," *Proceedings of the 7th International. Brick Masonry Conference*, Melbourne, Australia.

Durrani, A.J., and Luo, Y.H., 1994, "Seismic Retrofit of Flat-Slab Buildings with Masonry Infills," in *Proceedings of the NCEER Workshop on Seismic Response of Masonry Infills*, D.P. Abrams editor, National Center for Earthquake Engineering Research, Technical Report NCEER-94-0004.

Flanagan, R.D. and Bennett, R.M., 1994, "Uniform Lateral Load Capacity of Infilled Frames," *Proceed-*

ings of the Structures Congress '94, Atlanta, Georgia, ASCE, 1: 785-790.

Focardi, F. and Manzini, E., 1984, "Diagonal tension tests on reinforced and non-reinforced brick panels," *Proceedings of the 8th World Conference on Earthquake Engineering*, San Francisco, California, VI: 839-846.

Freeman S. A., 1994 "The Oakland Experience During Loma Prieta - Case Histories," *Proceedings of the NCEER Workshop on Seismic Response of Masonry Infills*, D.P. Abrams editor, National Center for Earthquake Engineering Research, Technical Report NCEER-94-0004.

Gergely, P., White, R.N., and Mosalam, K.M., 1994, "Evaluation and Modeling of Infilled Frames," *Proceedings of the NCEER Workshop on Seismic Response of Masonry Infills*, D.P. Abrams editor, National Center for Earthquake Engineering Research, Technical Report NCEER-94-0004, pp. 1-51 to 1-56.

Gergely, P., White, R.N., Zawilinski, D., and Mosalam, K.M., 1993, "The Interaction of Masonry Infill and Steel or Concrete Frames," *Proceedings of the 1993 National Earthquake Conference, Earthquake Hazard Reduction in the Central and Eastern United States: A Time for Examination and Action*; Memphis, Tennessee, II: 183-191.

Hamburger, R.O. and Chakradeo, A.S., 1993, "Methodology for seismic capacity evaluation of steel-frame buildings with infill unreinforced masonry," *Proceedings of the 1993 National Earthquake Conference, Earthquake Hazard Reduction in the Central and Eastern United States: A Time for Examination and Action*; Memphis, Tennessee, II: 173-182.

Hill, James A., 1994, "Lateral Response of Unreinforced Masonry Infill Frame," *Proceedings of the Eleventh Conference* (formerly Electronic Computation Conference) held in conjunction with ASCE Structures Congress '94 and International Symposium '94, Atlanta, Georgia, pp. 77-83.

Holmes, M., 1961, "Steel frames with brickwork and concrete infilling," *Proceedings of the Institute of Civil Engineers*, 19: 473.

Kadir, M.R.A., 1974, *The structural behavior of masonry infill panels in framed structures*, Ph.D. thesis, University of Edinburgh.

Kahn, L.F. and Hanson, R.D., 1977, "Reinforced concrete shear walls for a seismic strengthening," *Proceedings of the 6th World Conf. on Earthquake Engineering*, New Delhi, India, III: 2499-2504.

Klingner, R.E. and Bertero, V.V., 1976, *Infilled frames in earthquake resistant construction*, Earthquake Engineering Research Centre, University of California at Berkeley, Report No. EERC 76-32.

Klingner, R.E. and Bertero, V.V., 1978, "Earthquake resistance of infilled frames," *Journal of the Structural Division, Proc. ASCE*, (104)6.

Kodur, V.K.R., Erki, M.A., and Quenneville, J.H.P., 1995, "Seismic design and analysis of masonry-infilled frames," *Journal of Civil Engineering*, 22: 576-587.

Liauw, T.C. and Lee, S.W., 1977, "On the behavior and the analysis of multi-story infilled frames subjected to lateral loading," *Proceedings of the Institute of Civil Engineers*, 63: 641-656.

Liauw, T.C., 1979, "Tests on multi-storey infilled frames subject to dynamic lateral loading," *ACI Journal*, (76)4: 551-563.

Liauw, T.C. and Kwan, K.H., 1983a, "Plastic theory of infilled frames with finite interface shear strength," *Proceedings of the Institute of Civil Engineers*, (2)75: 707-723.

Liauw, T.C. and Kwan, K.H., 1983b, "Plastic theory of non-integral infilled frames," *Proceedings of the Institute of Civil Engineers*, (2)75: 379-396.

Maghaddam, H.A. and Dowling, P.J., 1987, *The State of the Art in Infilled Frames*, Civil Engineering Department, Imperial College, ESEE Research Report No. 87-2, London.

Mainstone, R.J. and Weeks, G.A., 1970, "The influence of bounding frame on the racking stiffness and strength of brick walls," *2nd International Brick Masonry Conference.*

Mainstone, R.J., 1971, "On the stiffness and strength of infilled frames," *Proceedings of the Institute of Civil Engineers* Sup., pp. 57-90.

Mallick, D.V. and Garg, R.P., 1971, "Effect of openings on the lateral stiffness of infilled frames," *Proceedings of the Institute of Civil Engineers*, 49: 193-209.

Mander J. B., Aycardi, L.E., and Kim, D-K, 1994, "Physical and Analytical Modeling of Brick Infilled Steel Frames," *Proceedings of the NCEER Workshop on Seismic Response of Masonry Infills*, D.P. Abrams editor, National Center for Earthquake Engineering Research, Technical Report NCEER-94-0004.

Mander, J.B., Chen, S.S., and Pekcan, G., 1994, "Low-cycle fatigue behavior of semi-rigid top-and-seat angle connections", *AISC Engineering Journal*, (31)3: 111-122.

Mander, J.B., and Dutta, A., 1997, "How Can Energy Based Seismic Design Be Accommodated In Seismic Mapping," *Proceedings of the FHWA/NCEER Workshop on the National Representation of Seismic Ground Motion for New and Existing Highway Facilities, Technical Report,* National Center for Earthquake Engineering Research, NCEER-97-0010, pp 95-114.

Mander, J.B., and Nair, B., 1993a, "Seismic Resistance of Brick-Infilled Steel Frames With and Without Retrofit," *The Masonry Society Journal*, 12(2): 24-37.

Mander, J.B., Nair, B., Wojtkowski, K., and Ma, J., 1993b, *An Experimental Study on the Seismic Performance of Brick Infilled Steel Frames*, National Center for Earthquake Engineering Research, Technical Report NCEER-93-0001.

Mander, J.B., Pekcan, G., and Chen, S.S., 1995, "Low-cycle variable amplitude fatigue modeling of top-and-seat angle connections," *AISC Engineering Journal*, American Institute of Steel Construction, (32)2: 54-62.

Mander, J.B., Waheed, S.M., Chaudhary, M.T.A., and Chen, S.S., 1993, *Seismic Performance of Shear-Critical Reinforced Concrete Bridge Piers,* National Center for Earthquake Engineering Research, Technical Report NCEER-93-0010.

Mehrabi, A.B., Shing, P.B., Schuller, M.P. and Noland J.L., 1996, "Experimental evaluation of masonry-infilled RC frames," *Journal of Structural Engineering.*

Mosalam, K.M., Gergely, P., and White, R., 1994, "Performance and Analysis of Frames with "URM" Infills," *Proceedings of the Eleventh Conference* (formerly Electronic Computation Conference) held in conjunction with ASCE Structures Congress '94 and International Symposium '94, Atlanta, Georgia, pp. 57-66.

Parducci, A. and Mezzi, M., 1980, "Repeated horizontal displacement of infilled frames having different stiffness and connection systems--Experimental analysis", *Proceedings of the 7th World Conference on Earthquake Engineering*, Istanbul, Turkey, 7: 193-196.

Paulay, T. and Priestley, M.J.N., 1992, *Seismic Design of Reinforced Concrete and Masonry Buildings*, John Wiley & Sons, New York.

Polyakov, S.V., 1956, *Masonry in framed buildings*, pub. by Gosudarstvennoe Izdatelstvo po Stroitelstvu I Arkhitekture (Translation into English by G.L.Cairns).

Prawel, S.P. and Lee, H.H., 1994, "Research on the Seismic Performance of Repaired URM Walls," *Proc. of the US-Italy Workshop on Guidelines for Seismic Evaluation and Rehabilitation of Unreinforced Masonry Buildings*, Department of Structural Mechanics, University of Pavia, Italy, June 22-24, Abrams, D.P. et al. (eds.) National Center for Earthquake Engineering Research, SUNY at Buffalo, pp. 3-17 - 3-25.

Priestley, M.J.N., 1996, "Displacement-based seismic assessment of existing reinforced concrete buildings," *Bulletin of the New Zealand National Soc. for Earthquake Eng.*, (29)4: 256-271.

Priestley, M.J.N., Seible, F., and Calvi, G.M., 1996, *Seismic Design and Retrofit of Bridges*, John Wiley & Sons, New York, 686 pp.

Reinhorn, A.M., Madan, A., Valles, R.E., Reichmann, Y., and Mander, J.B., 1995, *Modeling of Masonry Infill Panels for Structural Analysis*, National Center for Earthquake Engineering Research, Technical Report NCEER-95-0018.

Riddington, J. and Stafford-Smith, B., 1977, "Analysis of infilled frames subject to racking with design recommendations," *Structural Engineers*, (52)6: 263-268.

Riddington, J.R., 1984, "The influence of initial gaps on infilled frame behavior," *Proceedings of the Institute of Civil Engineers*, (2)77: 259-310.

Sachanski, S., 1960, "Analysis of earthquake resistance of frame buildings taking into consideration the carring capacity of the filling masonry," *Proceedings of the 2nd World Conference on Earthquake Engineering*, Japan, 138: 1-15.

Saneinejad, A and Hobbs, B., 1995, "Inelastic design of infilled frames," *Journal of Structural Engineering*, (121)4: 634-650.

Shapiro, D., Uzarski, J., and Webster, M., 1994, *Estimating Out-of-Plane Strength of Cracked Masonry Infills*, University of Illinois at Urbana-Champaign, Report SRS-588, 16 pp.

Shen, J. and Zhu, R., 1994, "Earthquake response simulation of reinforced concrete frames with infilled brick walls by pseudo-dynamic test," *Proc. of the Second International Conference on Earthquake Resistant Construction and Design*, Berlin, A. Balkema, Rotterdam, pp. 955-962.

Shing, P.B., Mehrabi, A.B., Schuller, M. and Noland J.D., 1994, "Experimental evaluation and finite element analysis of masonry-infilled R/C frames," *Proc. of the Eleventh Conference* (formerly Electronic Computation Conference) held in conjunction with ASCE Structures Congress '94 and International Symposium '94, Atlanta, Georgia., pp. 84-93.

Stafford-Smith, B.S., 1966, "Behavior of square infilled frames," *ASCE* (92)1: 381-403.

Stafford-Smith, B. and Carter, C., 1969, "A method of analysis for infilled frames," *Proceedings of the Institute of Civil Engineers*, 44: 31-48.

Thiruvengadam, V., 1985, "On the natural frequencies of infilled frames," *Earthquake Engineering and Structural Dynamics*, 13: 401-419.

Thomas, F.G., 1953, "The strength of brickwork," *J. Instnt. Struct. Engrs.*, (31)2: 35-46.

Wood, R.H., 1978, "Plasticity, composite action and collapse design of unreinforced shear wall panels in frames," *Proceedings of the Institute of Civil Engineers*, 2: 381-411.

Yoshimura, K. and Kikuchi, K., 1995, "Experimental study on seismic behavior of masonry walls confined by R/C frames," *Proceedings of the Pacific Conference on Earthquake Engineering*, Melbourne, Australia, Parkville, Victoria, 3: 97-106.

Zarnic, R. and Tomazevic, M., 1984, "The behavior of masonry infilled reinforced concrete frames subjected to seismic loading," *Proceedings of the 8th World Conference on Earthquake Engineering*, California, VI: 863-870.

Zarnic, R. and Tomazevic, M., 1985a, "Study of the behavior of masonry infilled reinforced concrete frames subjected to seismic loading," *Proc. 7th Intl. Brick Masonry Conf.*, Melbourne, Australia.

Zarnic, R. and Tomazevic, M., 1985b, *Study of the behavior of masonry infilled reinforced concrete frames subjected to seismic loading, Part 2*. A report to the research community of Slovenia, ZRMK/IKPI - 8502, Ljubljana.

6. Analytical Studies

6.1 Overview

Analytical studies were conducted as part of this project to serve two broad objectives: (1) to assess the effects of damage from a prior earthquake on the response of single-degree-of-freedom oscillators to a subsequent, hypothetical performance-level earthquake, and (2) to evaluate the utility of simple, design-oriented methods for estimating the response of damaged structures. Previous analytical studies were also reviewed.

To assess the effects of prior damage on response to a performance-level earthquake, damage to a large number of single-degree-of-freedom (SDOF) oscillators was simulated. The initially "damaged" oscillators were then subjected to an assortment of ground motions. The response of the damaged oscillators was compared with that of their undamaged counterparts to identify how the damage affected the response.

The oscillators ranged in initial period from 0.1 to 2.0 seconds, and the strength values were specified such that the oscillators achieved displacement ductility values of 1, 2, 4, and 8 for each of the ground motions when using a bilinear force-displacement model. The effects of damage were computed for these oscillators using several Takeda-based force-displacement models. Damage was parameterized independently in terms of ductility demand and strength reduction.

Ground motions were selected to represent a broad range of frequency characteristics in each of the following categories: Short-duration (SD) records were selected from earthquakes with magnitudes less than about 7, while long-duration (LD) records were generally selected from stronger earthquakes. A third category, forward directivity (FD), consists of ground motions recorded near the fault rupture surface for which a strong velocity pulse may be observed very early in the S-wave portion of the record. Six motions were selected for each category, representing different frequency characteristics, source mechanisms, and earthquakes occurring in locations around the world over the last half-century.

The utility of simple, design-oriented methods for estimating response was evaluated for the damaged and undamaged SDOF oscillators. The displacement coefficient method is presented in FEMA 273 (FEMA, 1997a) and the capacity spectrum and secant stiffness methods is presented in ATC-40 (ATC, 1996). Estimates of peak displacement response were determined according to these methods and compared with computed values obtained in the dynamic analyses for the damaged and undamaged structures. In addition, the ratio of the peak displacement estimates of damaged and undamaged structures was compared with the ratio obtained from the displacements computed in the nonlinear dynamic analyses.

This chapter summarizes related findings by previous investigators in Section 6.2. The dynamic analysis framework is described in detail in Section 6.3, and results of the nonlinear dynamic analyses are presented in Section 6.4. The design-oriented nonlinear static procedures are described in Section 6.5, and the results of these analyses are compared with the results computed in the dynamic analyses in Section 6.6. Conclusions and implications of the work are presented in Section 6.7.

6.2 Summary of Previous Findings

Previous studies have addressed several issues related to this project. Relevant analytical and experimental findings are reviewed in this section.

6.2.1 Hysteresis Models

Studies of response to recorded ground motions have used many force-displacement models that incorporate various rules for modeling hysteretic response. By far, the most common of these are the bilinear and stiffness-degrading models, which repeatedly attain the strengths given by the monotonic or envelope force-displacement relation. The response of oscillators modeled using bilinear or stiffness-degrading models is discussed below.

6.2.1.1 Bilinear and Stiffness-Degrading Models

Many studies (for example, Iwan,1977; Newmark and Riddell, 1979; Riddell, 1980; Humar, 1980; Fajfar and Fischinger, 1984; Shimazaki and Sozen, 1984; and Minami and Osawa, 1988) have examined the effect of the hysteresis model on the response of SDOF structures. These studies considered elastic-perfectly-plastic, bilinear (with positive post-yield stiffness), and stiffness-degrading models such as the Takeda model

and the Q model, as well as some lesser-known models. For the nonlinear models used in these studies, the post-yield stiffness of the primary curve ranged between 0 and 10% of the initial stiffness. It is generally found that for long-period structures with positive post-yield stiffness, peak displacement response tends to be independent of the hysteresis model, and it is approximately equal to the peak displacement of linear-elastic oscillators having the same initial stiffness. For shorter-period structures, however, peak displacement response tends to exceed the response of linear-elastic oscillators having the same initial stiffness. The difference in displacement response is exacerbated in lower-strength oscillators. Fajfar and Fischinger (1984), found that for shorter-period oscillators, the peak displacements of elastic-perfectly-plastic models tend to exceed those of degrading-stiffness models (the Q-model), and these peak displacements tend to exceed those of the bilinear model. Riddell (1980), reported that the response of stiffness-degrading systems tends to "go below the peaks and above the troughs" of the spectra obtained for elastoplastic systems.

The dynamic response of reinforced concrete structures tested on laboratory shake tables has been compared with the response computed using different hysteretic models. The Takeda model was shown to give good agreement with measured response characteristics (Takeda et al., 1970). In a subsequent study, the Takeda model was shown to match closely the recorded response; acceptable results were obtained with the less-complicated Q-Hyst model (Saiidi, 1980). Time histories computed by these models were far more accurate than those obtained with the bilinear model.

Studies of a seven-story reinforced concrete moment-resisting frame building damaged in the 1994 Northridge earthquake yield similar conclusions. Moehle et al. (1997) reported that the response computed for plane-frame representations of the structure most nearly matched the recorded response when the frame members were modeled using stiffness-degrading models and strength- and stiffness-degrading force/displacement relationships; dynamic analysis results obtained using bilinear force/displacement relationships were not sufficiently accurate.

Iwan (1973) examined the effect of pinching and yielding on the response of SDOF oscillators to four records. It was found that the maximum displacement response of oscillators having an initial period equal to one second was very nearly equal to that computed for bilinear systems having the same initial stiffness and yield strength. For one-second oscillators having different system parameters and subjected to different earthquake records, the ratio of mean degrading-system peak displacement response to bilinear system response was 1.06, with standard deviation of 0.14. Iwan noted that for periods appreciably less than one second, the response of degrading systems was significantly greater than that for the corresponding bilinear system, but these effects were not quantified.

Iwan (1977) reported on the effects of a reduction in stiffness caused by cracking. Modeling the uncracked stiffness caused a reduction in peak displacement response for shorter-period oscillators with displacement ductility values less than four, when compared with the response of systems having initial stiffness equal to the yield-point secant stiffness.

Humar (1980) compared the displacement ductility demand calculated for the bilinear and Takeda models for SDOF and multi-degree-of-freedom (MDOF) systems. For the shorter-period SDOF oscillators, the displacement ductility demands exceeded the strength-reduction factor, particularly for the Takeda model. Five- and ten-story frames were designed with girder strengths set equal to 25% of the demands computed in an elastic analysis, and column strengths were set higher than the values computed in an elastic analysis. The Takeda model, which included stiffness degradation, generally led to larger interstory drifts and girder ductility demands than were computed with the bilinear model.

The studies described above considered hysteretic models for which the slope of the post-yield portion of the primary curve was greater than or equal to zero. Where negative post-yield slopes are present, peak displacement response is heightened (Mahin, 1980). The change in peak displacement response tends to be significantly larger for decreases in the post-yield slope below zero than for similar increases above zero. Even post-yield stiffness values equal to negative 1% of the yield stiffness were sufficient to cause collapse. These effects were found to be more pronounced in shorter-period systems and in relatively weak systems.

Rahnama and Krawinkler (1995) reported findings for SDOF structures subjected to 15 records obtained on rock sites. They found that higher lateral strength is required, relative to elastic demands to obtain target displacement ductility demands, for oscillators with

negative post-yield stiffness. The decrease in the strength-reduction factor is relatively independent of vibration period and is more dramatic with increases in target displacement ductility demand. These effects depend on the hysteresis model; the effect of negative post-yield stiffness on the strength-reduction factor is much smaller for stiffness-degrading systems than for bilinear systems. They note that stiffness-degrading systems behave similarly to bilinear systems for positive post-yield stiffness, and they are clearly superior to systems with negative values of post-yield stiffness.

Palazzo and DeLuca (1984) found that the strength required to avoid collapse of SDOF oscillators subjected to the Irpinia earthquake increased as the post-yield stiffness of the oscillator became increasingly negative. Xie and Zhang (1988) compared the response of stiffness-degrading models (having zero post-yield stiffness) with the response of models having a negative post-yield stiffness. The SDOF oscillators were subjected to 40 synthetic records having duration varying from 6 to 30 seconds. It appears that Xie and Zhang found that for shorter-period structures, negative post-yield stiffness models were more likely to result in collapse than were the stiffness-degrading models for all durations considered.

6.2.1.2 *Strength-Degrading Models*

The response of structures for which the attainable strength is reduced with repeated cyclic loading is discussed below.

Parducci and Mezzi (1984) used elasto-plastic force-displacement models to examine the effects of strength degradation. Yield strength was modeled as decreasing linearly with cumulative plastic deformation. Using accelerograms recorded in Italian earthquakes, The authors found that strength degradation causes an increase in displacement ductility demand for the stronger, shorter-period oscillators. For weaker oscillators, strength degradation amplifies ductility demand over a broader range of periods. The more rapid the degradation of strength, the greater the increase in ductility demand. An analogy can be made with the findings of Shimazaki and Sozen (1984): when strength degradation occurs, the increase in ductility demand can be kept small for shorter-period structures if sufficient strength is provided.

Nakamura and Tanida (1988) examined the effect of strength degradation and slip on the response of SDOF oscillators to white noise and to the 1940 NS El Centro motion. Figure 6-1 plots the force/displacement response curves obtained in this study for various combinations of hysteresis parameters for oscillators with a 0.2-sec period. The parameter D controls the

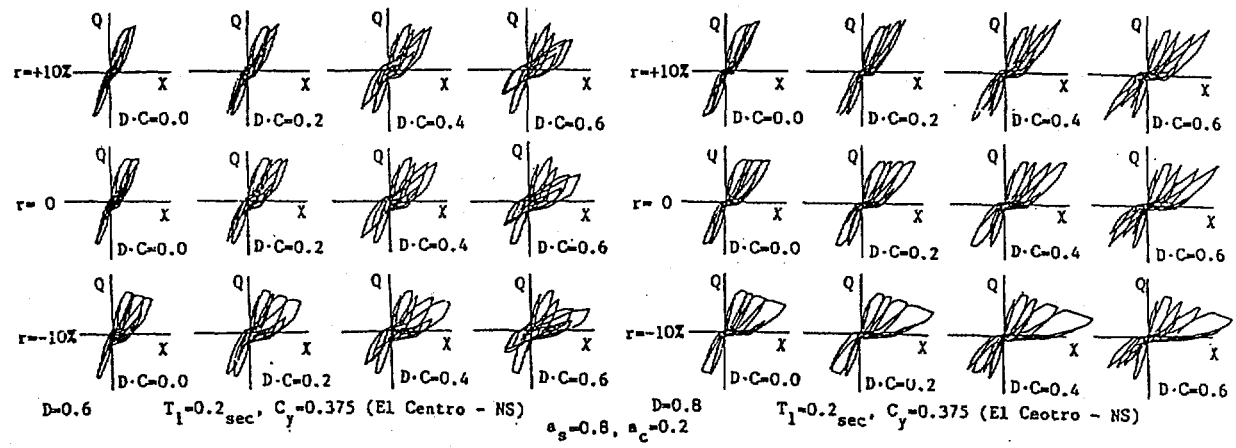

Figure 6-1 Effect of Hysteretic Properties on Response to 1940 NS El Centro Record (from Nakamura, 1988)

amount of slip, C controls the degraded loading stiffness, and a_s and a_c control the unloading stiffness for the slip and degrading components of the model. It is clear that peak displacement response tends to increase as slip becomes more prominent, as post-yield stiffness decreases or even becomes negative, and as loading stiffness decreases.

Rahnama and Krawinkler (1995) modeled strength degradation for SDOF systems as a function of dissipated hysteretic energy. Strength degradation may greatly affect the response of SDOF systems, and the response is sensitive to the choice of parameters by which the strength degradation is modeled. Results of such studies need to be tied to realistic degradation relationships to understand the practical significance of computed results.

6.2.2 Effect of Ground Motion Duration

As described previously, Xie and Zhang (1988) subjected a number of SDOF oscillators to 40 synthetic ground motions, which lasted from 6 to 30 seconds. For stiffness-degrading and negative post-yield stiffness models, the number of collapses increased, as ground motion duration increased. The incidence of collapse tended to be higher for shorter-period structures than longer-period structures. Shorter-duration ground motions that were just sufficient to trigger the collapse of short-period structures did not trigger the collapse of any longer-period structures.

Mahin (1980) reported on the evolution of ductility demand with time for SDOF oscillators subjected to five synthetic records, each having a 60-second duration. Peak evolutionary ductility demands were plotted at 10-second intervals for bilinear oscillators; ductility demand was found to increase asymptotically toward the peak values obtained at 60 seconds. This implies that increases in the duration of ground motion may cause relatively smaller increases in ductility demand.

Sewell (1992) studied the effect of ground-motion duration on elastic demand, constant-ductility strength-reduction factors, and inelastic response intensity, using a set of 262 ground-motion records. He found that the spectral acceleration of elastic and inelastic systems is not correlated with duration, and that strength-reduction factors can be estimated using elastic response ordinates. These findings suggest that the effect of duration on inelastic response is contained within representations of elastic response quantities.

6.2.3 Residual Displacement

Kawashima et al. (1994) studied the response of bilinear systems with periods between 0.1 and 3 seconds that were subjected to Japanese ground-motion records. According to this study, residual displacement values are strongly dependent on the post-yield stiffness of the bilinear system; that is, systems with larger post-yield stiffness tend to have significantly smaller residual displacements, and systems with zero or negative post-yield stiffness tend to have residual displacements that approach the peak response displacement. They also found that the magnitude of residual displacement, normalized by peak displacement, tends to be independent of displacement ductility demand, based on displacement ductility demands of two, four, and six. The results also indicated that the magnitude of residual displacement is not strongly dependent on the characteristic period of the ground motion, the magnitude of the earthquake, or the distance from the epicenter.

In shake-table tests of reinforced concrete wall and frame/wall structures, Araki et al. (1990) reported that residual drifts for all tests were less than 0.2% of structure height. These tests included wall structures exhibiting displacement ductility demands up to about 12 and frame/wall structures exhibiting displacement ductility demands up to about 14. The small residual drifts in this study were attributed to the presence of restoring forces (acting on the mass of the structure), which are generated as the wall lengthens when displaced laterally. Typical response analyses do not model these restoring forces. These results appear to be applicable to systems dominated by flexural response. However, larger residual displacements have been observed in postearthquake reconnaissance.

6.2.4 Repeated Loading

In the shake-table tests, Araki et al. (1990) also subjected reinforced concrete wall and frame-wall structures to single and repeated motions. It appears that a synthetic ground motion was used. It was found that the low-rise structures subjected to repeated shake-table tests displaced to approximately twice as much as they did in a single test. For the mid-rise and high-rise structures, repeated testing caused peak displacements that were approximately 0 to 10% larger than those obtained in single tests.

Wolschlag (1993) tested three-story reinforced concrete walls on a shake table. In one test series, an undamaged structure was subjected to repeated ground motions of the same intensity. In the repeat tests, the peak displacement response at each floor of the damaged specimen hardly differed from the response measured for the initially undamaged structure.

Cecen (1979) tested two identical ten-story, three-bay, reinforced concrete frame models on a shake table. The two models were subjected to sequences of base motions of differing intensity, followed by a final test using identical base motions. When the structures were subjected to the repeated base motion, the peak displacement response at each story was only slightly affected by the previous shaking of the same intensity. When the two structures were subjected to the same final motion, peak displacement response over the height of the two structures was only slightly affected by the different prior sequences. Floor acceleration response, however, was prone to more variation.

Mahin (1980) investigated the analytical response of SDOF oscillators to repeated ground motions. He reported minor-to-moderate increases in displacement ductility demand across all periods, and weaker structures were prone to the largest increases. For bilinear models with negative post-yield stiffness, increased duration or repeated ground motions tended to cause significant increases in displacement ductility demand (Mahin and Boroschek, 1991).

6.3 Dynamic Analysis Framework

6.3.1 Overview

This section describes the dynamic analyses determining the effects of damage from prior earthquakes on the response to a subsequent performance-level earthquake. In particular, this section describes the ground motion and hysteresis models, the properties of the undamaged oscillators, and the assumptions and constructions used to establish the initially-damaged oscillators. Results of the dynamic analyses are presented in Section 6.4.

6.3.2 Dynamic Analysis Approach

The aim of dynamic analysis was to quantify the effects of a damaging earthquake on the response of a SDOF oscillator to a subsequent, hypothetical, performance-event earthquake. Two obvious approaches may be taken: the first simulates the damaging earthquake, and the second simulates the damage caused by the damaging earthquake.

To simulate the damaging earthquake, oscillators can be subjected to an acceleration record that is composed of an initial, damaging ground motion record, a quiescent period, and a final ground motion record specified as the performance-level event. This approach appears to simulate reality well, but it is difficult to determine *a priori* how to specify the intensity of the damaging ground motion. One rationale would be to impose damaging earthquakes that cause specified degrees of ductility demand. This would result in oscillators having experienced prior ductility demand and residual displacement at the start of the performance-level ground motion.

In the second approach, taken in this study, the force-displacement curve of the oscillator is modified prescriptively to simulate prior ductility demand, and these analytically "damaged" oscillators are subjected to only the performance-level ground motion. To identify the effects of damage (through changes in stiffness and strength of the oscillator force/displacement response), the possibility of significant residual displacements resulting from the damaging earthquake was neglected. Thus, the damaging earthquake is considered to have imposed prior ductility demands (PDD), possibly in conjunction with strength reduction or strength degradation, on an initially-undamaged oscillator. Initial stiffness, initial unloading stiffness, and strength of the oscillators at the start of the performance-level ground motion may be affected. Response of the initially-damaged structure is compared with the response of the undamaged structure under the performance-level motion. This approach presumes that an engineer will be able to assess changes in lateral stiffness and strength of a real structure based on the nature of damage observed after the damaging earthquake.

While a number of indices may be used to compare response intensity, peak displacement response is preferred here because of its relative simplicity, its immediate physical significance, and its use as the basic parameter in the nonlinear static procedures (described in Section 6.5). The utility of the nonlinear static procedures is assessed vis-a-vis their ability to estimate accurately the peak displacement response.

It should be recognized that predicting the capacity of wall and infill elements may be difficult and prone to uncertainty, whether indexed by displacement, energy,

or other measures. When various modes of response may contribute significantly to an element's behavior, existing models may not reliably identify which mode will dominate. Uncertainty in the dominant mode necessarily leads to uncertainty in estimates of the various capacity measures.

6.3.3 Ground Motions

Several issues were considered when identifying ground motion records to be used in the analyses. First, the relative strength of the oscillators and the duration of ground motion are thought to be significant because these parameters control the prominence of inelastic response. Second, it is known that ground motions rich in frequencies just below the initial frequency of the structure tend to exacerbate damage, because the period of the structure lengthens as yielding progresses. Third, information is needed on the characteristics of structural response to near-field motions having forward-directivity effects.

The analyses were intended to identify possible effects of duration and forward directivity on the response of damaged structures. Therefore, three categories of ground motions were established: short duration (SD), long duration (LD), and Forward Directivity (FD). The characteristics of several hundred ground motions were considered in detail in order to select the records used in each category. Ground motions within a category were selected to represent a broad range of frequency content. In addition, it was desired to use some records that were familiar to the research community, and to use some records obtained from the Loma Prieta, Northridge, and Kobe earthquakes. Within these constraints, records were selected from a diverse worldwide set of earthquakes in order to avoid systematic biases that might otherwise occur. Six time series were used in each category to provide a statistical base on which to interpret response trends and variability. Table 6-1 identifies the ground motions that compose each category, sorted by characteristic period.

Record duration was judged qualitatively in order to sort the records into the short duration and long duration categories. The categorization is intended to discriminate broadly between records for which the duration of inelastic response is short or long. Because the duration of inelastic response depends fundamentally on the oscillator period, the relative strength, and the force/displacement model, a suitable scalar index of record duration is not available.

The physical rupture process tends to correlate ground-motion duration and earthquake magnitude. It can be observed that earthquakes with magnitudes less than 7 tended to produce records that were categorized as short-duration motions, while those with magnitudes greater than 7 tended to be categorized as long-duration motions.

Ground motions recorded near a rupturing fault may contain relatively large velocity pulses if the fault rupture progresses toward the recording station. Motions selected for the forward directivity category were identified by others as containing near-field pulses (Somerville et al., 1997). Recorded components aligned most nearly with the direction perpendicular to the fault trace were selected for this category.

The records shown in Table 6-1 are known to come from damaging earthquakes. The peak ground acceleration values shown in Table 6-1 are in units of the acceleration of gravity. The actual value of peak ground acceleration does not bear directly on the results of this study, because oscillator strength is determined relative to the peak ground acceleration in order to obtain specified displacement ductility demands.

Identifiers in Table 6-1 are formulated using two characters to represent the earthquake, followed by two digits representing the year, followed by four characters representing the recording station, followed by three digits representing the compass bearing of the ground-motion component. Thus, IV40ELCN.180 identifies the South-North component recorded at El Centro in the 1940 Imperial Valley earthquake. Various magnitude measures are reported in the literature and repeated here for reference: M_L represents the traditional local or Richter magnitude, M_W represents moment magnitude, and M_S represents the surface-wave magnitude.

Detailed plots of the ground motions listed in Table 6-1 are presented in Figures 6-2 through 6-19. The plots present ground motion acceleration, velocity, and displacement time-series data, as well as spectral-response quantities. In all cases, ground acceleration data were used in the response computations, assuming zero initial velocity and displacement. For most records, the ground velocity and displacement data presented in the figures were prepared by others. For the four records identified with an asterisk (*) in Table 6-1, informal integration procedures were used to obtain the ground velocity and displacement values shown.

(Text continued on page 120)

Table 6-1 Recorded Ground Motions Used in the Analyses

Identifier	Earthquake Date	Mag.	Station	Com-ponent	PGA (g)	Epic. Dist. (km)	Char. Period (sec)
Short Duration (SD)							
WN87MWLN.090	Whittier Narrows 1 Oct 87	M_L=6.1	Mount Wilson Caltech Seismic Station	90	0.175	18	0.20
BB92CIVC.360	Big Bear 28 Jun 92	M_s=6.6	Civic Center Grounds	360	0.544	12	0.40
SP88GUKA.360 *	Spitak 7 Dec 88	M_s=6.9	Gukasyan, Armenia	360	0.207	57	0.55
LP89CORR.090	Loma Prieta 17 Oct 89	M_s=7.1	Corralitos Eureka Canyon Rd.	90	0.478	8	0.85
NR94CENT.360	Northridge 17 Jan 94	M_w=6.7	Century City	360	0.221	19	1.00
IV79ARY7.140	Imperial Valley 15 Oct 79	M_L=6.6	Array #7-14	140	0.333	27	1.20
Long Duration (LD)							
CH85LLEO.010	Central Chile 3 Mar 85	M_s=7.8	Llolleo-Basement of 1-Story Building	010	0.711	60	0.30
CH85VALP.070	Central Chile 3 Mar 85	M_s=7.8	Valparaiso University of Santa Maria	070	0.176	26	0.55
IV40ELCN.180	Imperial Valley 18 May 40	M_L=6.3	El Centro Irrigation District	180	0.348	12	0.65
TB78TABS.344 *	Tabas 16 Sep 78	M=7.4	Tabas	344	0.937	<3	0.80
LN92JOSH.360	Landers 28 Jun 92	M=7.5	Joshua Tree	360	0.274	15	1.30
MX85SCT1.270	Michoacan 19 Sep 85	M_s=8.1	SCT1-Secretary of Communication and Transportation	270	0.171	376	2.00
Forward Directivity (FD)							
LN92LUCN.250 *	Landers 28 Jun 92	M=7.5	Lucerne	250	0.733	42	0.20
IV79BRWY.315	Imperial Valley 15 Oct 79	M_L=6.6	Brawley Municipal Airport	315	0.221	43	0.35
LP89SARA.360	Loma Prieta 17 Oct 89	M_s=7.1	Saratoga Aloha Avenue	360	0.504	28	0.40
NR94NWHL.360	Northridge 17 Jan 94	M_w=6.7	Newhall LA County Fire Station	360	0.589	19	0.80
NR94SYLH.090	Northridge 17 Jan 94	M_w=6.7	Sylmar County Hospital Parking Lot	090	0.604	15	0.90
KO95TTRI.360 *	Hyogo-Ken Nambu 17 Jan 95	M_L= 7.2	Takatori-kisu	360	0.617	11	1.40

* Indicates that informal integration procedures were used to calculate the velocity and displacement histories shown in Figures 6-2 through 6-19.

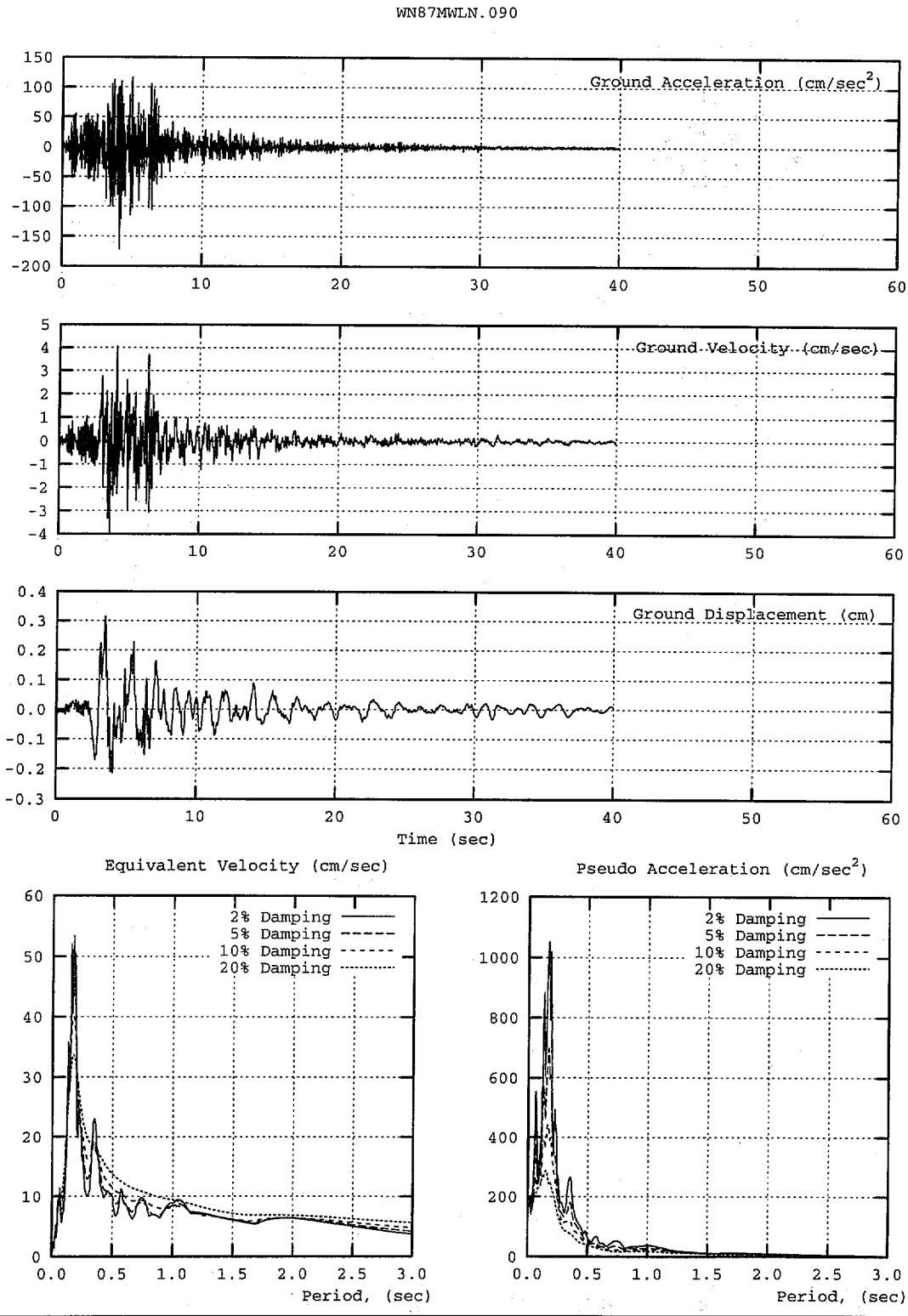

Figure 6-2 ***Characteristics of the WN87MWLN.090 (Mount Wilson) Ground Motion***

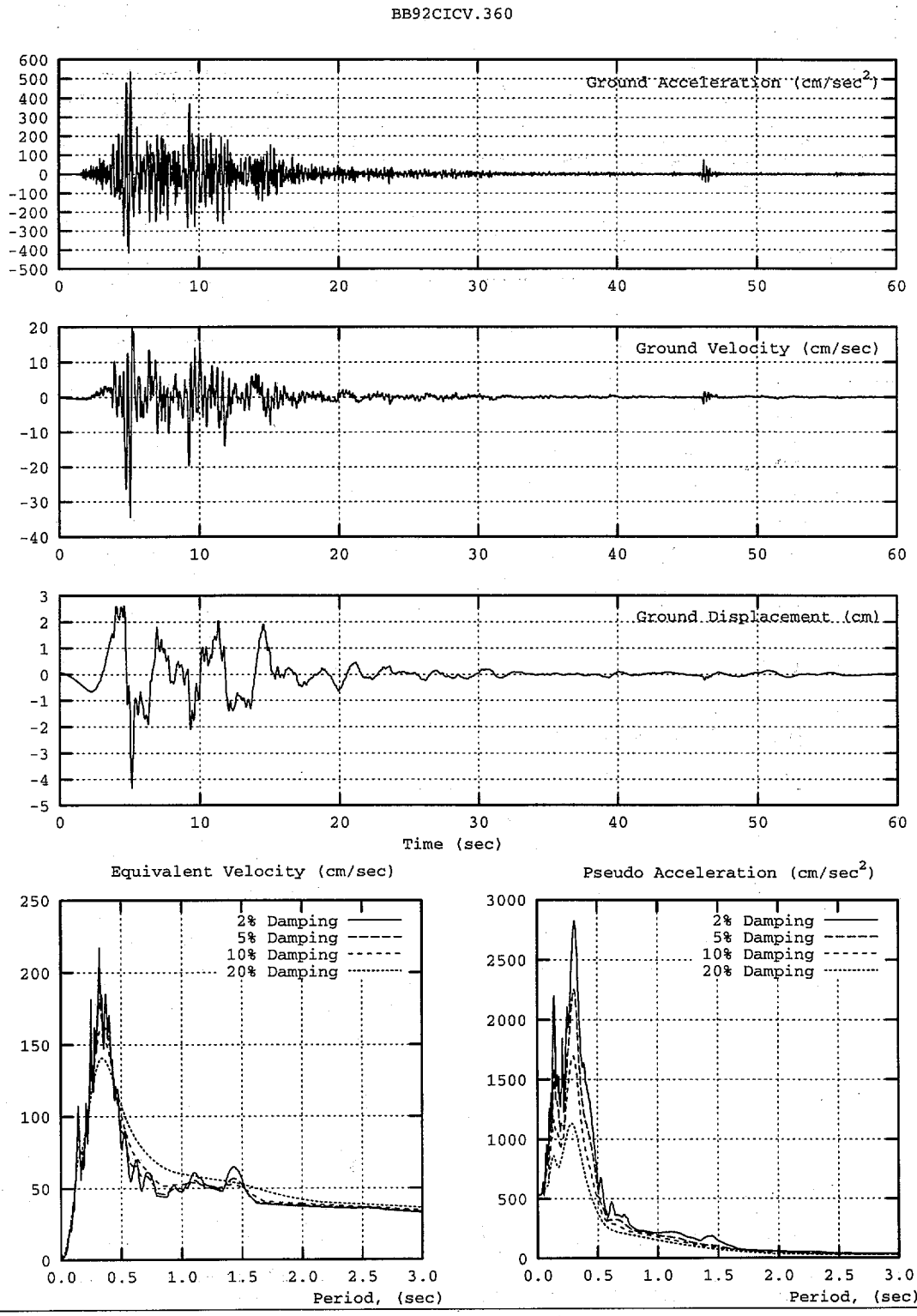

Figure 6-3 ***Characteristics of the BB92CIVC.360 (Big Bear) Ground Motion***

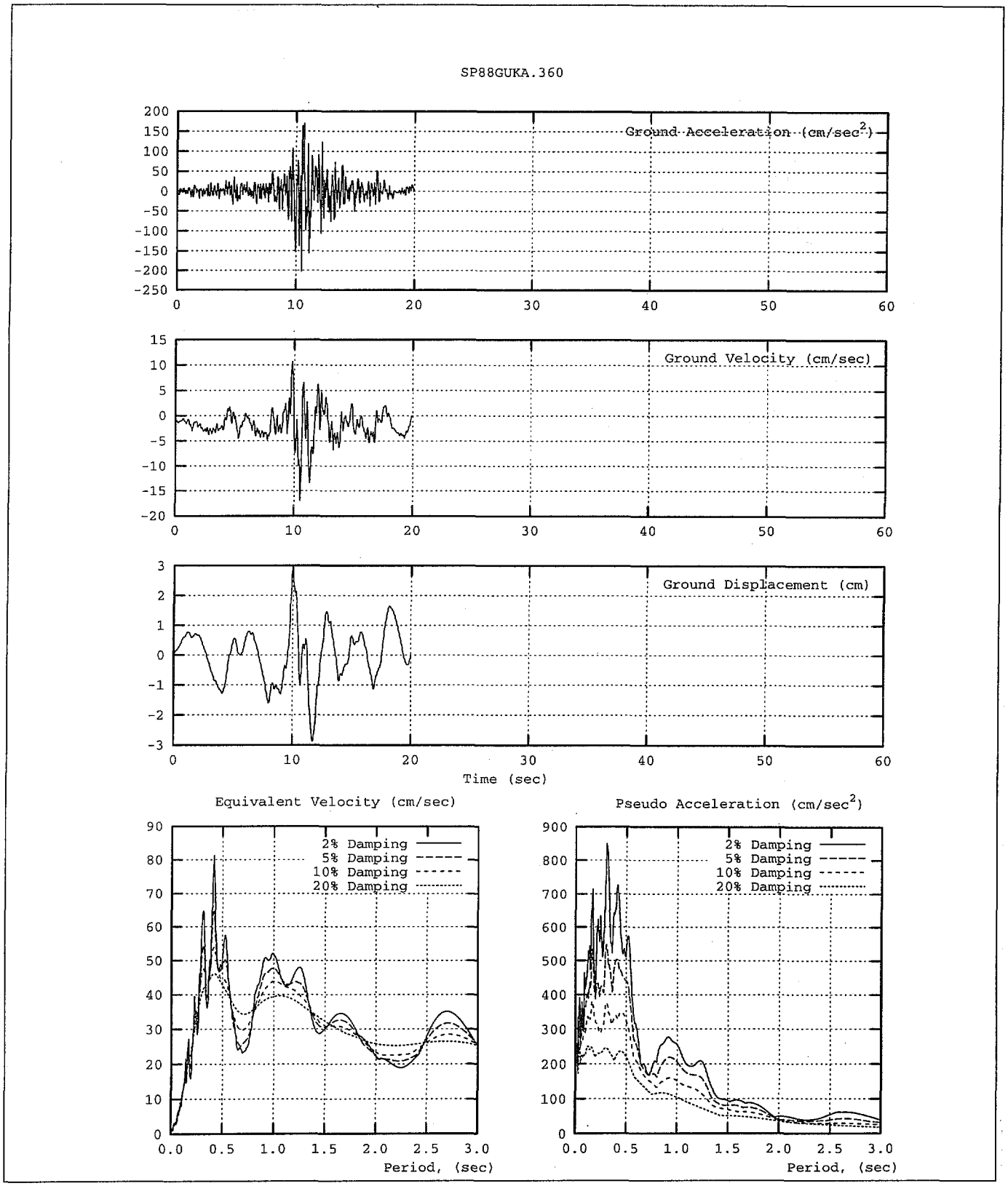

Figure 6-4 ***Characteristics of the SP88GUKA.360 (Spitak) Ground Motion***

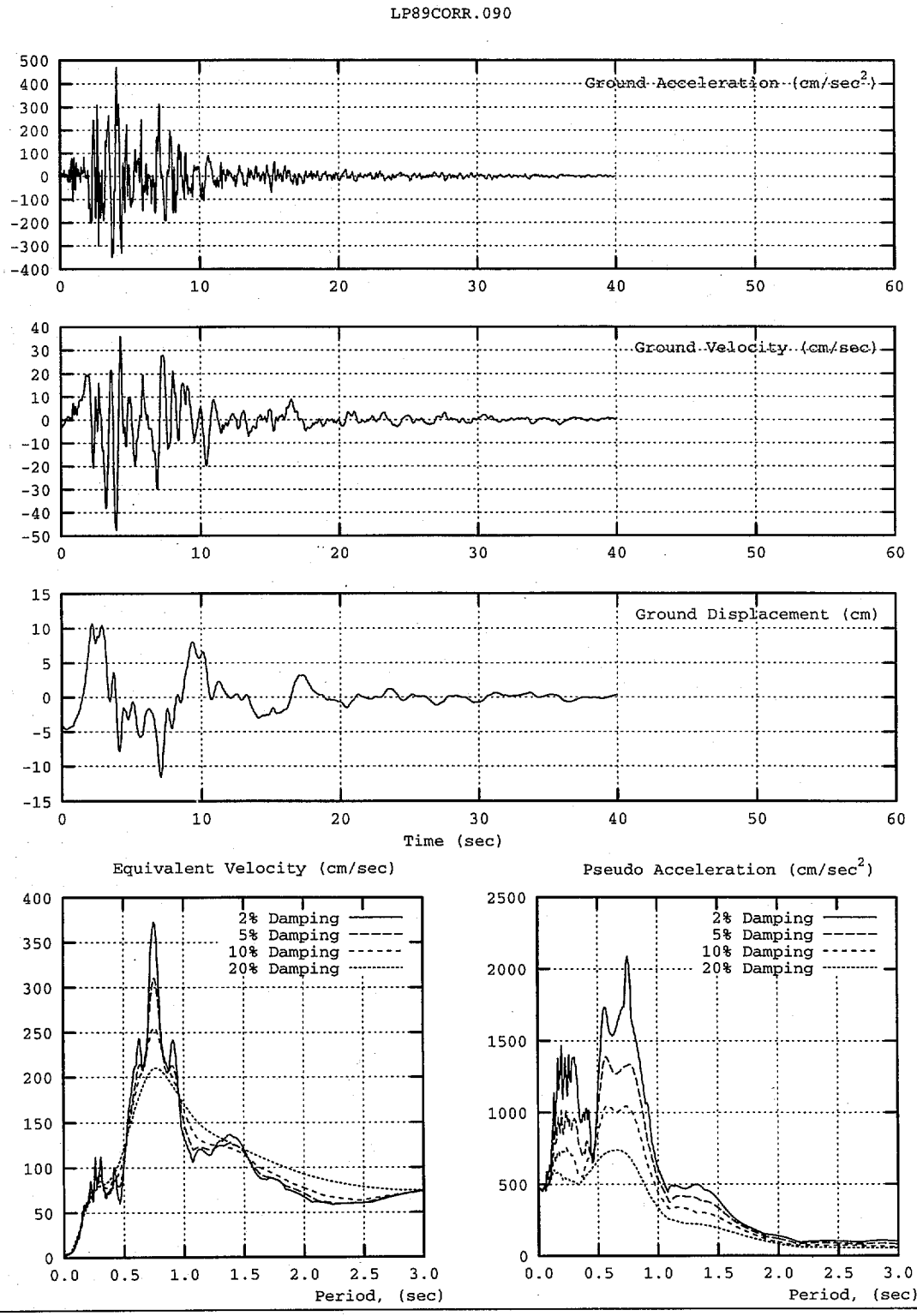

Figure 6-5 ***Characteristics of the LP89CORR.090 (Corralitos) Ground Motion***

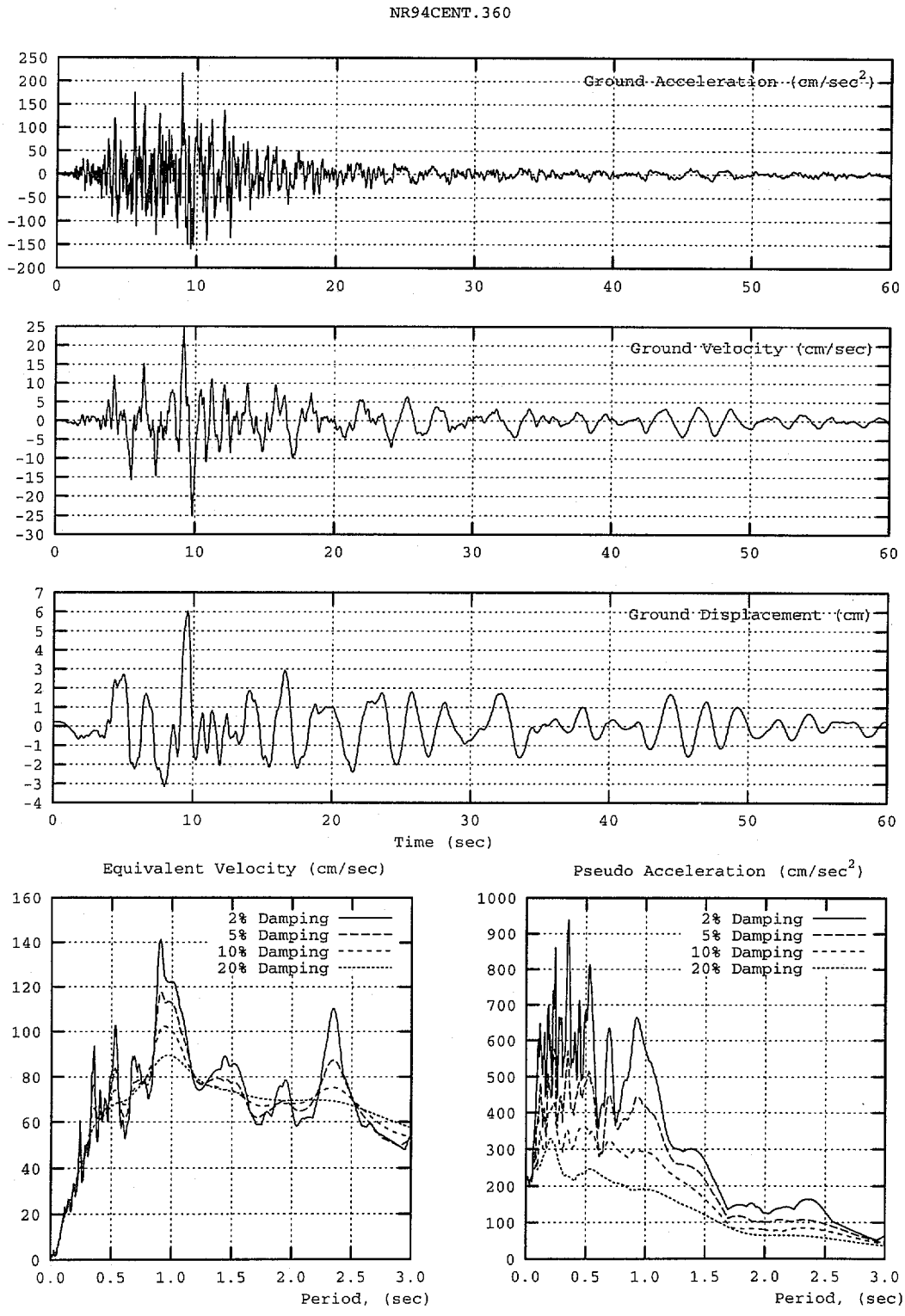

Figure 6-6 Characteristics of the NR94CENT.360 (Century City) Ground Motion

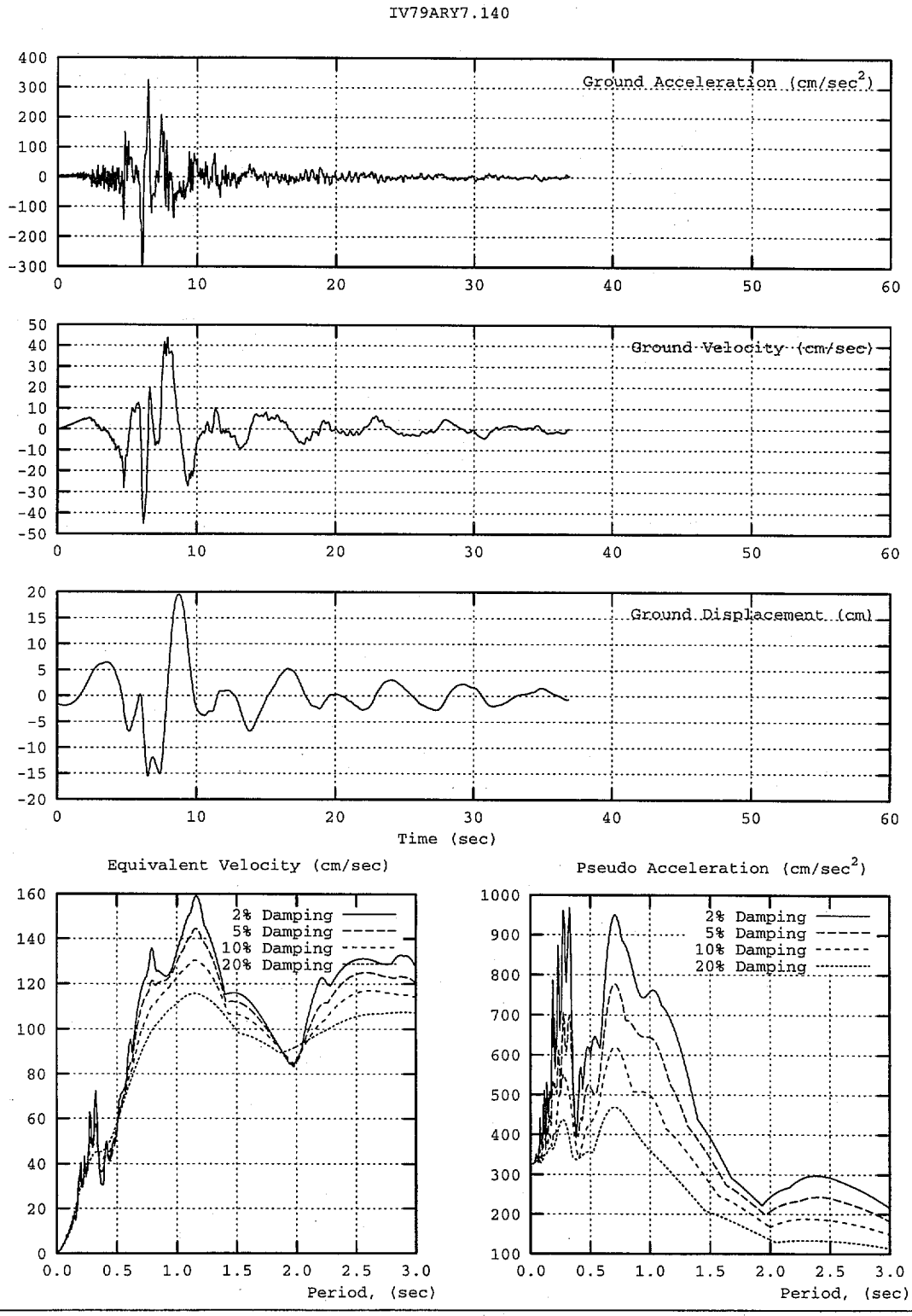

Figure 6-7 Characteristics of the IV79ARY7.140 (Imperial Valley Array) Ground Motion

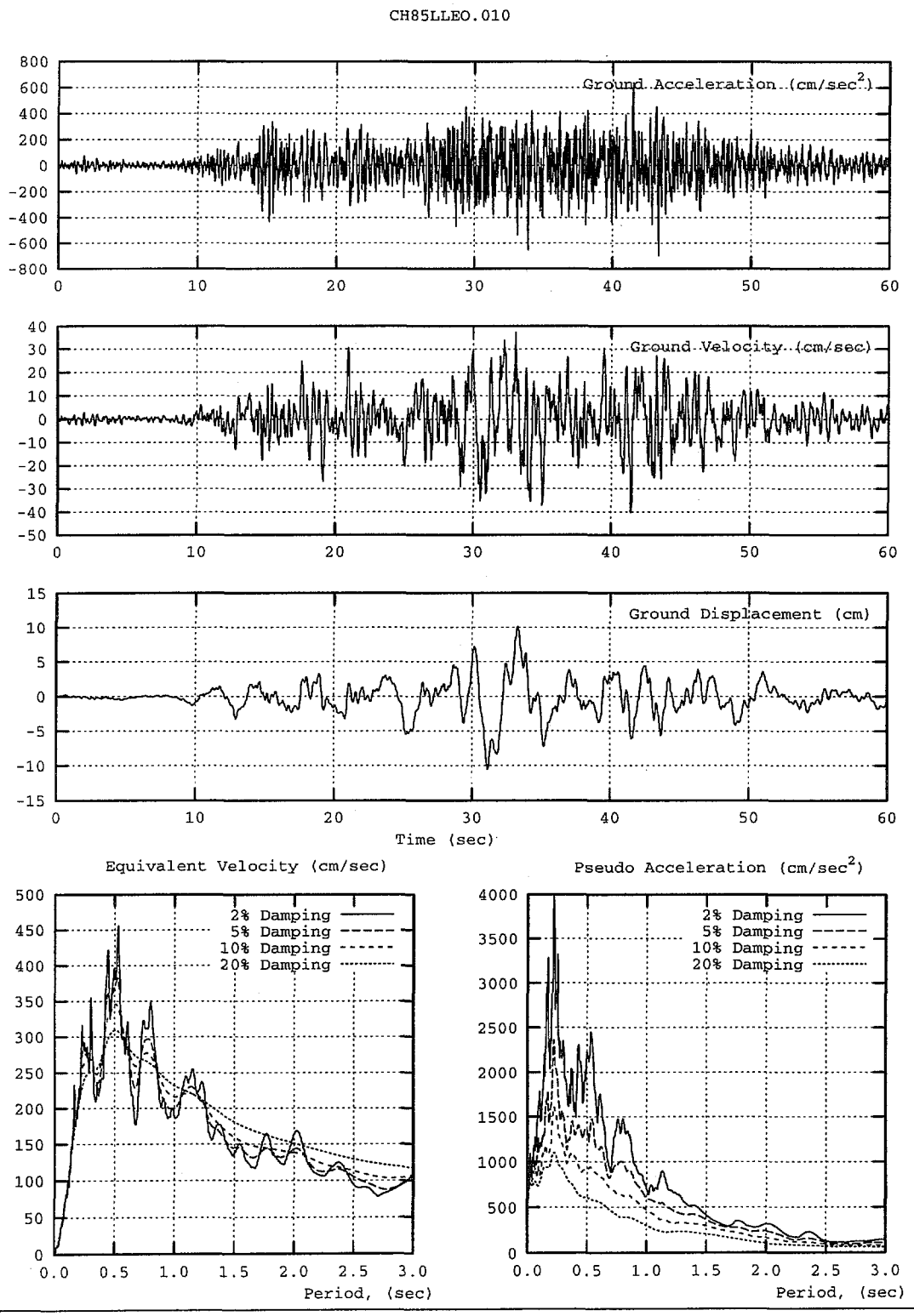

Figure 6-8 ***Characteristics of the CH85LLEO.010 (Llolleo) Ground Motion***

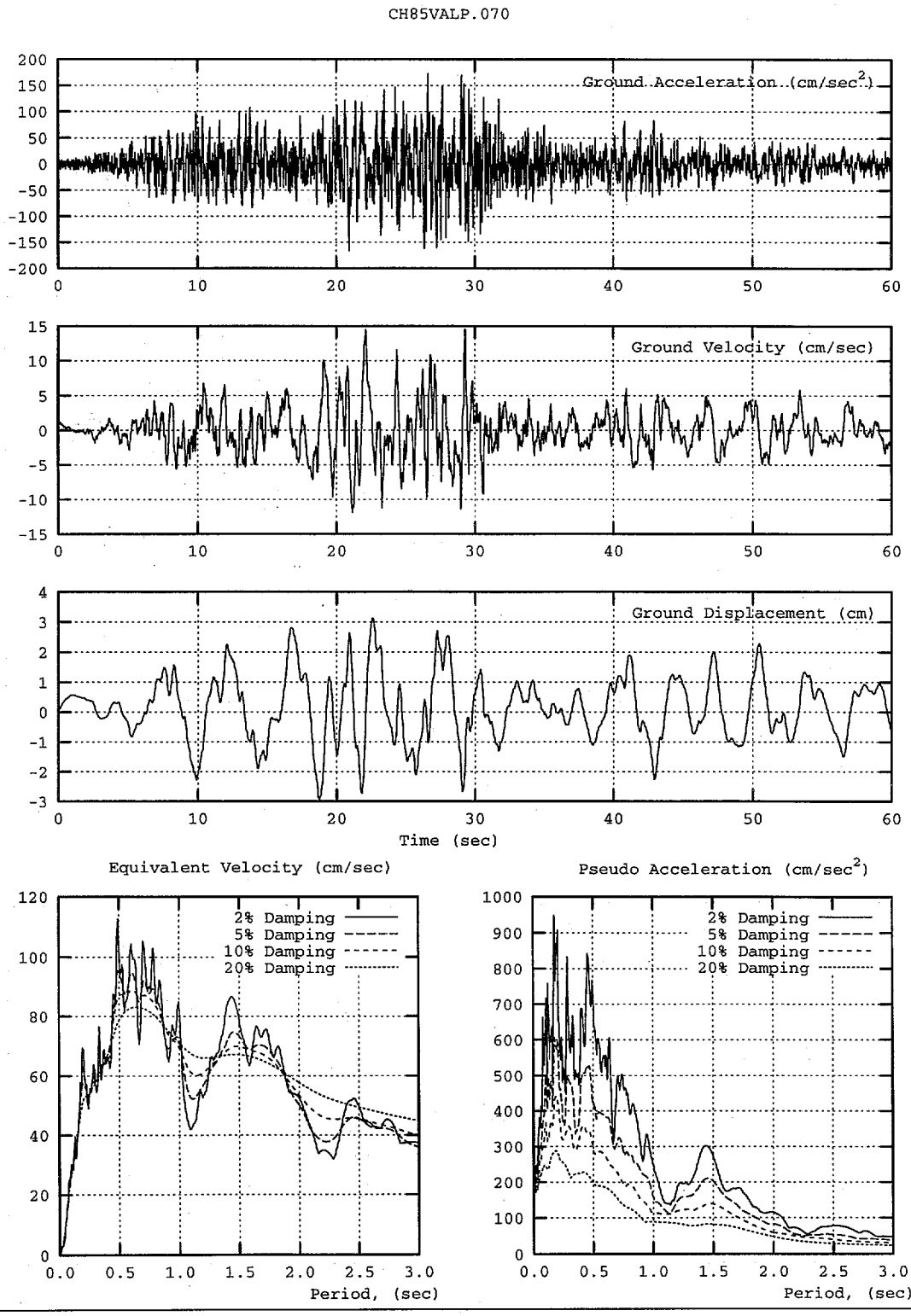

Figure 6-9 ***Characteristics of the CH85VALP.070 (Valparaiso University) Ground Motion***

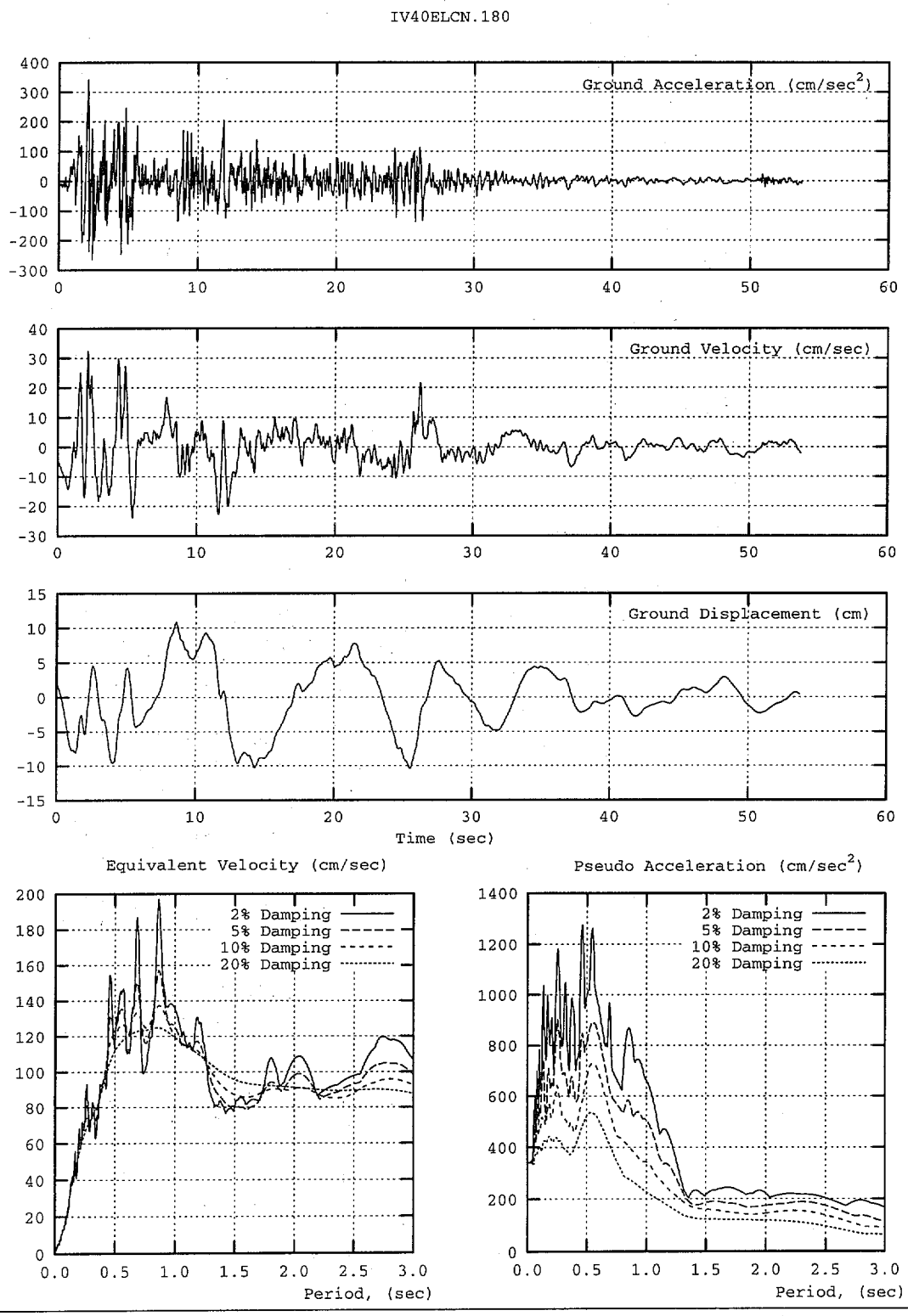

Figure 6-10 ***Characteristics of the IV40ELCN.180 (El Centro) Ground Motion***

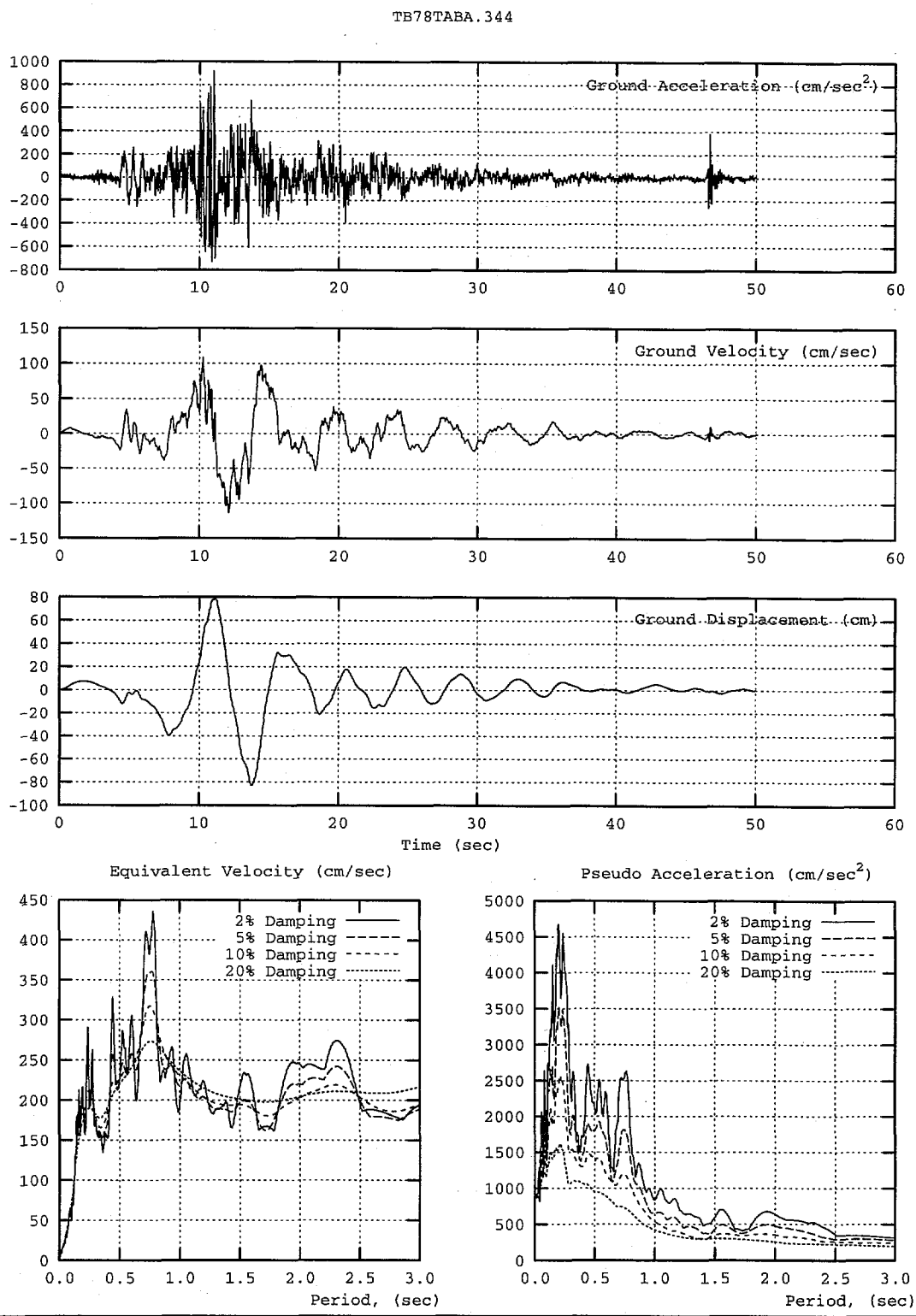

Figure 6-11 ***Characteristics of the TB78TABS.344 (Tabas) Ground Motion***

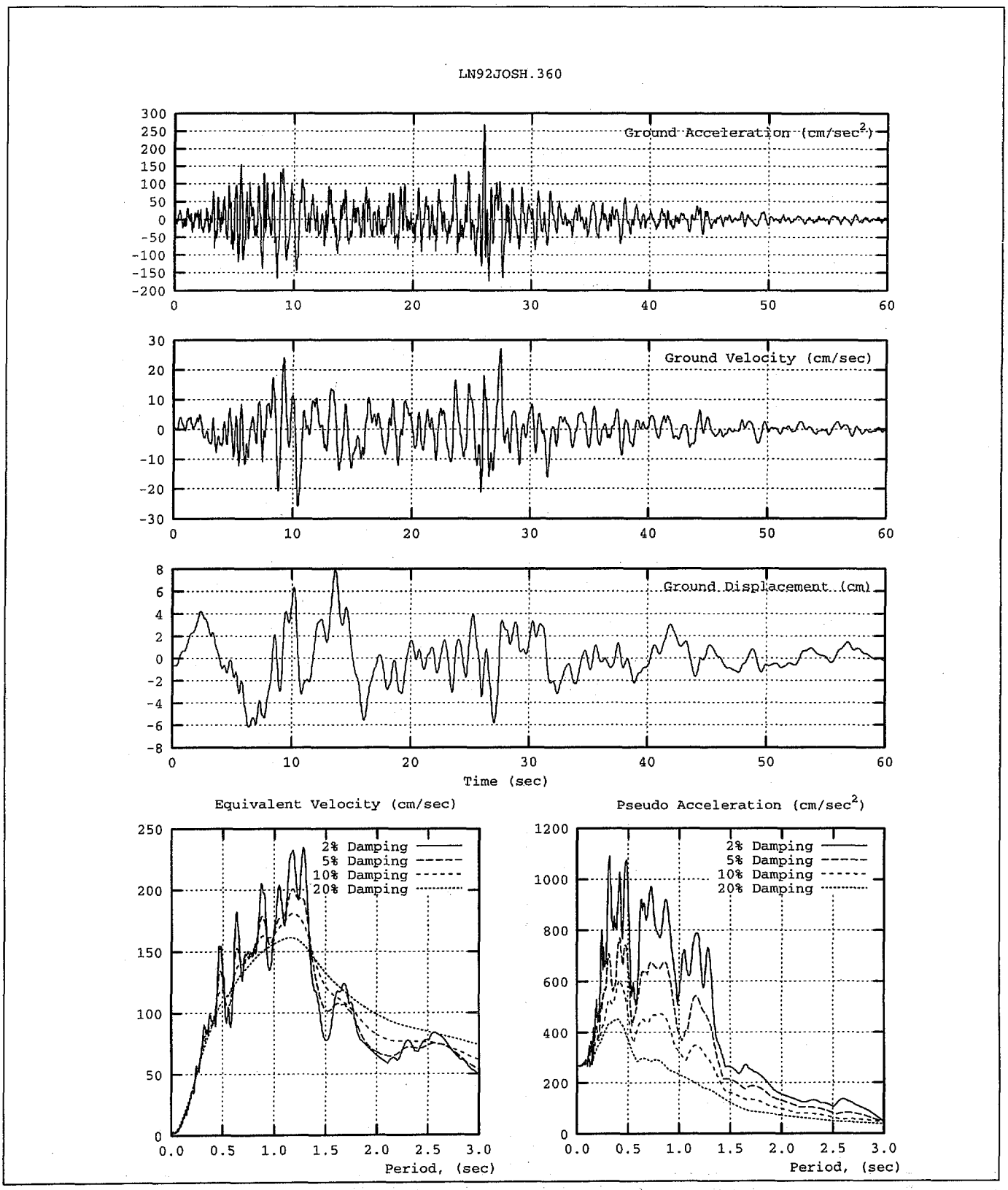

Figure 6-12 ***Characteristics of the LN92JOSH.360 (Joshua Tree) Ground Motion***

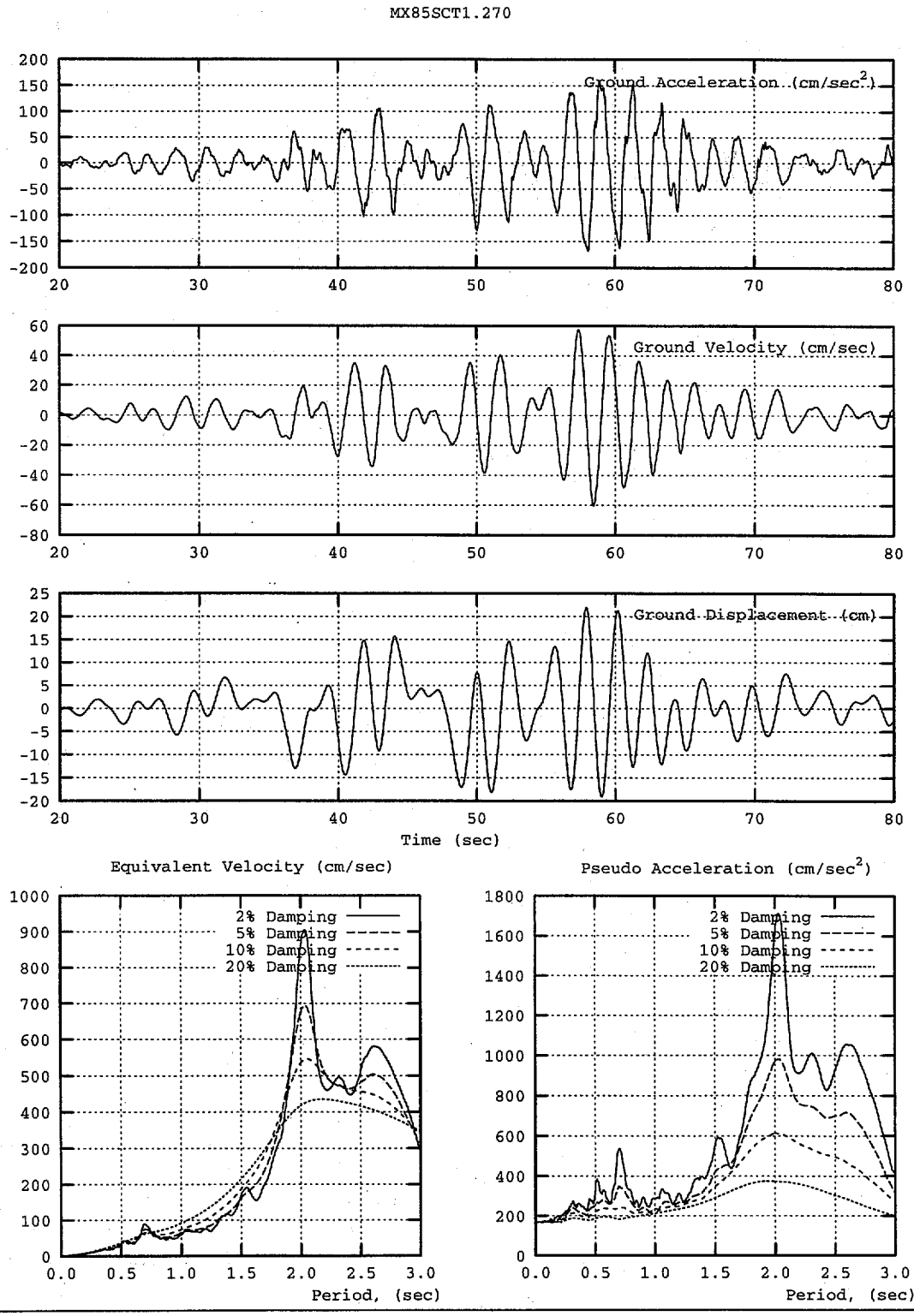

Figure 6-13 Characteristics of the MX85SCT1.270 (Mexico City) Ground Motion

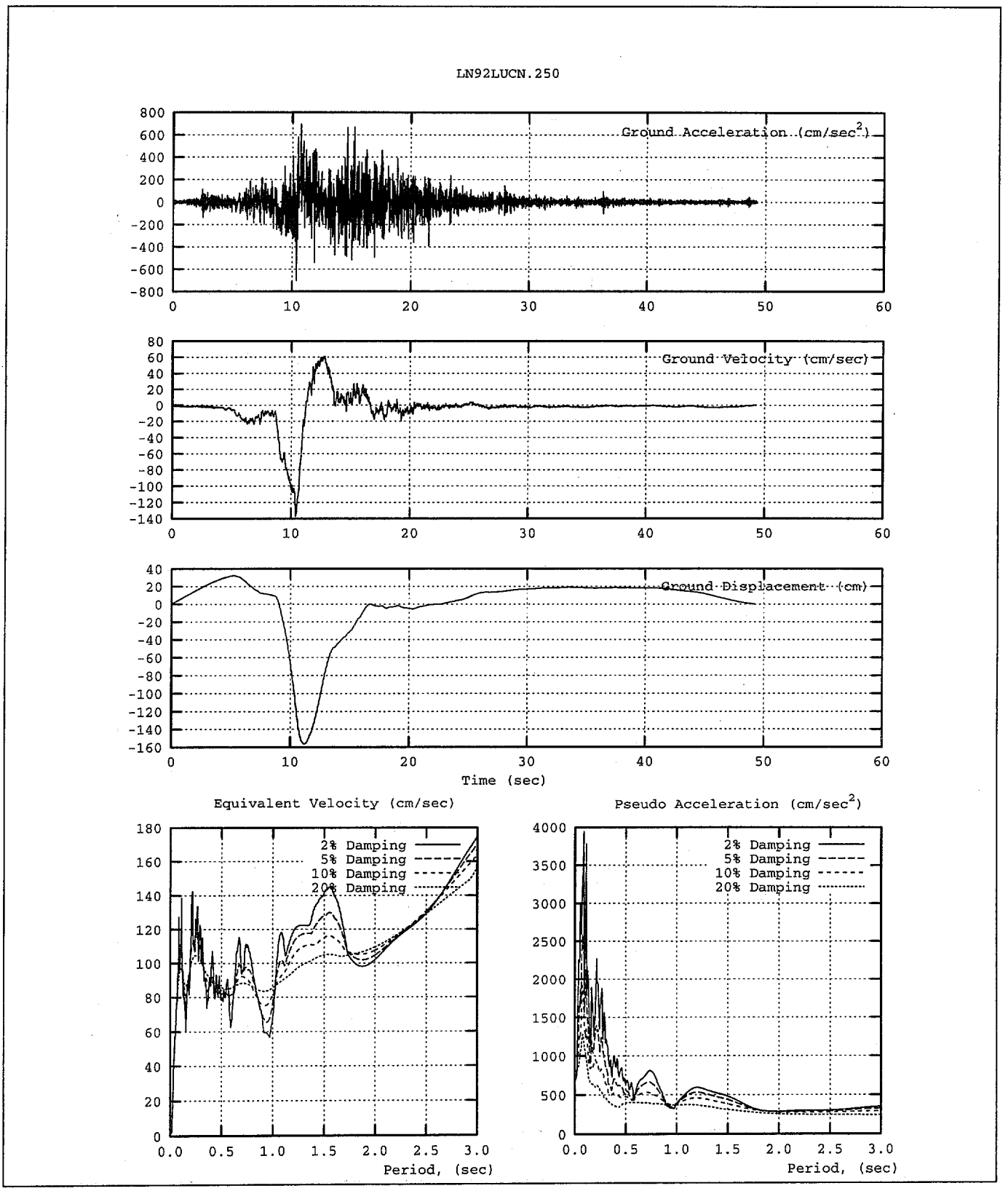

Figure 6-14 Characteristics of the LN92LUCN.250 (Lucerne) Ground Motion

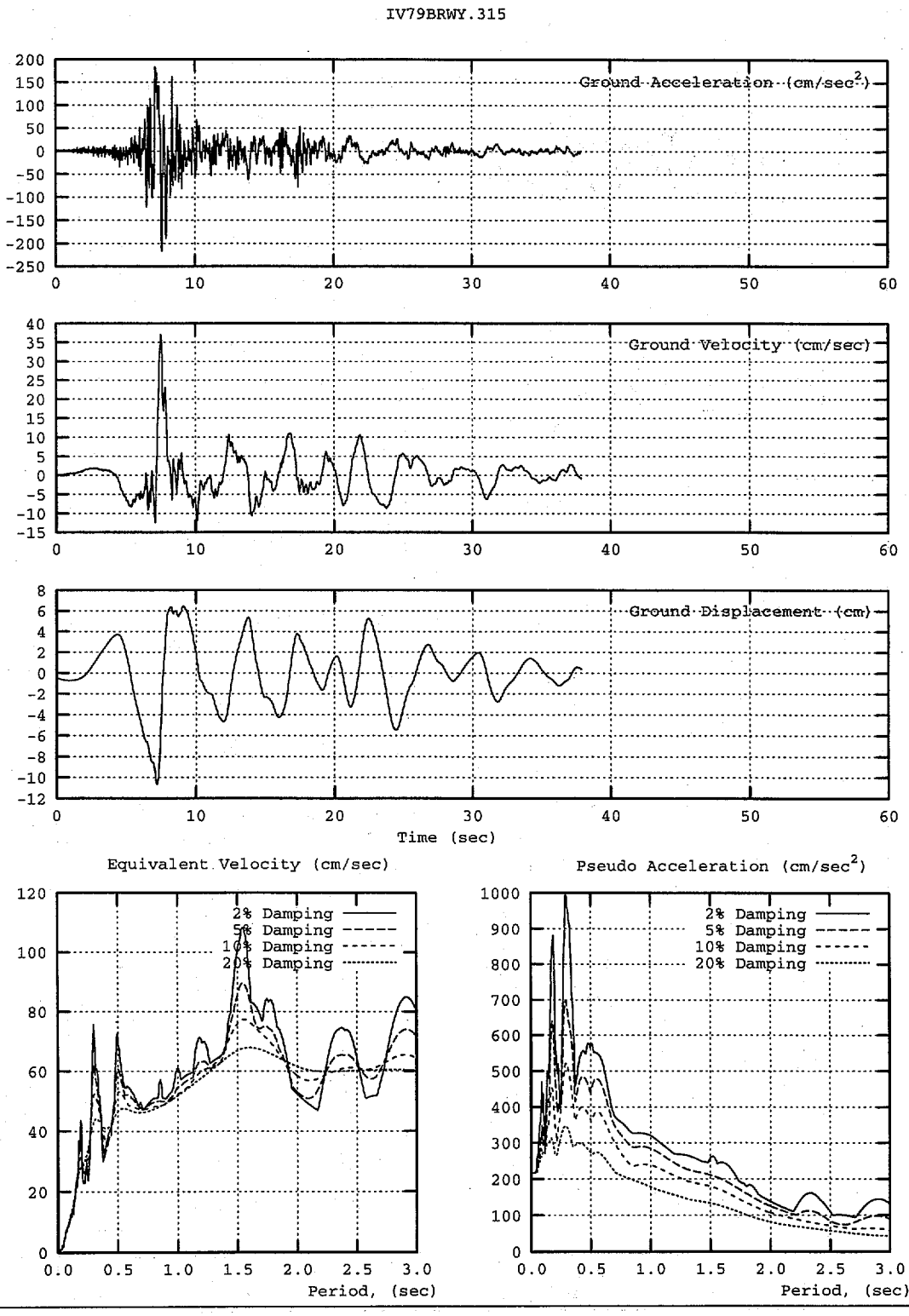

Figure 6-15 ***Characteristics of the IV79BRWY.315 (Brawley Airport) Ground Motion***

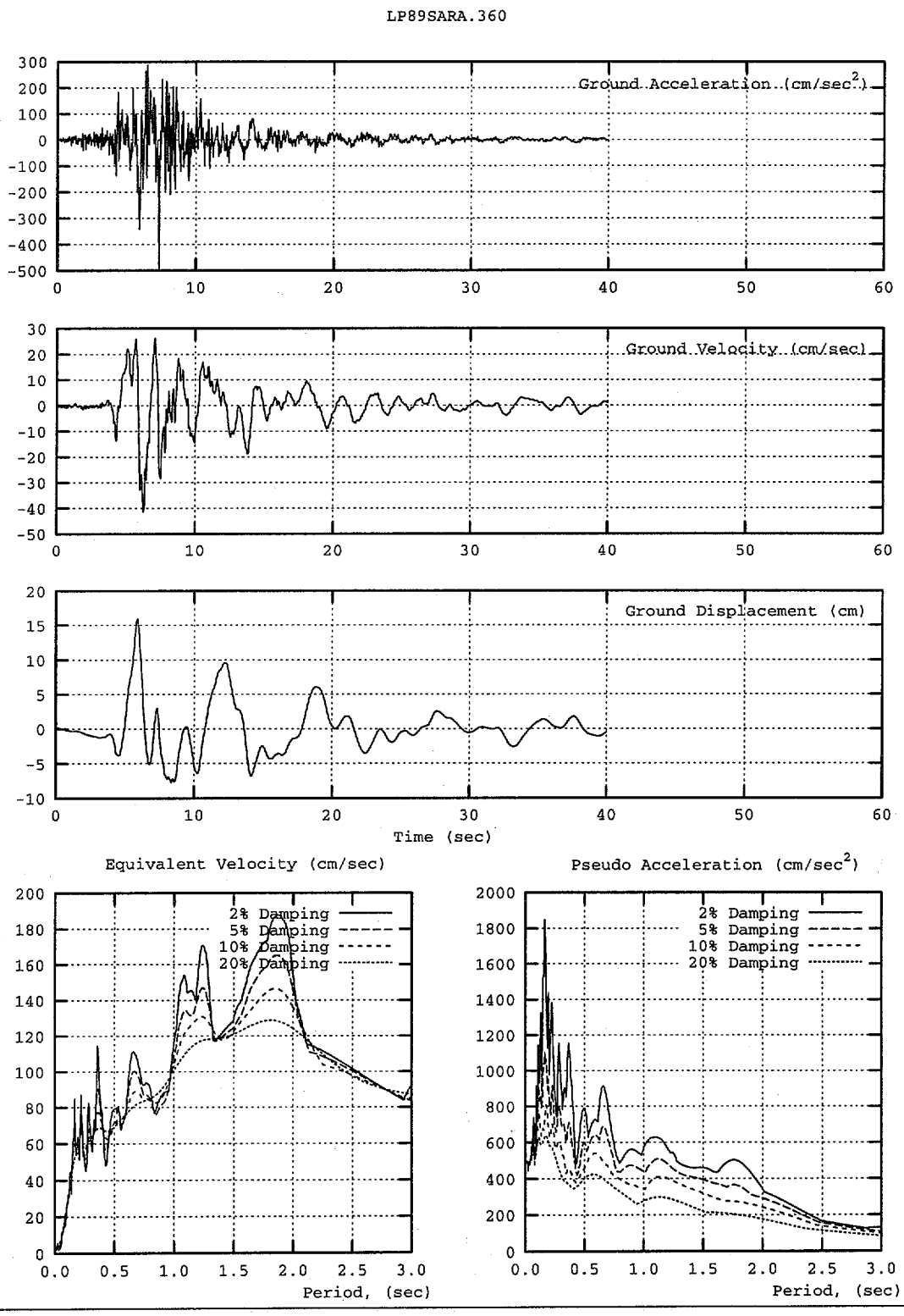

Figure 6-16 ***Characteristics of the LP89SARA.360 (Saratoga) Ground Motion***

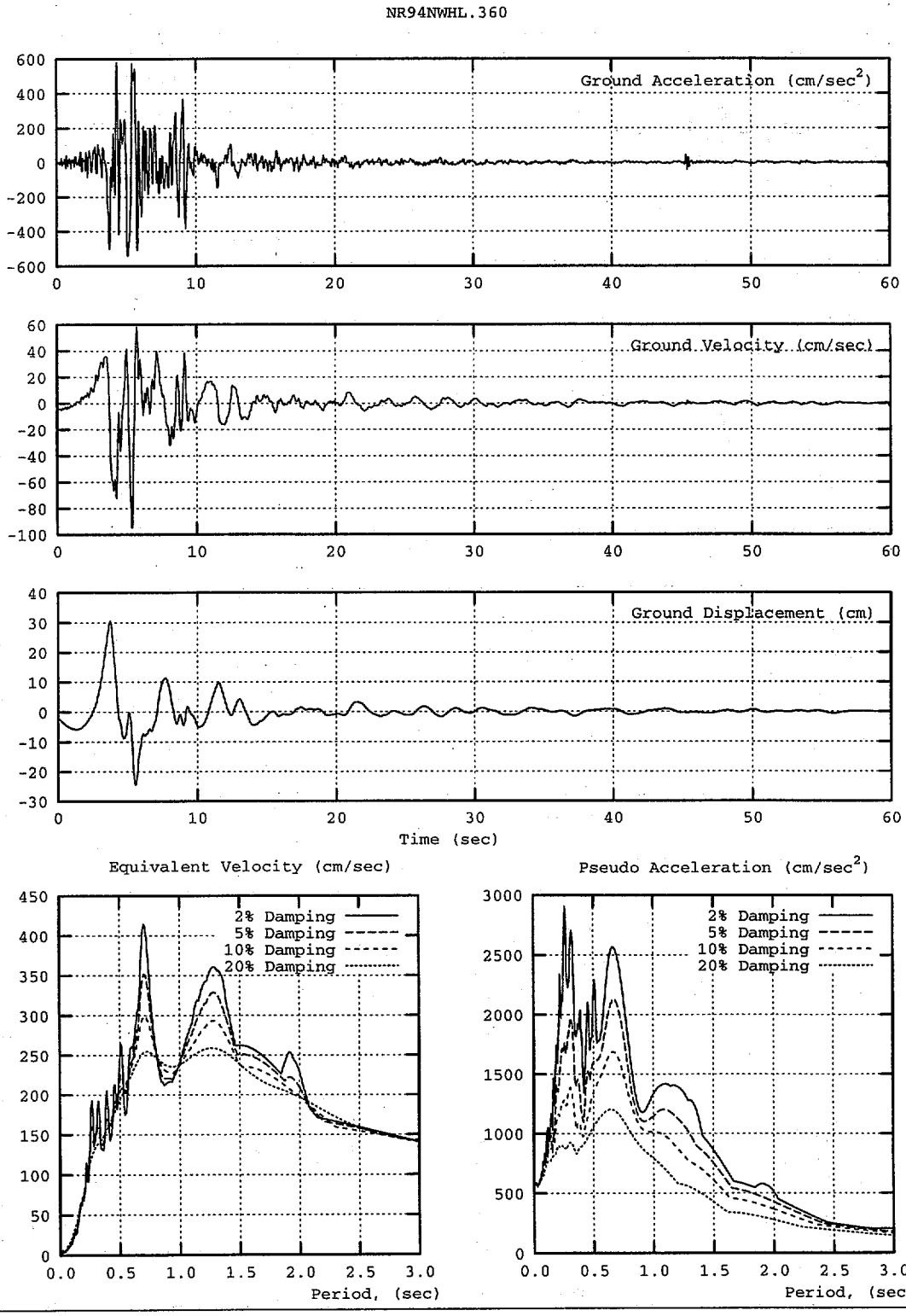

Figure 6-17 ***Characteristics of the NR94NWHL.360 (Newhall) Ground Motion***

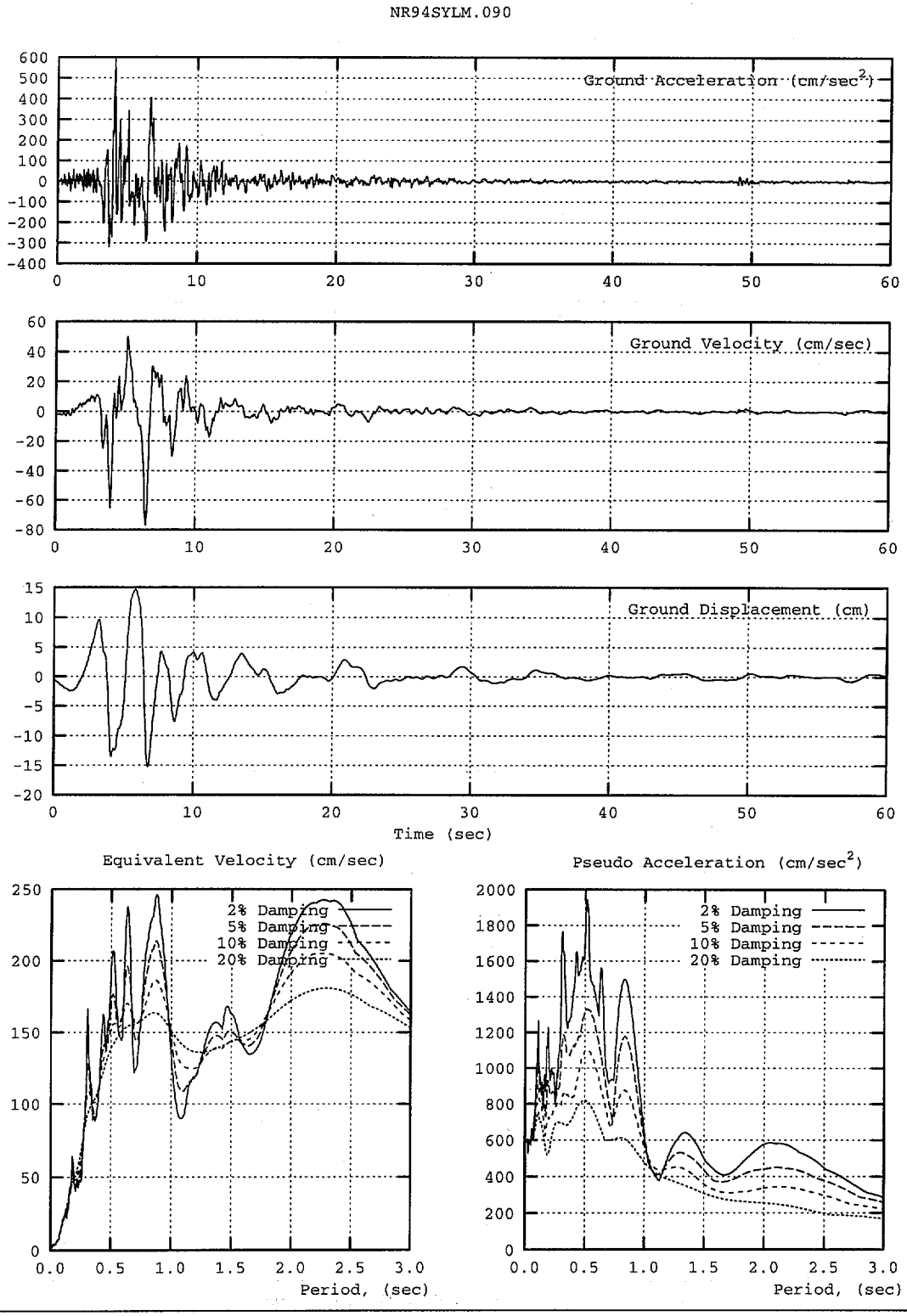

Figure 6-18 ***Characteristics of the NR94SYLH.090 (Sylmar Hospital) Ground Motion***

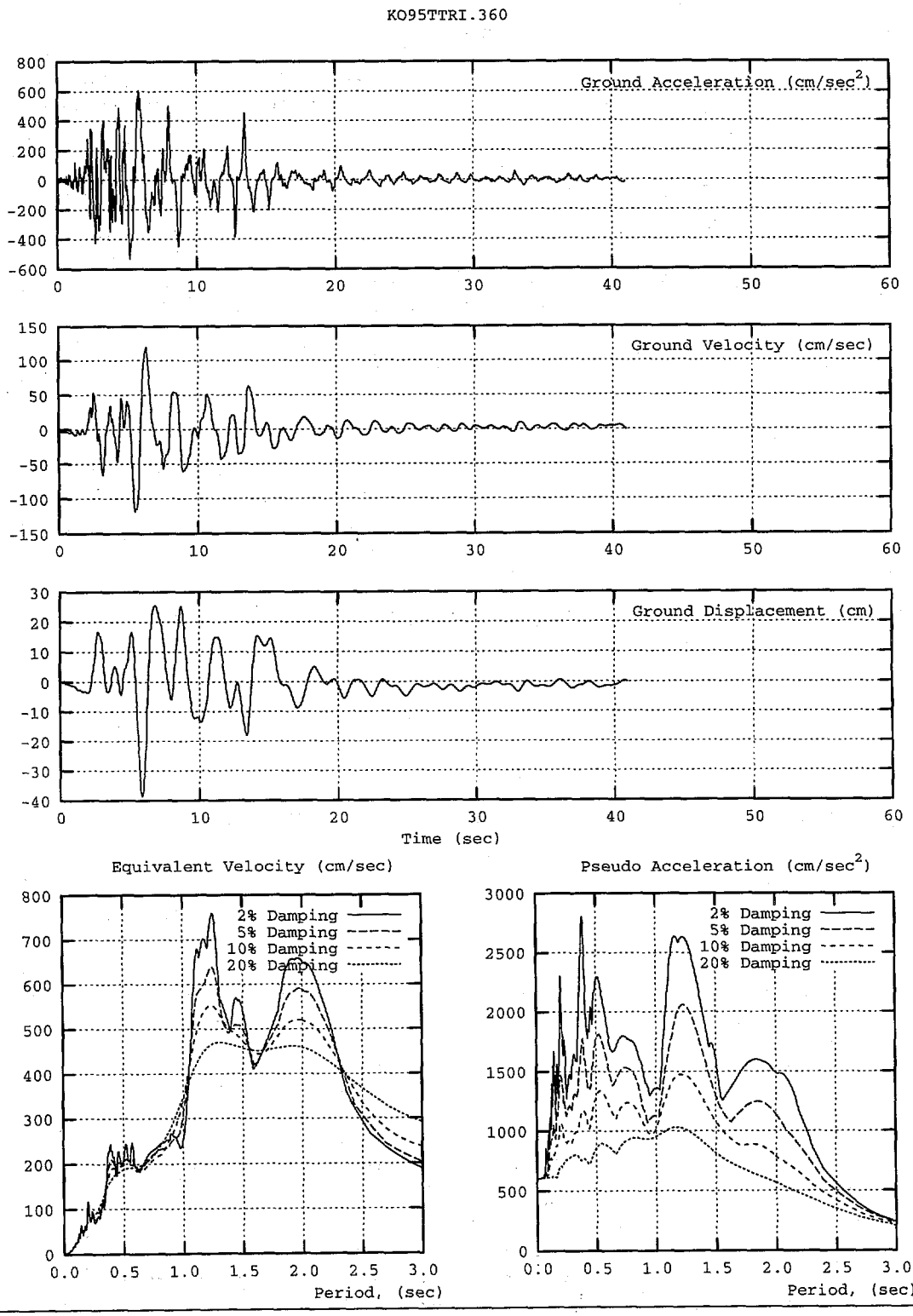

Figure 6-19 ***Characteristics of the KO95TTRI.360 (Takatori) Ground Motion***

The characteristic period, T_g, of each ground motion was established assuming equivalent-velocity spectra and pseudo-acceleration spectra for linear elastic oscillators having 5% damping. The equivalent velocity, V_m, is related to input energy, E_m, and ground acceleration and response parameters by the following expression:

$$\frac{1}{2}mV_m^2 = E_m = m\int \ddot{x}_g \dot{x} dt \qquad (6\text{-}1)$$

where m= mass of the single-degree-of-freedom oscillator, $\ddot{x}_g$ = the ground acceleration, and $\dot{x}$ = the relative velocity of the oscillator mass (Shimazaki and Sozen, 1984). The spectra present peak values calculated over the duration of the record.

The characteristic periods were determined according to engineering judgment to correspond approximately to the first (lowest-period) peak of the equivalent-velocity spectrum, and, at the same time, the period at which the transition occurs between the constant-acceleration and constant-velocity portions of a smooth design spectrum fitted to the 5% damped spectrum (Shimazaki and Sozen, 1984; Qi and Moehle, 1991; and Lepage, 1997). Characteristic periods were established prior to the dynamic analyses.

Other criteria are available to establish characteristic periods. For example, properties of the site, characterized by variation of shear-wave velocity with depth, may be used to establish T_g. Alternatively, the characteristic period may be defined as the lowest period for which the equal-displacement rule applies, and thus becomes a convenient reference point to differentiate between short- and long-period systems.

6.3.4 Force/Displacement Models

The choice of force/displacement model influences the response time-history and associated peak response quantities. Ideally, the force/displacement model should represent behavior typical of wall buildings, including strength degradation and stiffness degradation.

Actual response depends on the details of structural configuration and component response, which in turn, depend on the material properties, dimensions, and strength of the components, as well as the load environment and the evolving dynamic load history (which can influence the type and onset of failure). The objective of the dynamic analyses is to identify basic trends in how prior damage affects system response in future earthquakes. Fulfilling this objective does not require the level of modeling precision that would be needed to understand the detailed response of a particular structure or component. For this reason, we selected relatively simple models that represent a range of behaviors that might be expected in wall buildings. Three broad types of system response can be distinguished:

Type A: Stiffness-degrading systems with positive post-yield stiffness (Figure 6-20a).

Type B: Stiffness-degrading systems with negative post-yield stiffness (Figure 6-20b).

Type C: Pinched systems exhibiting strength and stiffness degradation Figure 6-20c).

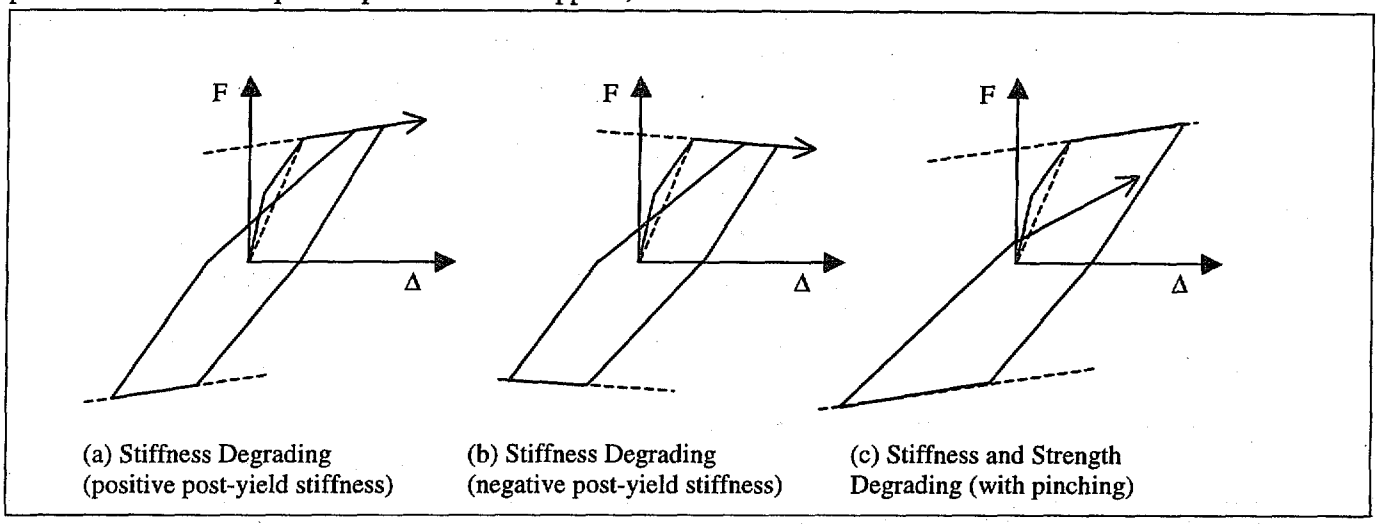

(a) Stiffness Degrading (positive post-yield stiffness)

(b) Stiffness Degrading (negative post-yield stiffness)

(c) Stiffness and Strength Degrading (with pinching)

Figure 6-20 Force-Displacement Hysteretic Models

Type A behavior typically represents wall systems dominated by flexural response. Type B behavior is more typical of wall systems that exhibit some degradation in response with increasing displacement; degradation may be due to relatively brittle response modes. Type C behavior is more typical of wall systems that suffer degradation of strength and stiffness, including those walls in which brittle modes of response may predominate.

Type A behavior was represented in the analyses using the Takeda model (Takeda et al., 1970) with post-yield stiffness selected to be 5% of the secant stiffness at the yield point (Figure 6-21a). Previous experience (Section 6.2.1) indicates that this model represents stiffness degradation in reinforced concrete members exceptionally well. In addition, it is widely known by researchers, and it uses displacement ductility to parameterize stiffness degradation. The Takeda model features a trilinear primary curve that is composed of uncracked, cracked, and yielding portions. After yielding, the unloading stiffness is reduced in proportion to the square root of the peak displacement ductility. Additional rules are used to control other aspects of this hysteretic model. This model is subsequently referred to as "Takeda5".

Type B behavior was represented in the analyses using the Takeda model with post-yield stiffness selected to be –10% of the yield-point secant stiffness (Figure 6-21b). This model is subsequently referred to as "Takeda10".

Type C behavior was represented in the analyses by a modified version of the Takeda model (Figure 6-21c). The behavior is the same as for Type A, except for modifications to account for pinching and cyclic strength degradation. The pinching point is defined independently in the first and third quadrants (Figure 6-22). The pinching-point displacement is set equal to 30% of the current maximum displacement in the quadrant. The pinching-point force level is set equal to 10% of the current maximum force level in the quadrant. Cyclic strength degradation incorporated in this model is described in Section 6.3.6. This model is subsequently referred to as "TakPinch".

Collectively, the Takeda5, Takeda10, and TakPinch models are referred to as degrading models in the body of this section. For these models, dynamic analyses were used to identify the effects of prior damage on response to future earthquakes. The analyses covered a number of relative strength values, initial periods of vibration, damage intensities, and performance-level earthquakes. For all dynamic analyses, damping was set equal to 5% of critical damping, based on the period of vibration that corresponds to the yield-point secant stiffness.

In addition, a bilinear model (Figure 6-23) was selected to establish the strength of the degrading oscillators, which were set equal to the strength required to achieve bilinear displacement ductility demands of 1 (elastic), 2, 4, and 8 for each reference period and for each of the 18 ground motions. The bilinear model does not exhibit stiffness or strength degradation. Besides establishing

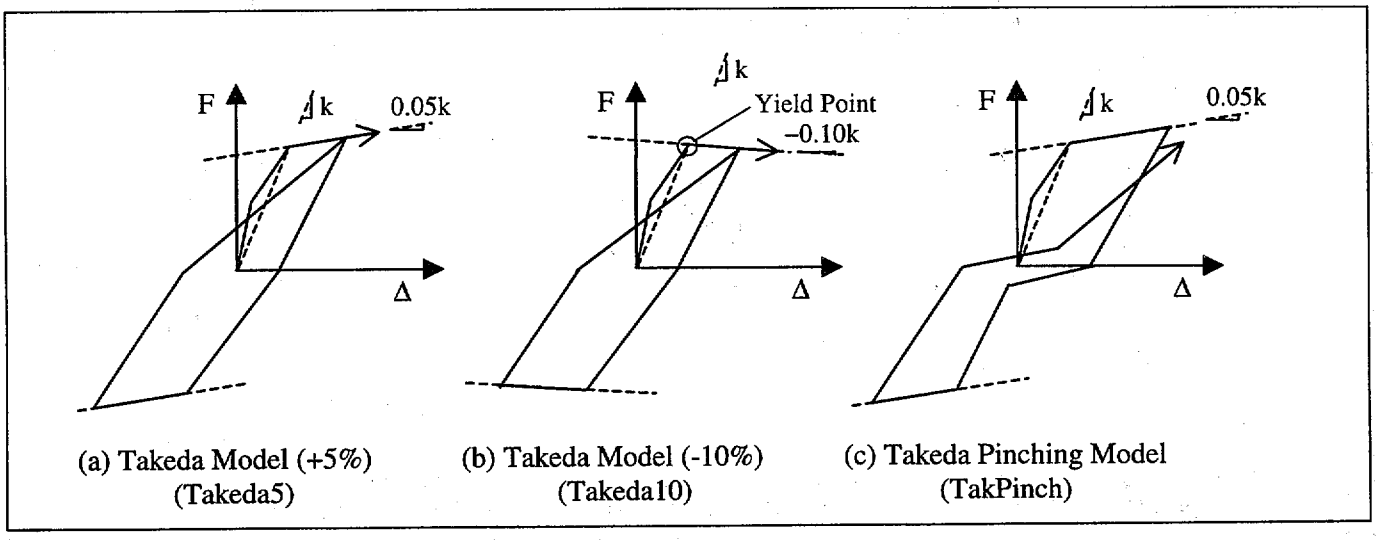

(a) Takeda Model (+5%) (Takeda5)

(b) Takeda Model (-10%) (Takeda10)

(c) Takeda Pinching Model (TakPinch)

Figure 6-21 Degrading Models Used in the Analyses

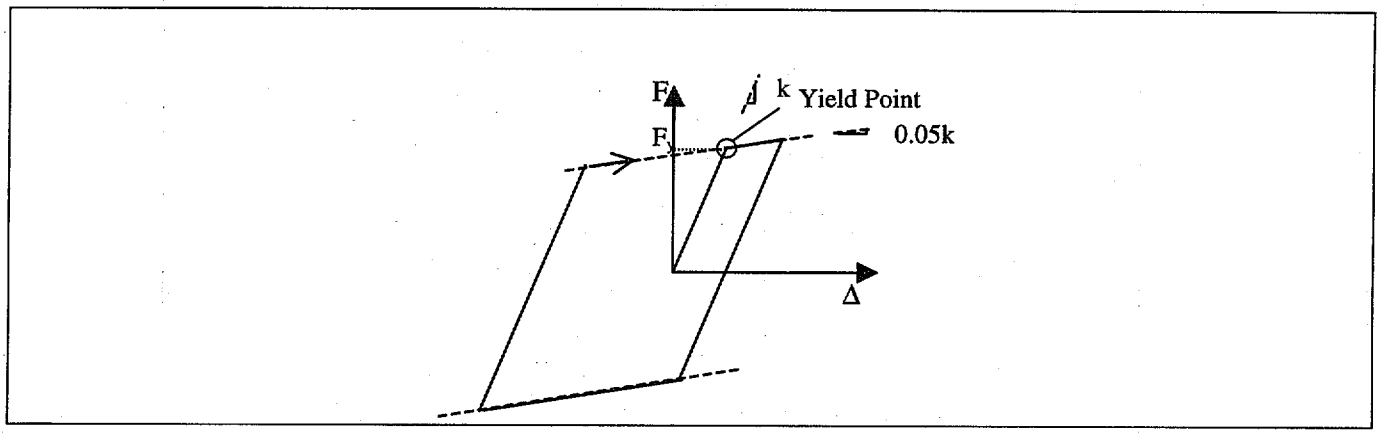

Figure 6-22 Bilinear Model Used to Determine Strengths of Degrading Models

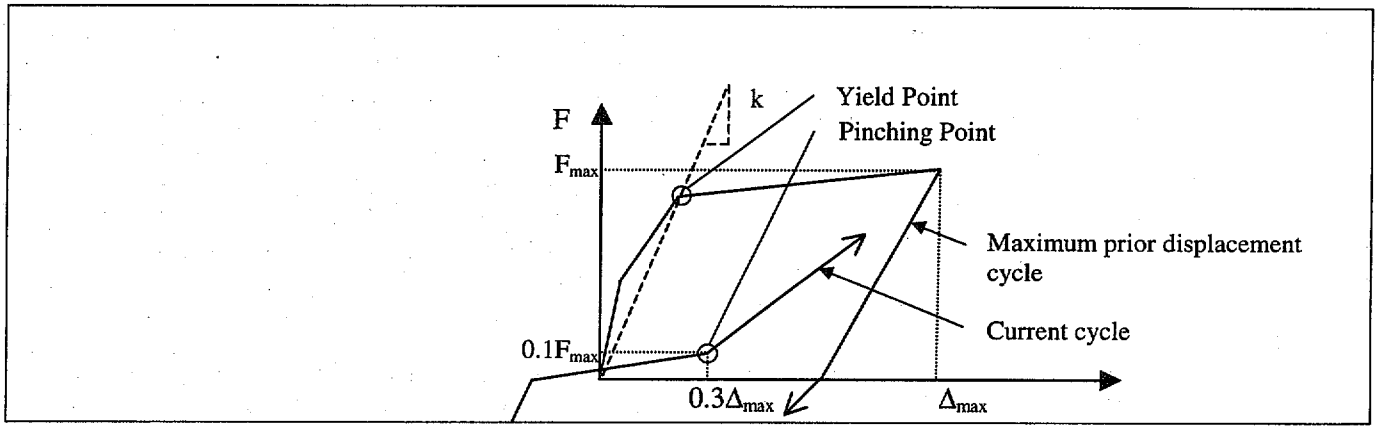

Figure 6-23 Specification of the Pinching Point for the Takeda Pinching Model

the strength of the oscillators, this model serves two additional purposes. First, results obtained in this study with the bilinear model can be compared with those obtained by other researchers to affirm previous findings and, at the same time, to develop confidence in the methods and techniques used in this study. Second, the bilinear model provides a convenient point of departure from which the effects of stiffness and strength degradation can be compared.

6.3.5 Undamaged Oscillator Parameters

To identify effects of damage on response, it is first necessary to establish the response of initially-undamaged oscillators to the same ground motions. The response of the undamaged oscillators is determined using the degrading models of Figure 6-21 for the performance-level ground motions.

The yield strength of all degrading models is set equal to the strength required to achieve displacement ductility demands (DDD) of 1 (elastic), 2, 4, and 8 using the bilinear model. This is done at each period and for each ground motion. For any period and ground motion considered, the yield strength of the initially-undamaged models is the same, but only the bilinear model achieves the target displacement ductility demand. Where the same target displacement ductility demand can be achieved for various strength values, the largest strength value is used, as implemented in the computer program PCNSPEC (Boroschek, 1991).

The initial stiffness of the models is established to achieve initial (reference) vibration periods of 0.1, 0.2, 0.3, 0.4, 0.5, 0.6, 0.8, 1.0, 1.2, 1.5, and 2.0 seconds. These periods are determined using the yield-point secant stiffness for all the models considered.

For the undamaged Takeda models, the cracking strength is set equal to 50% of the yield strength, and the uncracked stiffness is set equal to twice the yield-point secant stiffness (Figure 6-24).

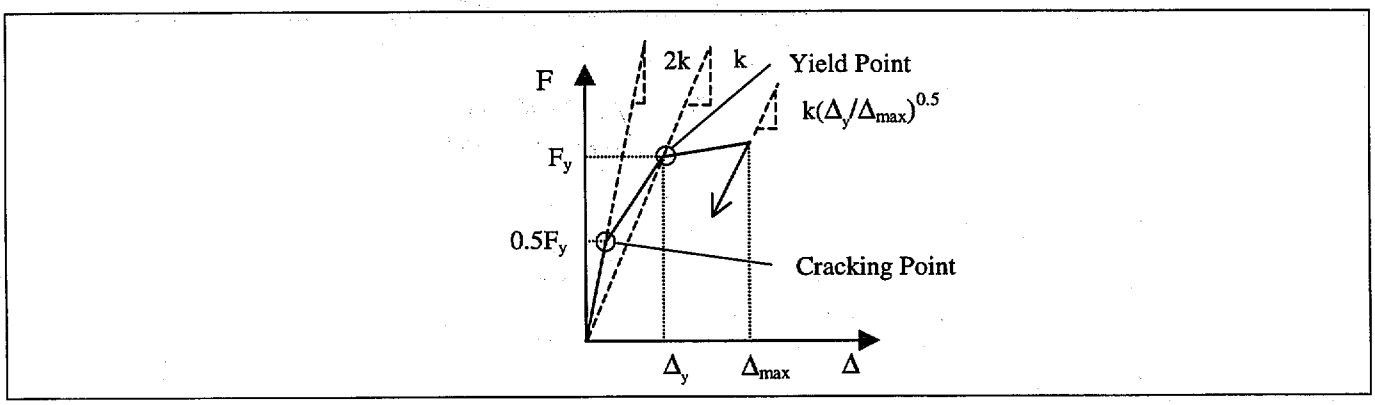

Figure 6-24 ***Specification of the Uncracked Stiffness, Cracking Strength, and Unloading Stiffness for the Takeda Models***

6.3.6 Damaged Oscillator Parameters

Damage is considered by assuming that the force-displacement curves of the oscillators are altered as a result of previous inelastic response. Reduction in stiffness caused by the damaging earthquake is parameterized by prior ductility demand. Strength degradation is parameterized by the reduced strength ratio.

Each of the initially-undamaged degrading oscillators is considered to have experienced prior ductility demand (PDD) equal to 1, 2, 4, or 8 as a result of the damaging earthquake. The construction of an initially-damaged oscillator force/displacement curve is illustrated for a value of PDD greater than zero in Figure 6-25. The prior ductility demand also regulates the unloading stiffness of the Takeda model until larger displacement ductility demands develop.

The analytical study considered damaging earthquakes of smaller intensity than the performance-level earthquake. Consequently, the PDD values considered must be less than or equal to the design displacement ductility (DDD). Thus, an oscillator with strength established to achieve a displacement ductility of 4 is analyzed only for prior displacement ductility demands of 1, 2, and 4. The undamaged Takeda oscillators sometimes had ductility demands for the performance-level earthquake that were lower than their design values (DDD). Again, because the damaging earthquake is considered to be less intense than the performance-level event, oscillators having PDD in excess of the undamaged oscillator response were not considered further.

The Takeda models of the undamaged oscillators represent cracking behavior by considering the uncracked stiffness and the cracking strength. The effects of cracking in a previous earthquake were assessed by comparing the peak displacement response

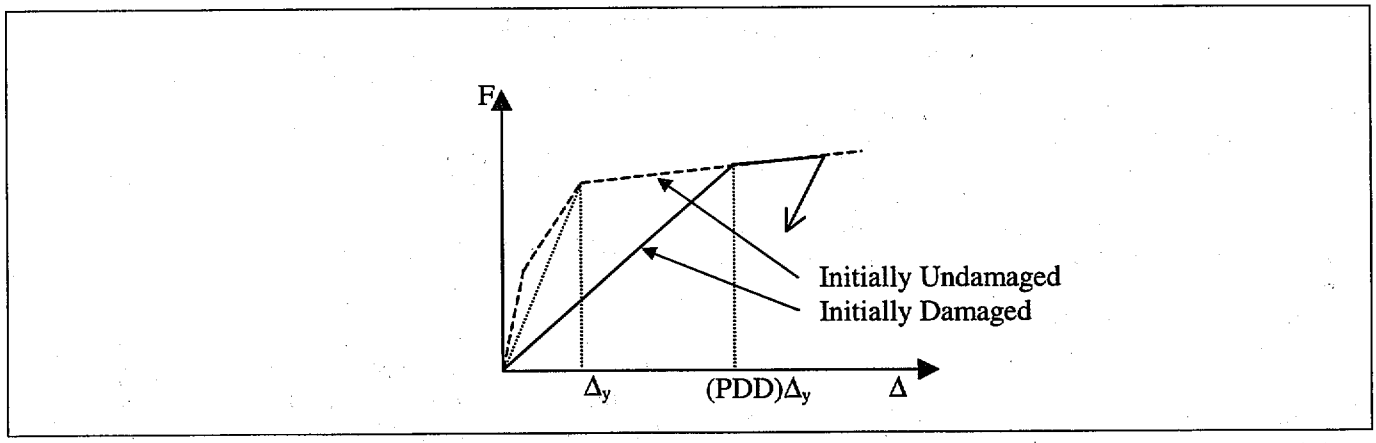

Figure 6-25 ***Construction of Initial Force-Displacement Response for Prior Ductility Demand > 0 and Reduced Strength Ratio = 1***

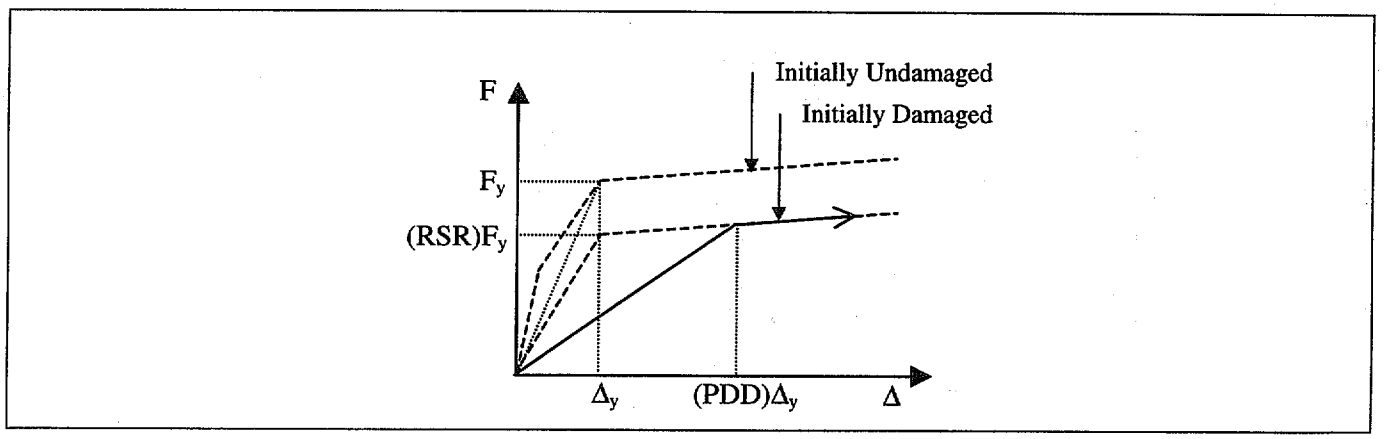

Figure 6-26 ***Construction of Initial Force-Displacement Response for PDD> 0 and RSR< 1 for Takeda5 and Takeda10 Models***

of initially-uncracked oscillators to the response of oscillators that are initially cracked; that is, Takeda oscillators having a PDD of one. When larger PDD values are considered, the reductions in initial loading and unloading stiffness are determined in accordance with the Takeda model.

It is not obvious what degree of strength degradation is consistent with the PDDs, nor just how the degradation of strength should be modeled to represent real structures. We used two approaches to gauge the extent to which strength degradation might affect the response:

1. Takeda5 and Takeda10 Oscillators: The initial strength of the damaged models was reduced to try to capture the gross effects of strength degradation on response. The initial response of the damaged oscillator was determined using the construction of Figure 6-26. The resulting curve may represent a backbone curve that is constructed to approximate the response of a strength-degrading oscillator. For example, a structure for which repeated cycling causes a 20% degradation in strength relative to the primary curve may be modeled as having an initial strength equal to 80% of the undegraded strength.

   If the backbone curve is established using the expected degraded-strength asymptotes, then the modeled structure tends to have smaller initial stiffness and larger displacement response relative to the ideal degrading structure. Consequently, the modeled response is expected to give an upper bound to the displacement response expected from the ideal model. If, instead, the backbone curve is selected to represent an average degraded response, using typical degraded-strength values rather than the lower asymptotic values, the computed response should more closely approximate the response of the ideal model.

2. TakPinch Oscillators: Rather than begin with a reduced strength, a form of cyclic strength degradation was explicitly modeled for the Takeda Pinching oscillators. A trilinear primary curve was established (Figure 6-27), identical to the envelope curve used in the Takeda5 model. The curve exhibits cracking, a yield strength determined from the response of the bilinear models, and a post-yield stiffness equal to 5% of the yield-point secant stiffness. A secondary curve is established, having the same yield displacement and post-yield stiffness as the primary curve, but having yield strength equal to the reduced strength ratio (RSR) times the primary yield strength. For displacements less than the current maximum displacement in the quadrant, a reduced-strength point is defined at the maximum displacement at $0.5^n(1\text{-}RSR)F_y$ above the secondary curve strength, where n is the number of cycles approaching the current maximum displacement. The oscillator may continue beyond this displacement, and once it loads along the primary curve, n is reset to one, to cause the next cycle to exhibit strength degradation. The term $(1\text{-}RSR)F_y$ is simply the strength difference between the primary and secondary curves, and the function 0.5^n represents an asymptotic approach toward the secondary curve with each cycle. In each cycle, the strength is reduced by half the distance remaining between the current curve and the secondary curve. Pinching and strength degradation are modeled independently in the first and third quadrants.

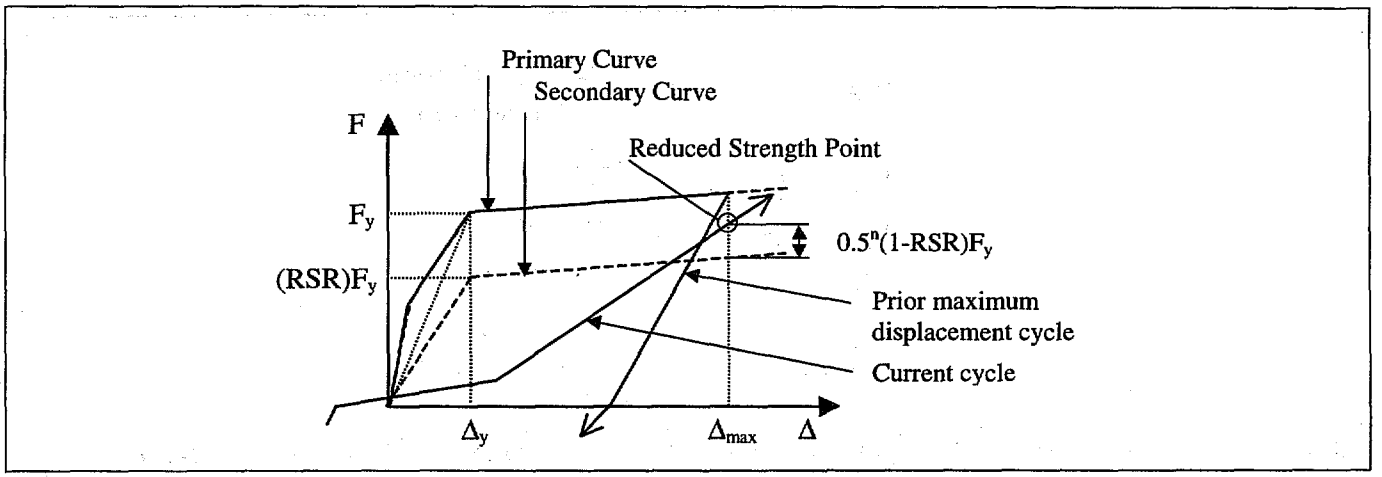

Figure 6-27 Strength Degradation for Takeda Pinching Model

For the TakPinch models, strength degradation is modeled with and without PDD. When PDD is present, the oscillator begins with *n* equal to one. This represents a single previous cycle to the PDD displacement, and corresponds to initial loading towards a reduced-strength point halfway between the primary and secondary curves at the PDD displacement (Figure 6-28).

For the other degrading models, strength reduction is considered possible only for PDDs greater than zero.

The parameter RSR is used to describe strength degradation in the context of the Takeda Pinching models and strength reduction in the context of the other degrading models. For this study, values of RSR were arbitrarily set at 100%, 80%, and 60%.

Oscillators were referenced by their initial, undamaged vibration periods, determined using the yield-point secant stiffness, regardless of strength loss and PDDs. Note that changes in strength further affect the initial stiffness of the damaged oscillators.

While the values of the parameters used to model Type A, B, and C behaviors, as well as the hysteresis rules themselves, were chosen somewhat arbitrarily, they were believed to be sufficiently representative to allow meaningful conclusions to be made regarding the effects of prior damage on response characteristics of various wall structures. Values of RSR and PDD were selected to identify trends in response characteristics, not to represent specific structures.

6.3.7 Summary of Dynamic Analysis Parameters

Nonlinear dynamic analyses were conducted for SDOF systems using various force/displacement models, various initial strength values, and for various degrees of damage. The analyses were repeated for the 18 selected ground-motion records. The analysis procedures are summarized below.

1. Initially-undamaged oscillators were established at eleven initial periods of vibration, equal to 0.1, 0.2, 0.3, 0.4, 0.5, 0.6, 0.8, 1.0, 1.2, 1.5, and 2.0 seconds. At these periods, the strength necessary to obtain design displacement ductilities (DDDs) of 1 (elastic), 2, 4, and 8 were obtained using the bilinear model for each earthquake. This procedure establishes 44 oscillators for each of 18 ground motions.
2. The responses of the oscillators designed in step 1 were computed using the three degrading models (Takeda5, Takeda10, and TakPinch). The yield strength of the degrading oscillators in this step is identical to that determined in the previous step for the bilinear model. The period of vibration of the degrading oscillators, when based on the yield-point secant stiffness, matches that determined in the previous step for the bilinear model.
3. Damage is accounted for by assuming that the force/displacement curves of the oscillators are altered as a result of previous inelastic response. The extent of prior damage is parameterized by PDD. For some cases, the strength of the oscillators is reduced as well. Each of the initially-undamaged, degrading oscillators was considered to have experienced a PDD equal to 1, 2, 4, or 8, but not in excess of the ductility demand for which the oscilla-

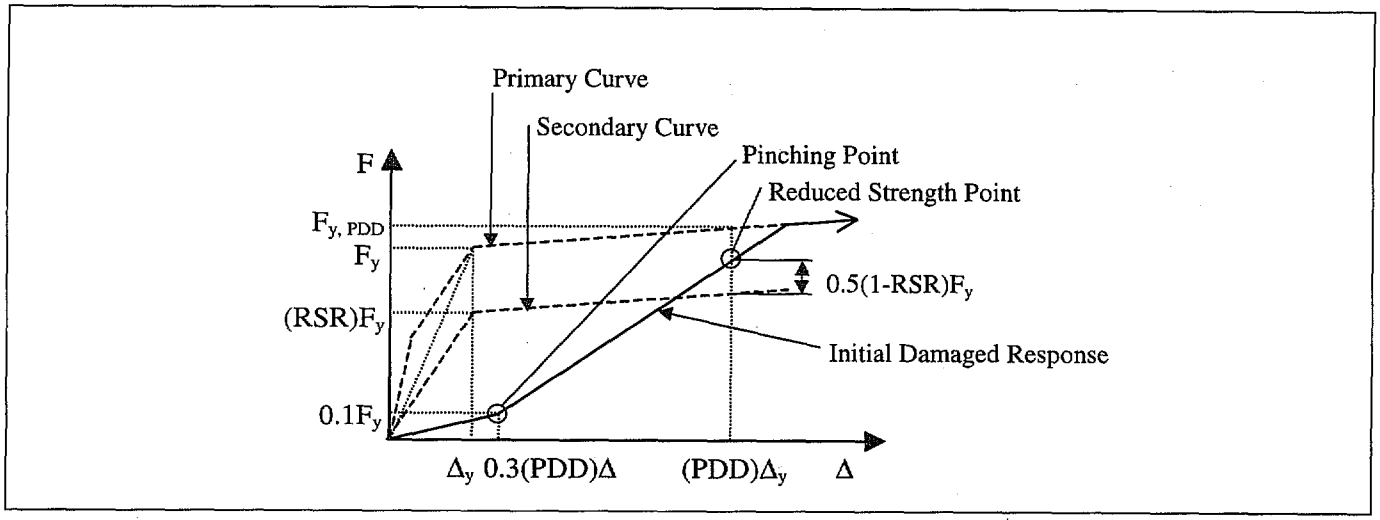

Figure 6-28 Construction of Initial Force-Displacement Response for PDD> 0 and RSR< 1 for Takeda Pinching Model

tor was designed. The effects of cracking on response were determined by considering a PDD of one. Where larger PDDs are considered, reductions in the initial loading and unloading stiffness were determined in accordance with the Takeda model.

4. Strength degradation was modeled explicitly in the TakPinch model. In the Takeda5 and Takeda10 models, strength degradation was approximated by reducing the initial strength of the damaged Takeda5 and Takeda10 models. RSRs equal to 100%, 80%, and 60% were considered. Although the strength reduction considered in the Takeda 5 and Takeda10 models does not model the evolution of strength loss, it suggests an upper bound for the effect of strength degradation on response characteristics.

6.3.8 Implementation of Analyses

Over 22,000 inelastic SDOF analyses were conducted using a variety of software programs. The strength of the oscillators was determined using constant-ductility iterations for the bilinear oscillators using the program PCNSPEC (Boroschek, 1991), a modified version of NONSPEC (Mahin and Lin , 1983). Response of the Takeda models was computed using a program developed by Otani (1981). This program was modified at the University of Illinois to include the effects of PDD, pinching, and strength degradation and to identify collapse states for models with negative post-yield stiffness.

6.4 Results Of Dynamic Analyses

6.4.1 Overview and Nomenclature

This section describes results obtained from the dynamic analyses. Section 6.4.2 characterizes the ground motions in terms of strength and displacement demand characteristics for bilinear oscillators, in order to establish that the ground motions and procedures used give results consistent with previous studies. Section 6.4.3 discusses the response of the Takeda models in some detail, for selected values of parameters. Section 6.4.4 presents summary response statistics for the Takeda models for a broader range of parameter values.

Several identifiers are used in the plots, as follows:

Records:
SD= Short-duration ground motions.
LD= Long-duration ground motions.
FD= Forward-directivity ground motions.

DDD: Design Displacement Ductility. Strength was determined to achieve the specified DDD response for bilinear oscillators having post-yield stiffness equal to 5% of the initial stiffness. Values range from 1 to 8.

PDD: Prior Ductility Demand. This represents a modification of loading and unloading stiffness, to simulate damage caused by

previous earthquakes. Values range from 1 to 8, but not in excess of DDD.

RSR: Reduced Strength Ratio. This represents a reduction or degradation of strength and associated changes in stiffness. Values ranges from 100% to 60%, as detailed in Figures 6-26, 6-27, and 6-28.

Displacements:

d_d = Peak displacement response of undamaged oscillator

d'_d = Peak displacement response of damaged oscillator

d_e = Peak displacement response of elastic oscillator having stiffness equal to the yield-point secant stiffness of the corresponding Takeda oscillator

Space constraints limit the number of included figures. Selected results for oscillators designed for a displacement ductility of 8 are presented below. Elastic response characteristics are presented as part of the ground motion plots in Figures 6-2 to 6-19.

6.4.2 Response of Bilinear Models

Figures 6-29 to 6-31 present the response of bilinear models to the SD, LD, and FD ground motions, respectively. The ratio of peak displacement of the inelastic model to the peak displacement response of an elastic oscillator having the same initial period, d_d/d_e, is presented in the upper plot of each figure. The lower plot presents the ratio of elastic strength demand to the yield strength provided in order to attain the specified DDD, which in this case equals 8.

When the strength reduction factor, R, has a value of 8, the inelastic design strength is 1/8 of the elastic strength. For DDD = 8, an R = 8 means that the reduced inelastic design strength and the resulting oscillator ductility are equal. If R is greater than 8, say 12, for DDD = 8, then the reduced inelastic design strength of the structure can be 1/12 of the expected elastic strength to achieve an oscillator ductility of 8. That is, for any R, the structure can be designed for $1/R$ times the elastic needed strength to achieve a ductility of DDD.

Response to each ground motion is indicated by the plotted symbols, which are ordered by increasing characteristic period, T_g. It was found that the displacement and strength data are better organized when plotted against the ratio T/T_g instead of the reference period, T. The plots present data only for $T/T_g < 4$ in order to reveal sufficient detail in the range $T/T_g < 1$.

The trends shown in Figures 6-29 through 6-31 resemble those reported by other researchers, for example, Shimazaki and Sozen (1984), Miranda (1991), and Nassar and Krawinkler (1991). However, it can be observed that the longer-period structures subjected to ground motions with forward-directivity effects show a peak displacement response in the range of approximately 0.5 to 2 times the elastic structure response, somewhat in excess of values typical of the other classes of ground motion. Additionally, strength-reduction factors, R, tend to be somewhat lower for the FD motions, representing the need to supply a greater proportion of the elastic strength demand in order to maintain prespecified DDDs.

6.4.3 Response of Takeda Models

The Takeda models were provided with lateral strength equal to that determined to achieve specified DDDs of 1, 2, 4, and 8 for the corresponding bilinear models, based on the yield-point secant stiffness.

Prior damage was parameterized by prior ductility demand (PDD), possibly in conjunction with strength reduction or strength degradation, which is parameterized by RSR. PDD greater than zero (damage present) and RSR less than one (strength reduced or degrading) both cause the initial period of the oscillator to increase. When previous damage has caused displacements in excess of the yield displacement (PDD>1), even small displacements cause energy dissipation through hysteretic response. No further attention is given to those oscillators for which the imposed PDD exceeds the response of the undamaged oscillator, and these data points are not represented on subsequent plots.

6.4.3.1 Response of the Takeda5 Model

It is of interest to observe how structures proportioned based on the bilinear model respond if their force/displacement response is represented more accurately by a Takeda model. This interest is based in part on the widespread use of the bilinear model in developing current displacement-based design approaches.

Figures 6-32 through 6-34 present the response of Takeda5 models in which the oscillator strength was set to achieve a bilinear displacement ductility demand of 8. The upper plot of each figure shows the ratio of peak displacement response to the peak response of an elastic

(Text continued on page 134)

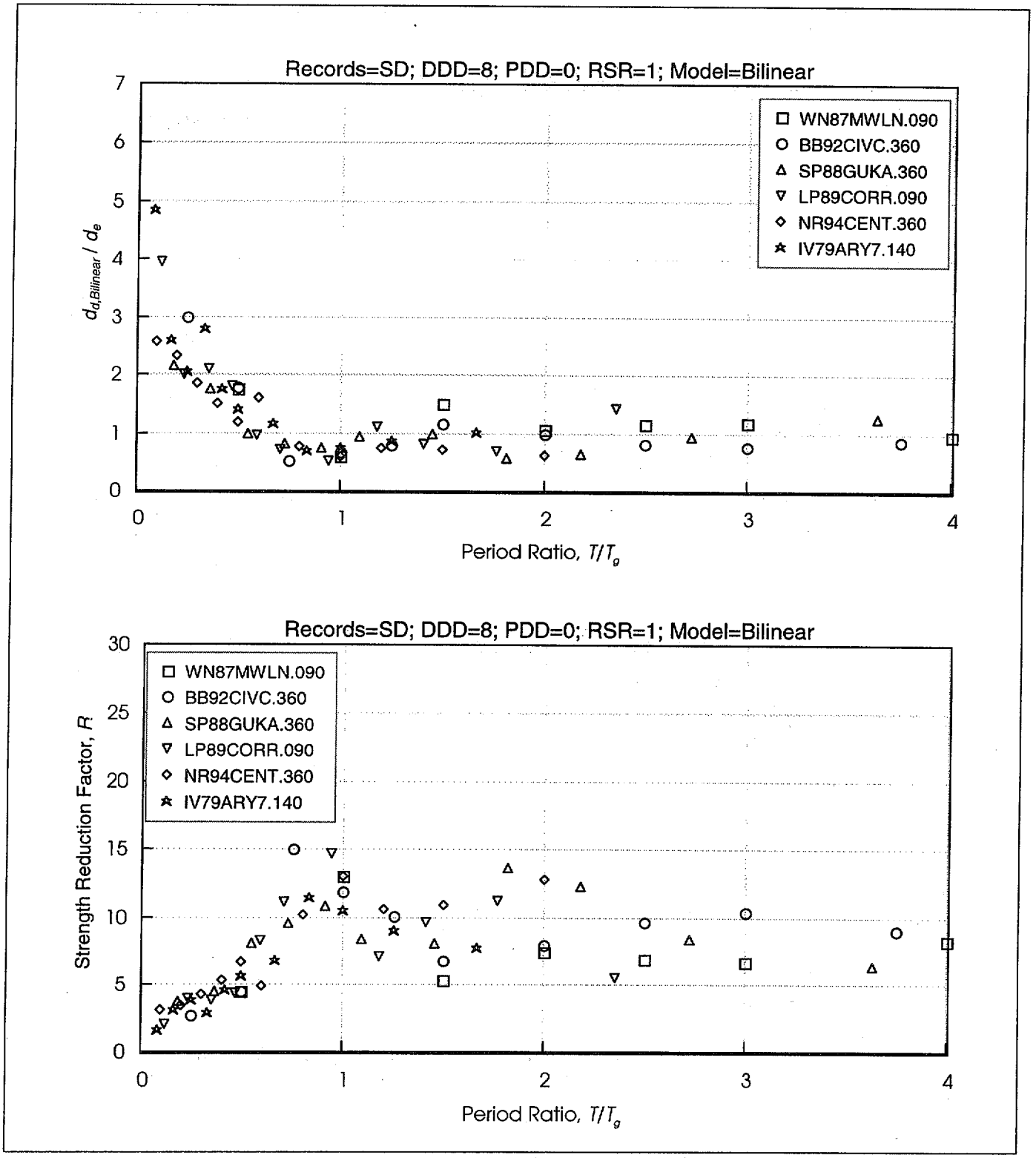

Figure 6-29 ***Response of Bilinear Oscillators to Short Duration Records (DDD= 8)***
DDD = Design Displacement Ductility; PDD = Prior Ductility Demand; RSR = Reduced Strength Ratio

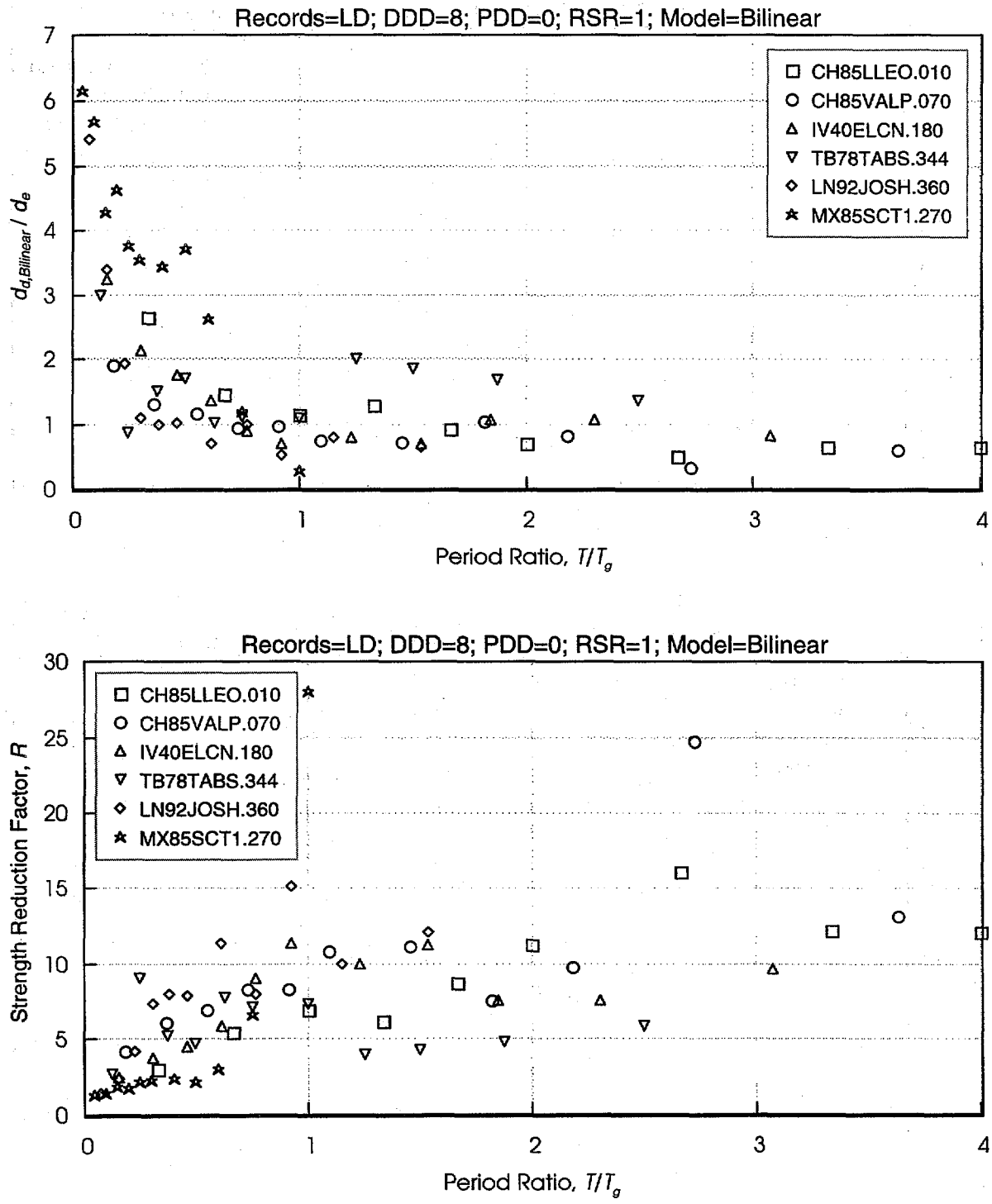

Figure 6-30 ***Response of Bilinear Oscillators to Long Duration Records (DDD= 8)***
DDD = Design Displacement Ductility; PDD = Prior Ductility Demand; RSR = Reduced Strength Ratio

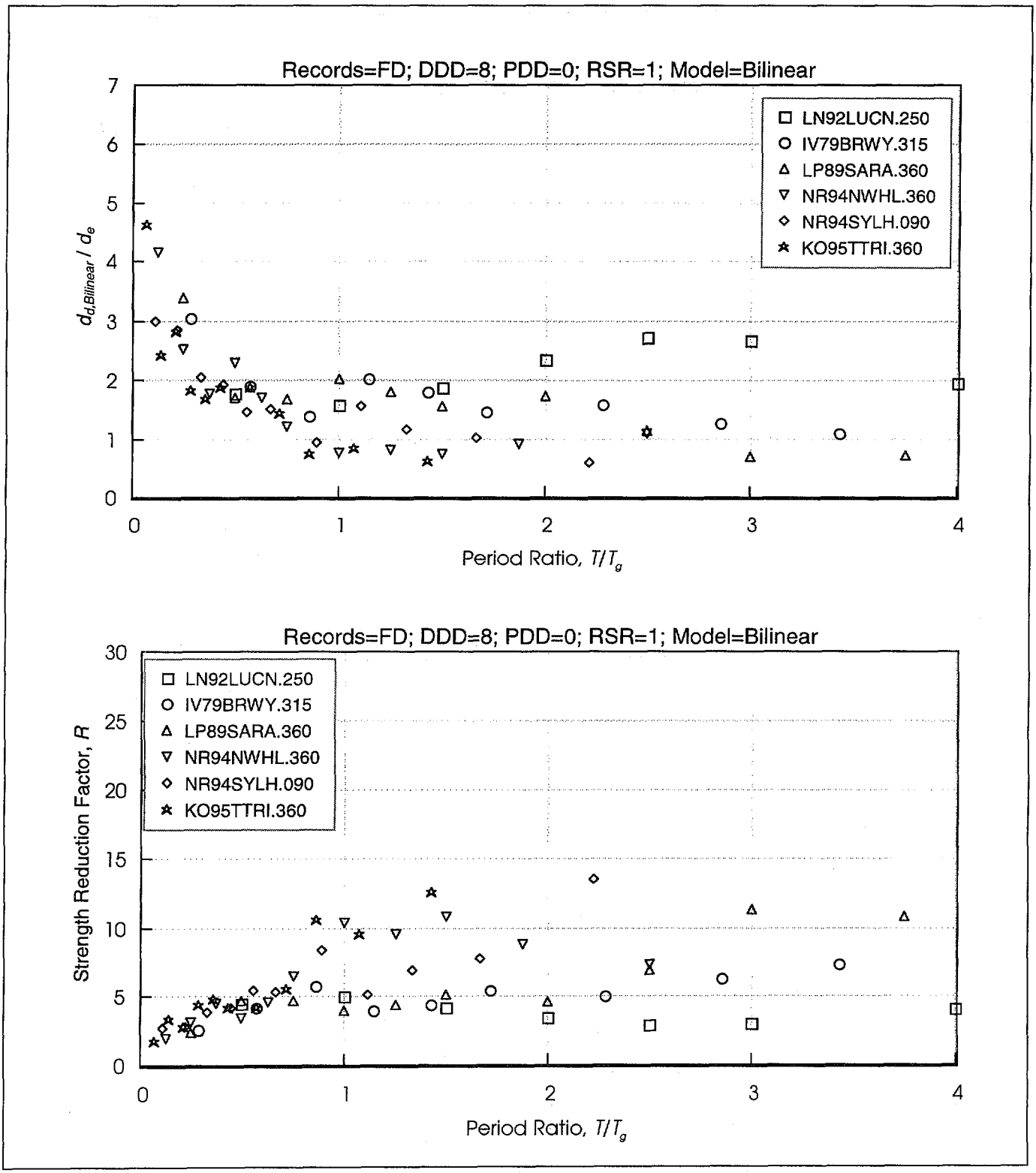

Figure 6-31 ***Response of Bilinear Oscillators to Forward Directive Records (DDD= 8)***
DDD = Design Displacement Ductility; PDD = Prior Ductility Demand; RSR = Reduced Strength Ratio

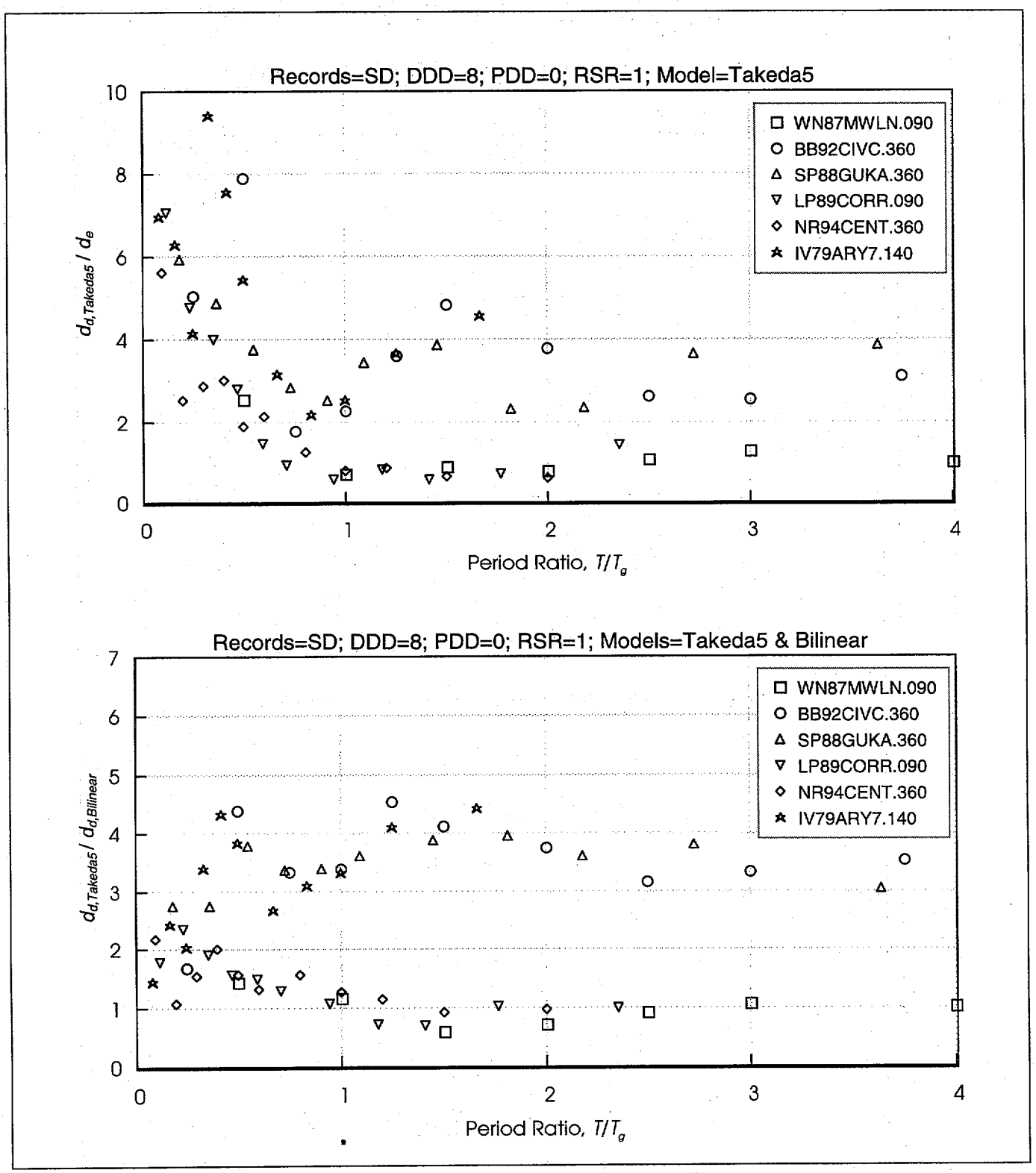

Figure 6-32 ***Displacement Response of Takeda Models Compared with Elastic Response and Bilinear Response, for Short-Duration Records (DDD= 8 and RSR= 1)***
DDD = Design Displacement Ductility; PDD = Prior Ductility Demand; RSR = Reduced Strength Ratio

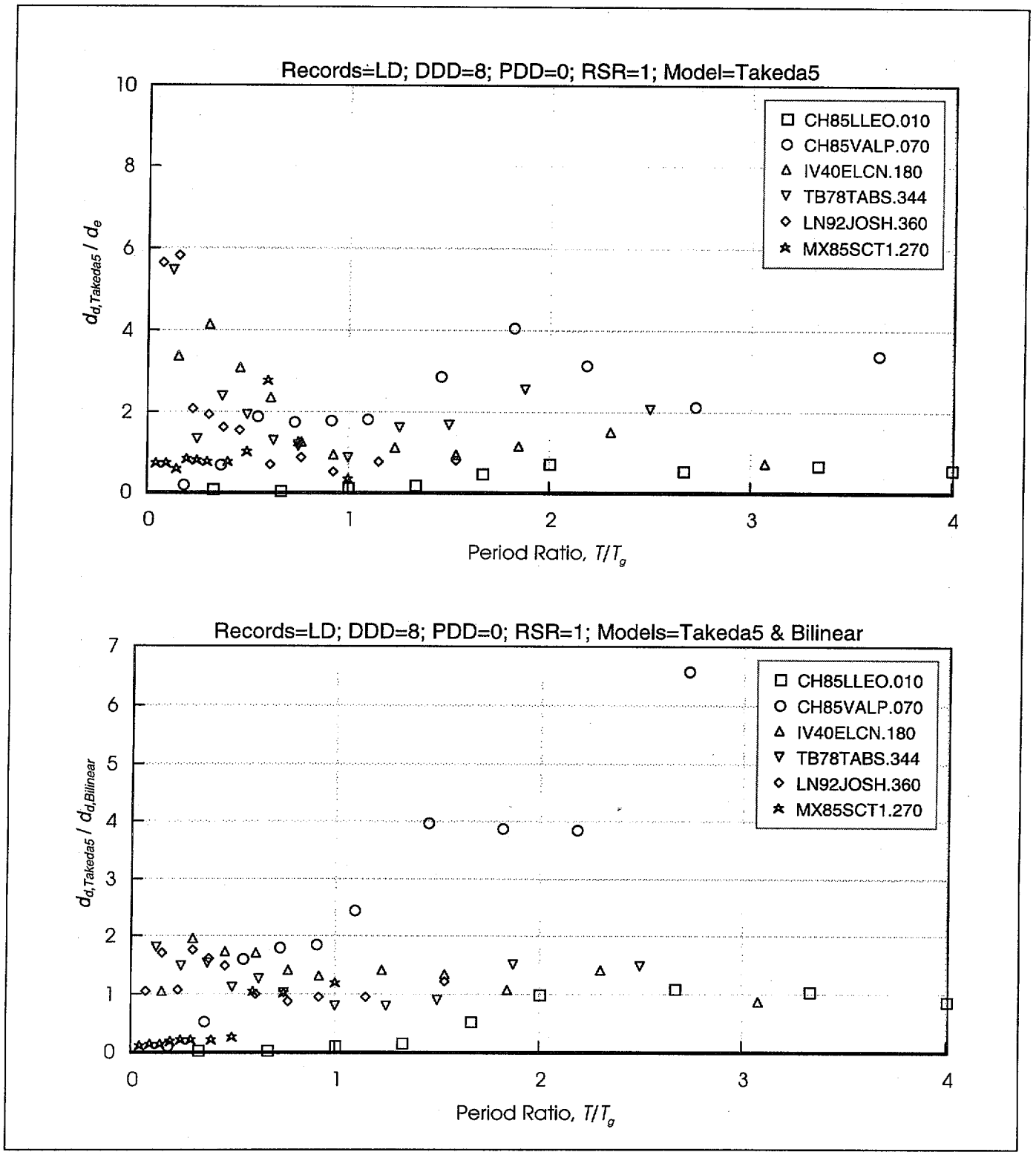

Figure 6-33 ***Displacement Response of Takeda Models Compared with Elastic Response and Bilinear Response for Long-Duration Records (DDD= 8 and RSR= 1)***
DDD = Design Displacement Ductility; PDD = Prior Ductility Demand; RSR = Reduced Strength Ratio

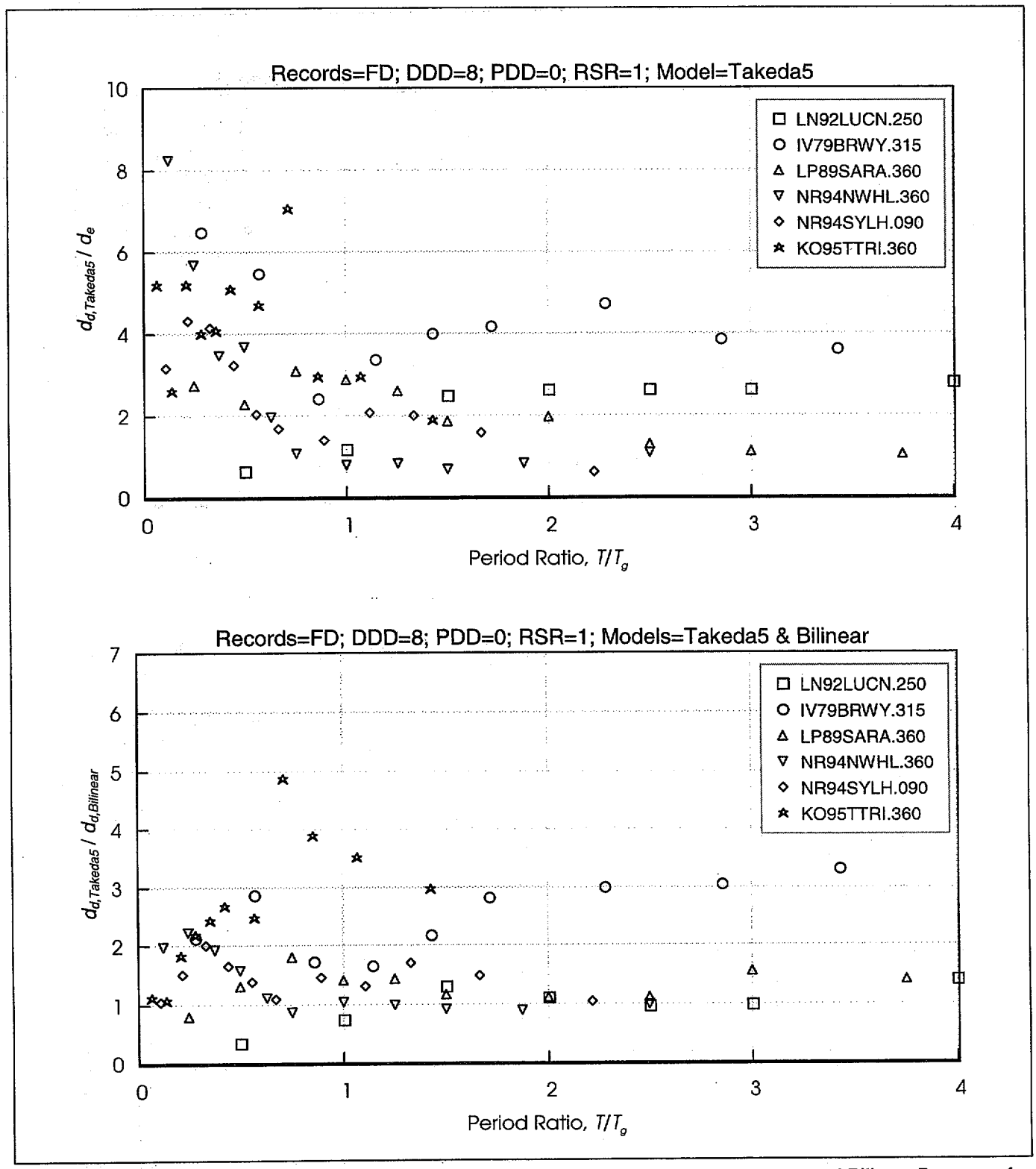

Figure 6-34 ***Displacement Response of Takeda Models Compared with Elastic Response and Bilinear Response for Forward Directive Records (DDD= 8 and RSR= 1)***
DDD = Design Displacement Ductility; PDD = Prior Ductility Demand; RSR = Reduced Strength Ratio

analog, d_d/d_e. The upper plots of Figures 6-32 through 6-34 are analogous to those presented in Figures 6-29 through 6-31.

The lower plots of Figures 6-32 through 6-34 show the ratio of the Takeda5 and bilinear ultimate displacements, $d_{d,Takeda5}/d_{d,Bilinear}$. It is clear that peak displacements of the Takeda model may be several times larger or smaller than those obtained with the corresponding bilinear model.

The effect of damage on the Takeda5 model is shown in Figures 6-35 through 6-40, for Takeda5 oscillators that were initially designed for a bilinear DDD of 8. The upper plot of each figure shows the response without strength reduction (RSR = 1); the lower plot shows response for RSR = 0.6.

Figures 6-35 through 6-37 show the effect of cracking on response. The displacement response, d'_d, of Takeda5 oscillators subjected to a PDD of one is compared with the response of the corresponding undamaged Takeda5 oscillators, d_d. Where no strength degradation occurs (RSR = 1), cracking rarely causes an increase in displacement demand; for the vast majority of oscillators, cracking is observed to cause a slight decrease in the peak displacement response. Reductions in strength typically cause a noticeable increase in displacement response, particularly for low T/T_g.

Figures 6-38 through 6-40 show the effect of a PDD of 8 on peak displacement, d'_d, relative to the response of the corresponding undamaged oscillators. Prior damage is observed to cause modest changes in displacement response where the strength is maintained (RSR = 1); displacements may increase or decrease. Where displacements increase, they rarely increase more than about 10% above the displacement of the undamaged oscillator for the short-duration and long-duration motions. For the forward directivity motions, they rarely increase more than about 30% above the displacement of the undamaged oscillator. The largest displacements tend to occur more frequently for $T<T_g$.

The above discussion concerned oscillators for which the strength is maintained. When strength is reduced (RSR = 0.6), prior ductility demand may cause displacements to increase or decrease, but the tendency for displacements to increase is more prominent than for RSR = 1. Furthermore, the increase in displacement tends to be larger than for RSR = 1. Reduction in strength, as represented in Figure 6-26, also causes reduction in stiffness, and both effects contribute to the tendency for displacements to increase.

To understand the effects of prior damage on the response of the Takeda5 models, it is helpful to consider several oscillators exposed to the IV40ELCN.180 (El Centro) record. Figures 6-41 to 6-45 plot the response of oscillators having initial (reference) periods of 0.2, 0.5, 1.0, 1.5, and 2.0 sec, respectively, to this ground motion. The oscillators have yield strength equal to that required to obtain displacement ductility demands of 8 for the bilinear model. Oscillators having PDD of 0 (undamaged), 1, 4, and 8 are considered. Displacement time-histories (40 sec) of the oscillators are plotted at the top of each figure. Details of the first 10 seconds of response are shown below these. The solid lines represent the response of the initially-undamaged oscillators, and the dashed and dotted lines represent oscillators with PDD > 0. Force/displacement plots for the first 10 sec of response of each oscillator are provided in the lower part of the figure, using the same PDD legend. It can be observed that even though the undamaged oscillators initially have greater stiffness, their displacement response tends to converge upon the response of the initially-damaged oscillators within a few seconds. The displacement response of the damaged oscillators tends to be in phase with that of the initially-undamaged oscillators, and maximum values tend to be similar to and to occur at approximately the same time as the undamaged oscillator peaks. Thus, it appears that prior ductility demands have only a small effect on oscillator response characteristics and do not cause a fundamentally different response to develop.

6.4.3.2 Response of the TakPinch Model

Figures 6-46 to 6-48 plot the ratio, d'_d/d_d, of damaged and undamaged displacement response for the TakPinch models having DDD = 8 and PDD = 8, for RSR = 1 and 0.6. Figure 6-49 plots the displacement time-history of TakPinch oscillators subjected to the NS component of the 1940 El Centro record, and Figure 6-50 plots results for oscillators having cyclic strength degradation given by RSR = 0.6. These oscillators have a reference period of one second, DDD = 8, and various PDDs.

By comparison with the analogous figures for the Takeda5 model (Figures 6-38 to 6-40 and 6-43), it can be observed that: (1) for RSR = 1 (no strength degradation), the effect of PDD on displacement response is typically small for the Takeda5 and TakPinch oscillators, and (2) the effect of cyclic strength degradation, as implemented here, is also relatively small. Thus, the observation that prior

(Text continued on page 151)

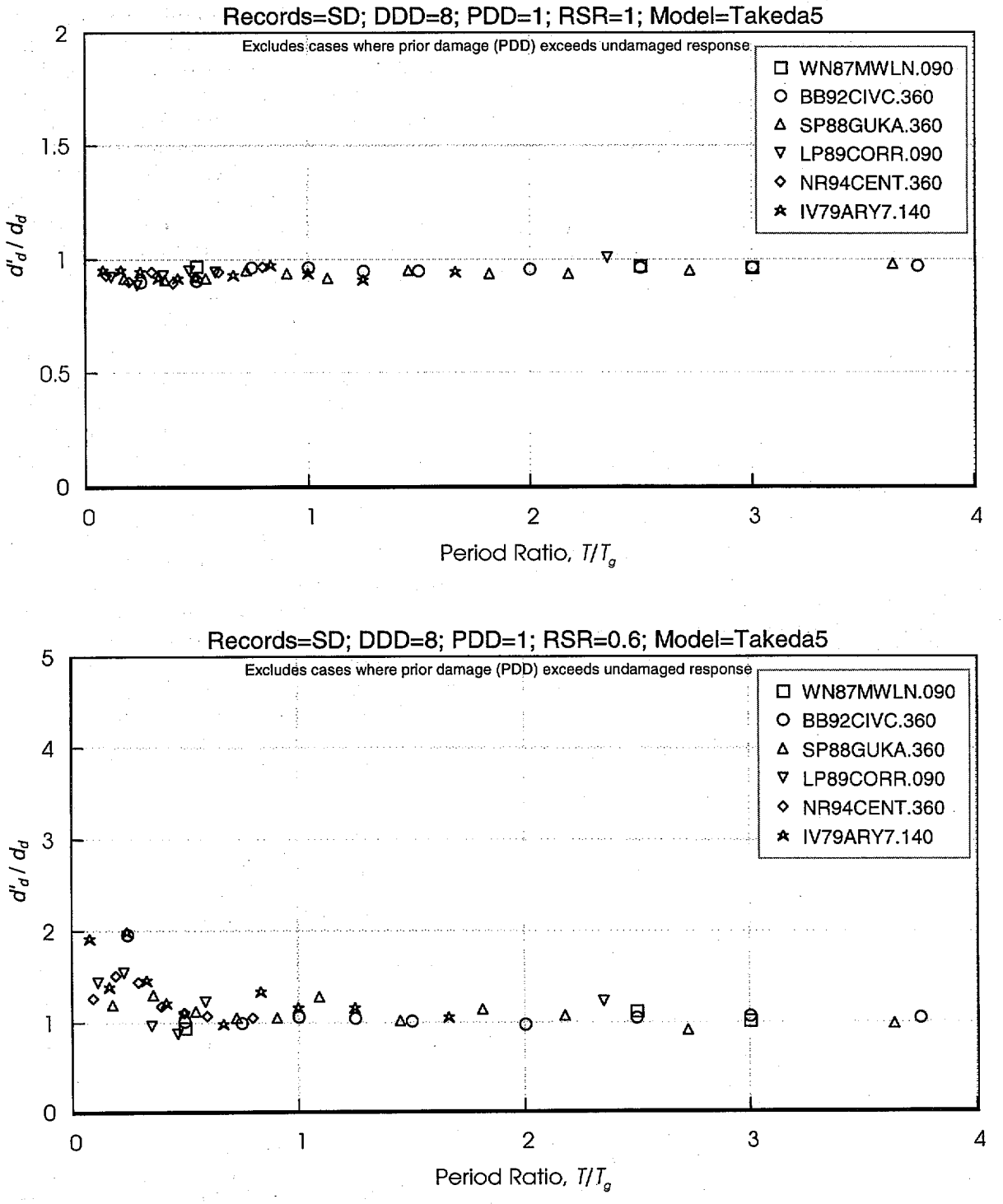

Figure 6-35 ***Effect of Cracking Without and With Strength Reduction on Displacement Response of Takeda5 Models, for Short-Duration Records (DDD= 8 and PDD= 1)***
DDD = Design Displacement Ductility; PDD = Prior Ductility Demand; RSR = Reduced Strength Ratio

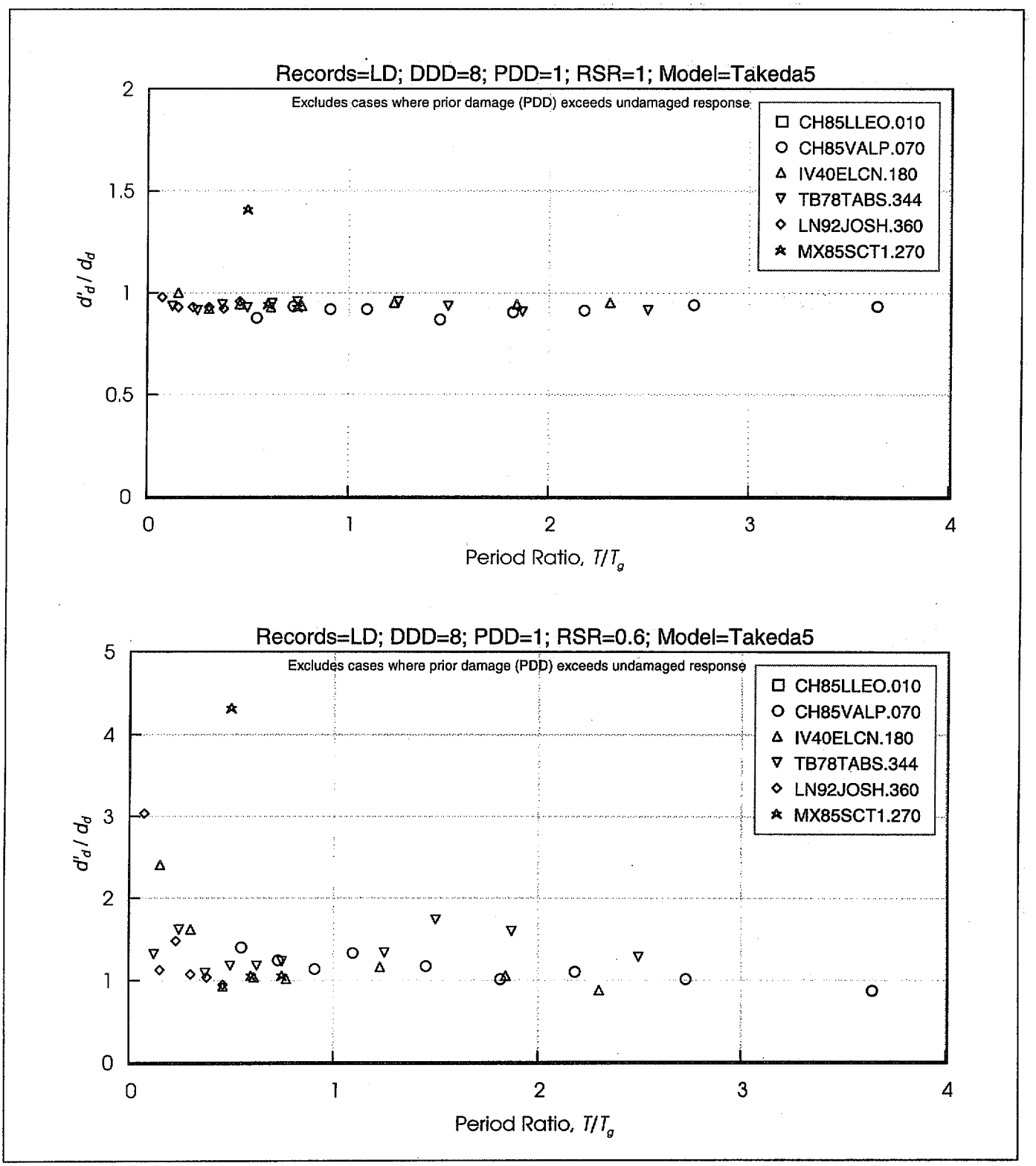

Figure 6-36 ***Effect of Cracking Without and With Strength Reduction on Displacement Response of Takeda5 Models, for Long-Duration Records (DDD= 8 and PDD= 1)***
DDD = Design Displacement Ductility; PDD = Prior Ductility Demand; RSR = Reduced Strength Ratio

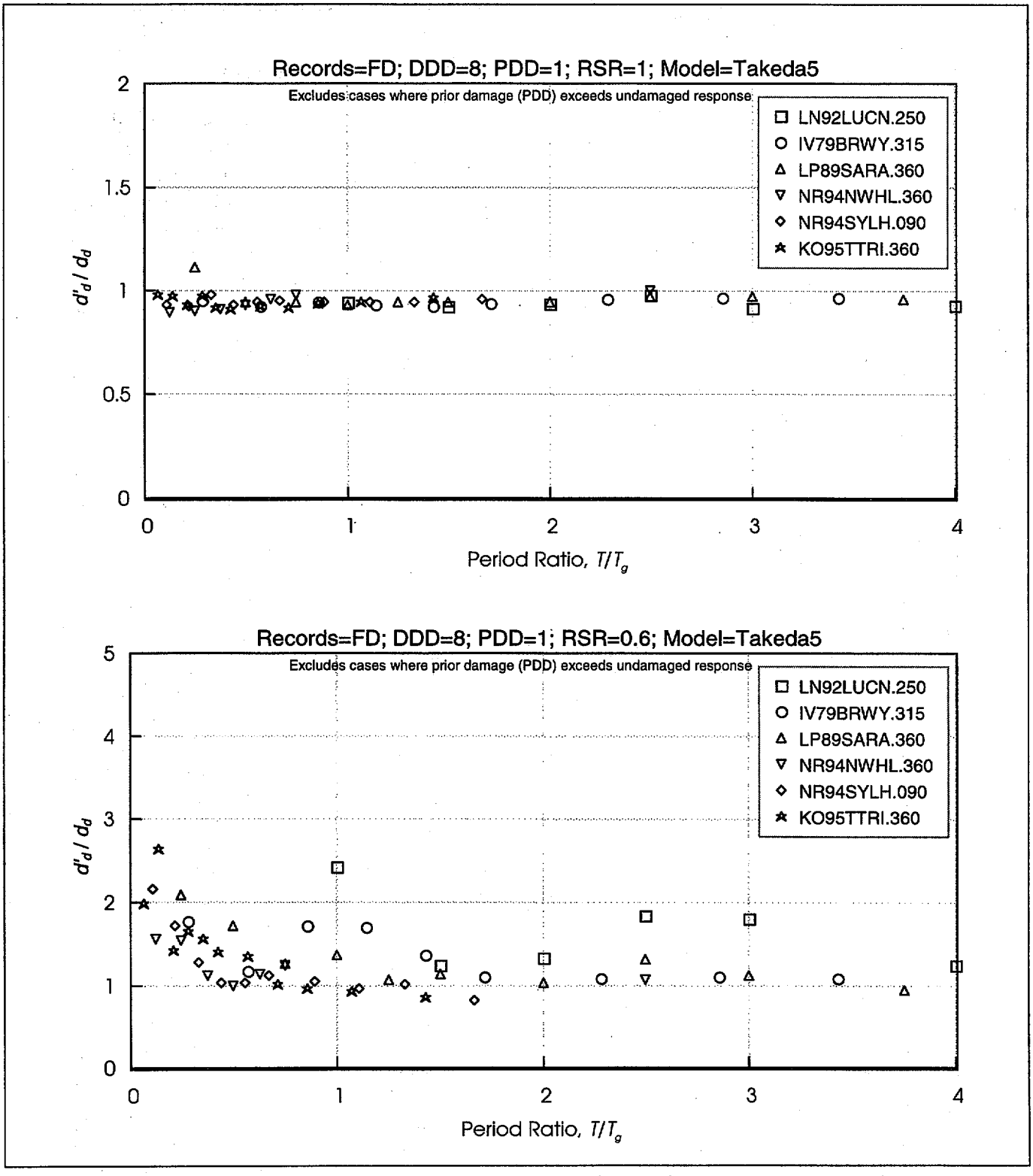

Figure 6-37 ***Effect of Cracking Without and With Strength Reduction on Displacement Response of Takeda5 Models, for Forward Directive Records (DDD= 8 and PDD= 1)***
DDD = Design Displacement Ductility; PDD = Prior Ductility Demand; RSR = Reduced Strength Ratio